POLITECNICO DI TORINO

Faculty of Engineering

Mechanical Design Engineering

Master Thesis

Nonlinear vibrating automotive devices: theoretical, numerical and experimental analyses

Supervisors:

Prof. Elvio Bonisoli

Dr. Luca Dimauro

Candidate:

Vincenzo Persano

October 2022

Index

Abstract

The real world is not only described by linear systems. It is rather generally explained by nonlinear structures, which have a richer behaviour with respect to linear ones. This thesis is devoted to better understand the nonlinear features of vibrating mechanical structures involved in automotive subsystems. It starts from a method to discretise a complex system using Lupos, a MATLAB based software because nowadays simulation and numerical analyses are essential for both linear and nonlinear structures. The device in question is the right lever of the LEVIT F173, projected and assembled at Valeo, Santena.

Then a deep look at the major distinctions of the two kinds of systems is performed, dealing with theoretical and practical aspects with the use of different approaches including Simulink numerical simulations of SDOF systems. To be more precise, their frequency contents are postprocessed with the use of:

- Spectrogram, that is based on the FFT, representing structures with summation of sines and cosines. It is used on a large scale to reduce the dimensions of the files that we daily handle;
- Wavelet, which employs waves of various shapes and now are widespread in the word of compressing sounds.

At the end, an experiment test is carried out and has its frequency contents examined in order to spot the nonlinear symptoms and characteristics described in the previous sections. In particular, a beam is employed with two sources of nonlinearity, i.e. magnets and a non-holonomic constraint. Moreover, numerical simulations with Lupos are executed with the idea of fully interpret the obtained results.

1. Pad Lever Right SW 2021 to Lupos

This chapter deals with the method of generating a frequency analysis of a simple assembly in SolidWorks 2021 and use both the results and the meshed geometry in Lupos, after properly exporting them from the abovementioned CAD software. Afterwards, the model is transformed into a parallelepipedal mesh, i.e. into a Minecraft model.
The components analysed in this document are part of a known system, which is the "Valeo Levit F173", the paddle-shift of a Ferrari production car. In particular the right pad and the lever, making up the up-shift system, are taken into account. The device is shown in Figure 1.1.

Figure 1.1 – Levit F173 and detail of the upshift-shift system.

Firstly, three new frequency studies are performed in SolidWorks, sharing an appropriate choice of the materials, the connections and fixtures of the components.
Afterwards, three discretisations with increasing grade of quality are carried out by using tetra4 elements (tetrahedrons that have a node for each vertex of the element) and three simulations are run to calculate eight natural frequencies and their corresponding mode shapes. Therefore, the first study has the coarsest mesh, whereas the third one contains the finest discretisation.
Next step is carefully exporting information about meshes, natural frequencies and mode shapes in order to utilise them in `BDFtoLUPOS.m` and `SW_CSVtoPhiW2.m`, which translate these files into Lupos ones.
This process appears to be simple at first glance, but there are many expedients that one needs to carefully exploit. Indeed, the procedure is detailed in the following sections of the report.
Eventually, the Lupos model becomes a Minecraft model, i.e. discretised into prisms with the proper material assigned to. This particular part requires a new MATLAB function that has many attentions to correctly perform the attribution.

1.1 CAD model

The simple assembly of Figure 1.1 is taken into account.
It is composed by two parts: E239483_PALETTA_DX_PANTOGRAFATA and BRACCIO_DX_E145589, that previously has been mentioned respectively as “pad” and “lever”.
It can be helpful to dissolve the original sub-assembly that contained the lever and save the assembly of Figure 1.1.1 as “MAIN_..”.

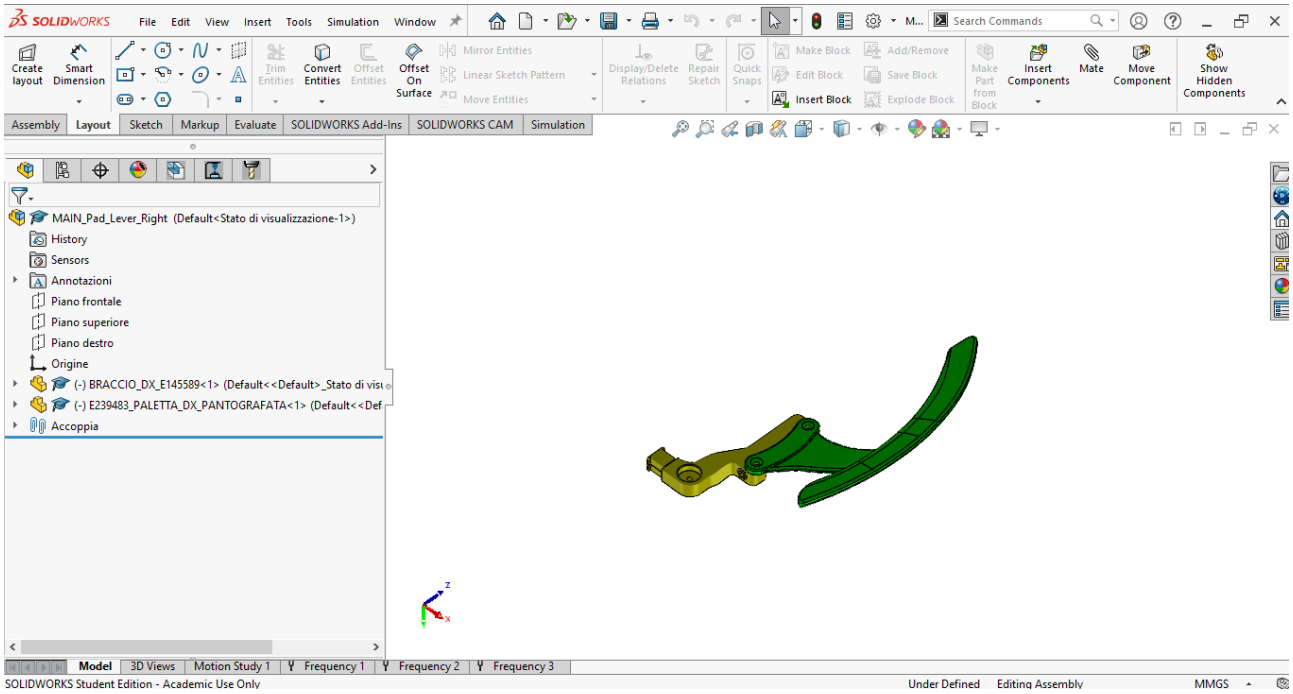

Figure 1.1.1 – MAIN CAD model.

1.2 FEM model files

After the definition of the FEM analysis, of the application of materials to the parts, constraints, external generalised forces and/or other parameters of simulation, the meshing step allows to approximate the CAD volumes to finite element discretisation. This is done by following the steps described in [1].
Tetrahedral mesh of the first order (draft quality mesh, tetra4) or the second order (tetra10) are suitable in SolidWorks, hence only this kind of elements is taken into account to be exported in MATLAB/Lupos.
In this particular example it is requested to choose two different types of aluminium alloy for the components in order to quickly change their colours in Lupos by modifying the file `.tet` that will be generated by the `BDFtoLUPOS.m` routine. More information about this function will be explained in § 1.4.1, § 1.5.3 and § 1.6.1.
Figure 1.2.1 shows the discretised model for the first study, i.e. the one with the roughest mesh.

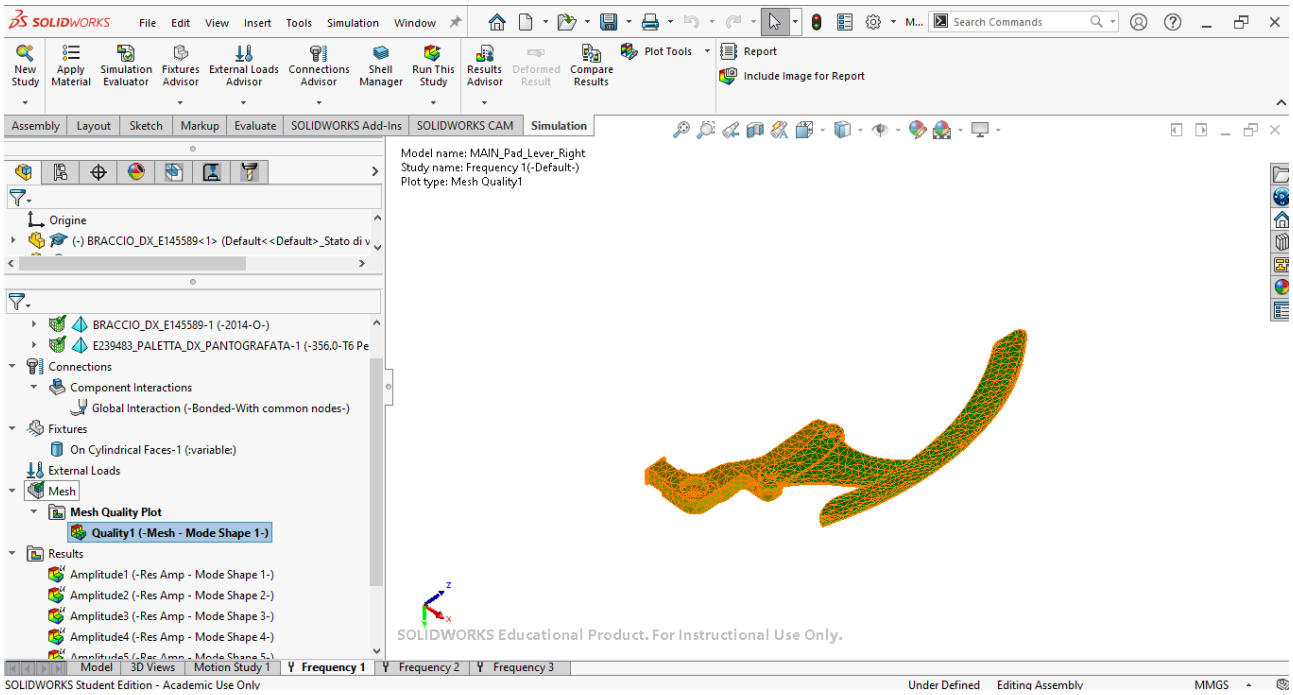

Figure 1.2.1 – Meshed model of the first frequency analysis.

It is crucial at this point to select the correct type and size of elements. As a matter of fact, using tetra10 instead of tetra4 does not improve the results since the above mentioned MATLAB routine only considers four nodes per tetrahedron, regardless if the element is a second order one.
Therefore, check if the components have “draft quality mesh”, as shown in Figure 1.2.2.
The steps to see the following screen are: right click on `Mesh`, select `Create Mesh`, select `Mesh Quality`

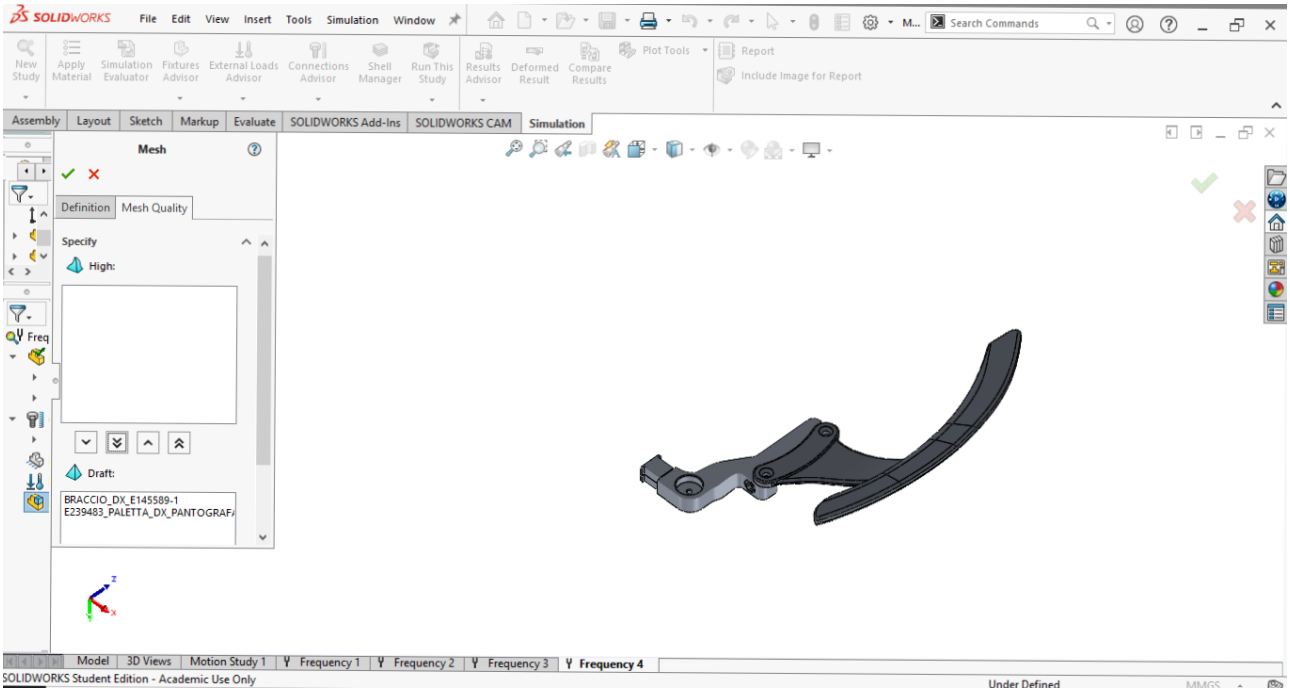

Figure 1.2.2 – Checking draft quality mesh.

As explained before, three discretisation fineness are utilised. The only changing parameter can be found by following this path: right click on `Mesh`, select `Create Mesh`, select the `Mesh Parameter` drop down menu and modify `Global Size`, like Figure 1.2.3

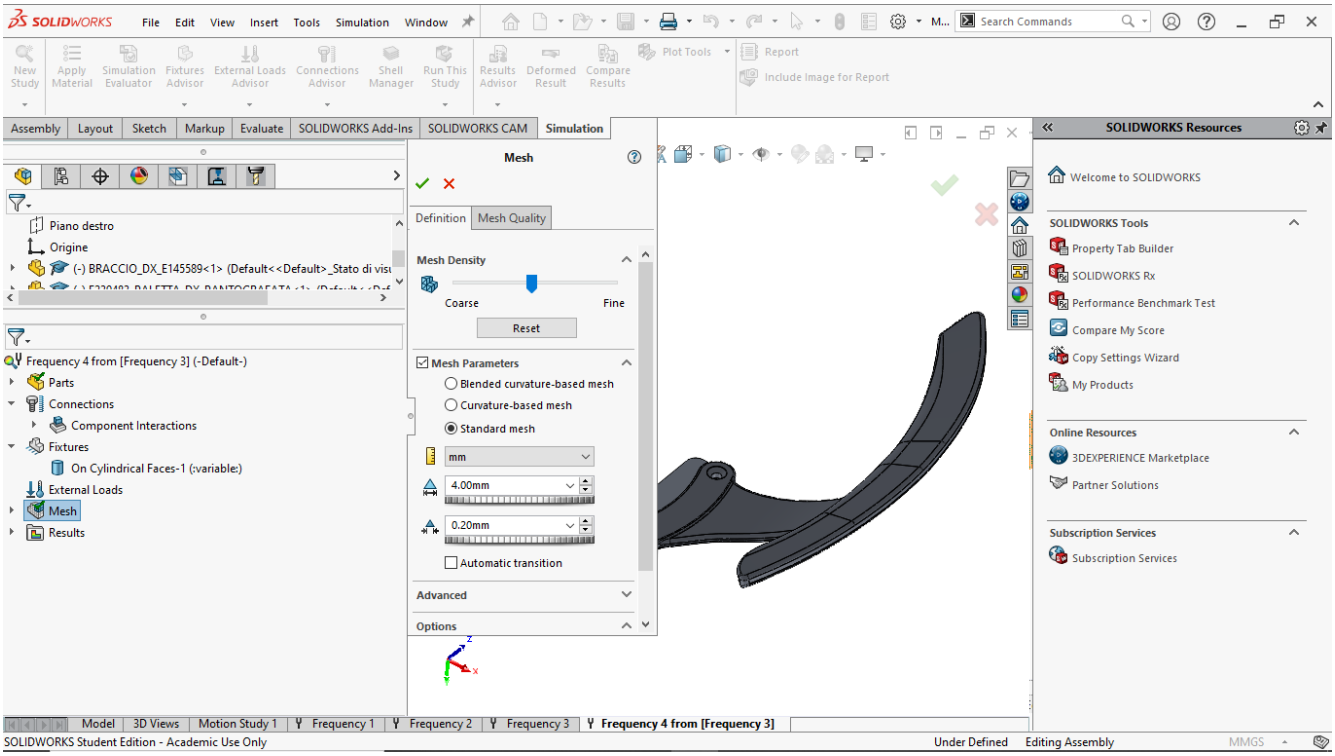

Figure 1.2.3 –Modifying mesh parameter.

The applied configurations are detailed in Table 1.2.1, as well as the number of nodes.

Table 1.2.1 – Configurations of the mesh parameters and nodes.

Frequency study	Global size [mm]	# Nodes	# Elements	# Dofs
1	4	4154	14299	12462
2	3	6762	25021	20286
3	2	15066	62592	45198

The number of the nodes, elements and dofs can be easily read in the `.log` file generated by SolidWorks.
A graphical comparison of the meshes can be seen in Figures 1.2.4-6.

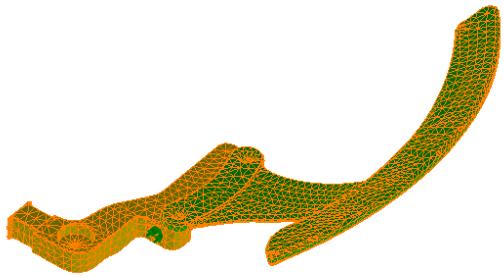

Figure 1.2.4 – Coarse mesh in SolidWorks.

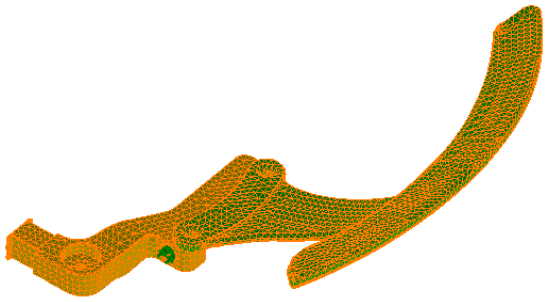

Figure 1.2.5 –Medium mesh in SolidWorks

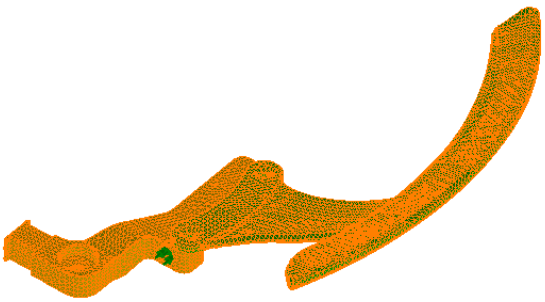

Figure 1.2.6 – Fine mesh in SolidWorks.

To export the model, select `Simulation`, then `Export…` as shown in Figure 1.2.7.
Then, select `NASTRAN files(*.dat)`, with `Options…`, `Short Fixed` (or `Long Fixed`) as shown in Figure 1.2.8.

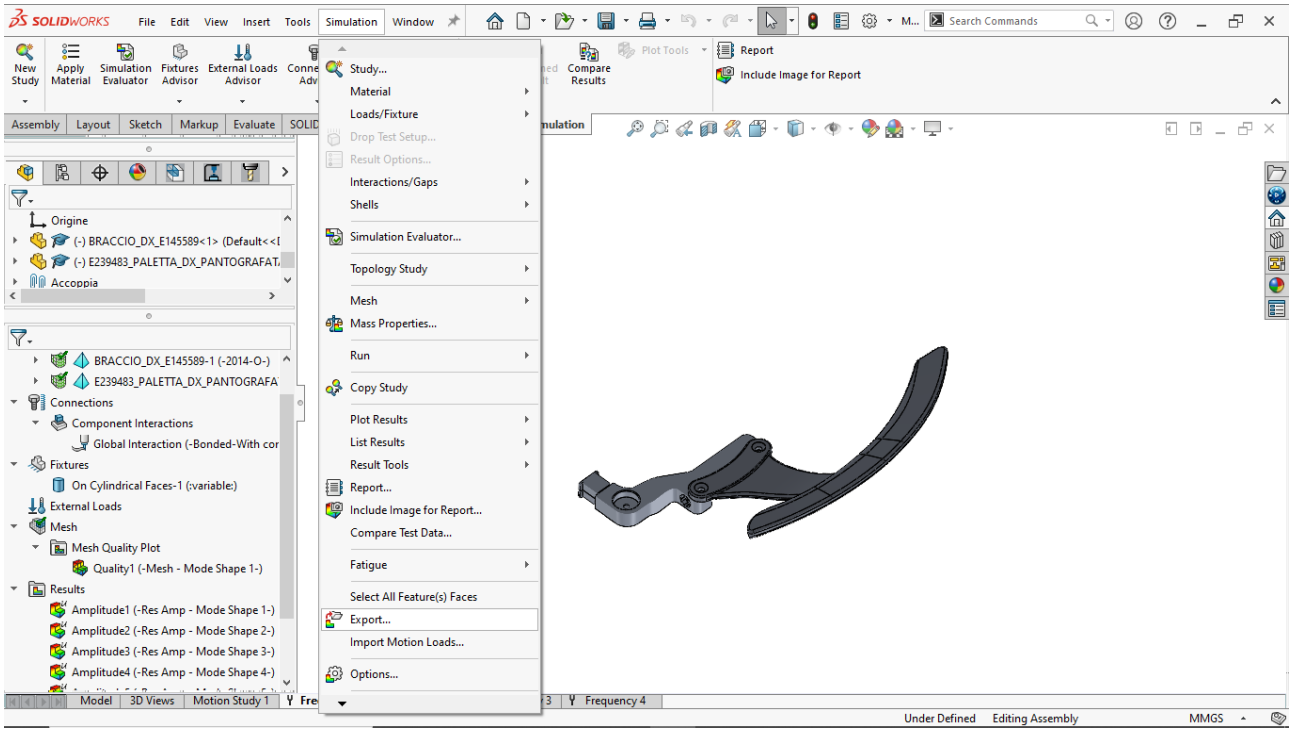

Figure 1.2.7 – Meshed model export.

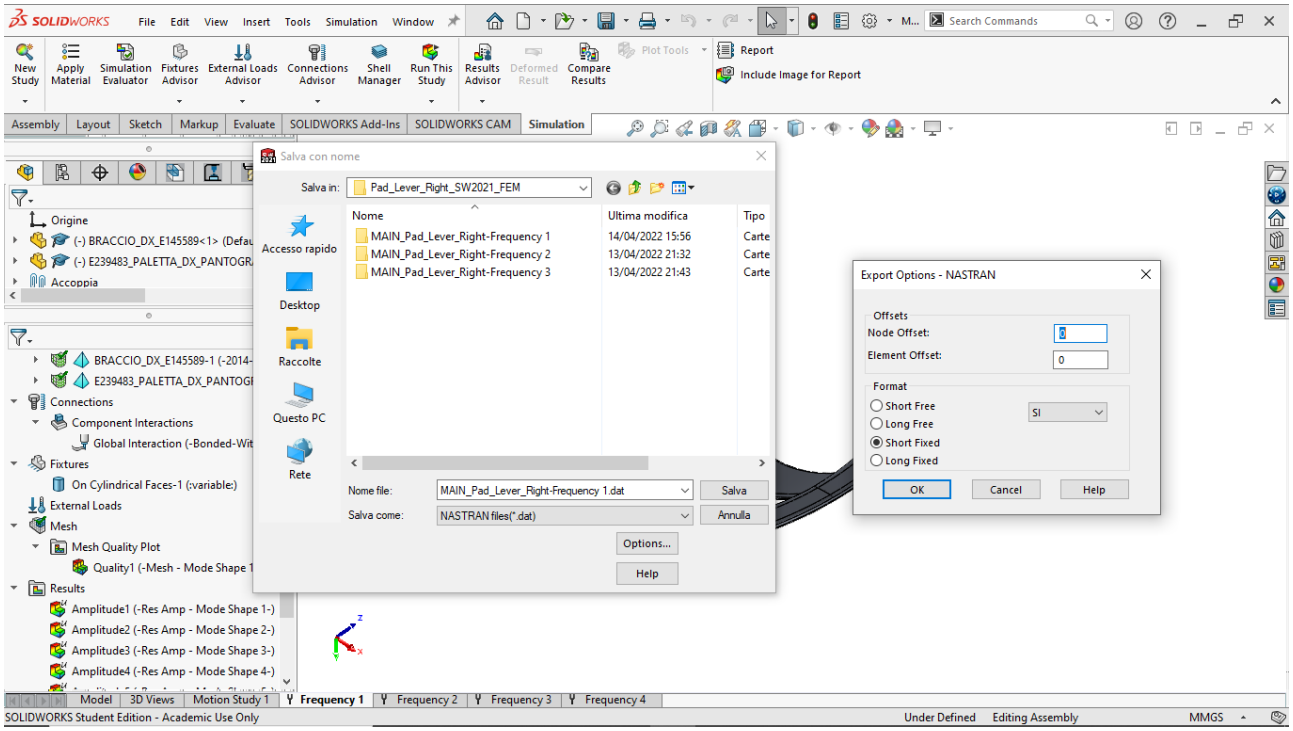

Figure 1.2.8 – Meshed model export.

Notes about `*.dat` files:

- the file contains all the three main parts of an MSC/Nastran file format (from `ID` to `CEND`, from `CEND` to `BEGIN BULK`, from `BEGIN BULK` to `ENDDATA`), hence not only the `bdf` part (from `BEGIN BULK` to `ENDDATA`);
- due to the previous note, some cards can exist in a not suitable way w.r.t. the translator file `BDFtoLUPOS.m`, i.e. `SPC = 1` in the part from `CEND` to `BEGIN BULK` part can create a row `1 nan nan` in the first row of the file `*.bcs`;
- these small problems have to be handled correcting manually the affected files;
- pay attention that, due to the Nastran short format, each field is composed by 8 characters only, hence to represent $\pi \cong 3.141592653589793$, the corresponding field is `3.141592` or `3.142+00` (without the symbol e and using two digits for the exponent);
- between the two alternatives long or short fixed files, the short format is suggested;
- in the `Export Options - NASTRAN` about the International Standard parameters, SI means [mm, tonnes, s] (default and suggested), MKS means [m, kg, s], IPS means [inch, pound, s] (absolutely to be avoided).

1.2.1 H-convergence analysis

It is worth, at this point, to perform the so-called *"h-convergence"* on the elaborated discretisation shown in Table 1.2.1. The analysis consists of evaluating the ratio between #nodes and #elements and relating it to the #elements itself. As theory explains ([2]), the graph with the just mentioned axis is limited by two curves:

- close volume (prismatic o spherical case), related to the densest volume, without any hole;
- maximum surface available (surface case), related to the case of an extreme ideal heat exchanger.

In this case, only tetra4 elements are used, in a configuration where a generic global cubic volume is discretised into twelve tetrahedrons. In Figure 1.2.1.1 is reported how the discretisation behaves in relation to the limit cases. Three other mesh have been added to the one of Table 2.1 and are reported in Table 1.2.1.1.

Table 1.2.1.1 – Six configurations of the mesh parameters and nodes.

Frequency study	Global size [mm]	# Nodes	# Elements	# Dofs
1	4	4154	14299	12462
2	3	6762	25021	20286
3	2	15066	62592	45198
4	1.5	28781	127753	86343
5	1	81531	394842	244593
6	0.5	161438	839394	484314

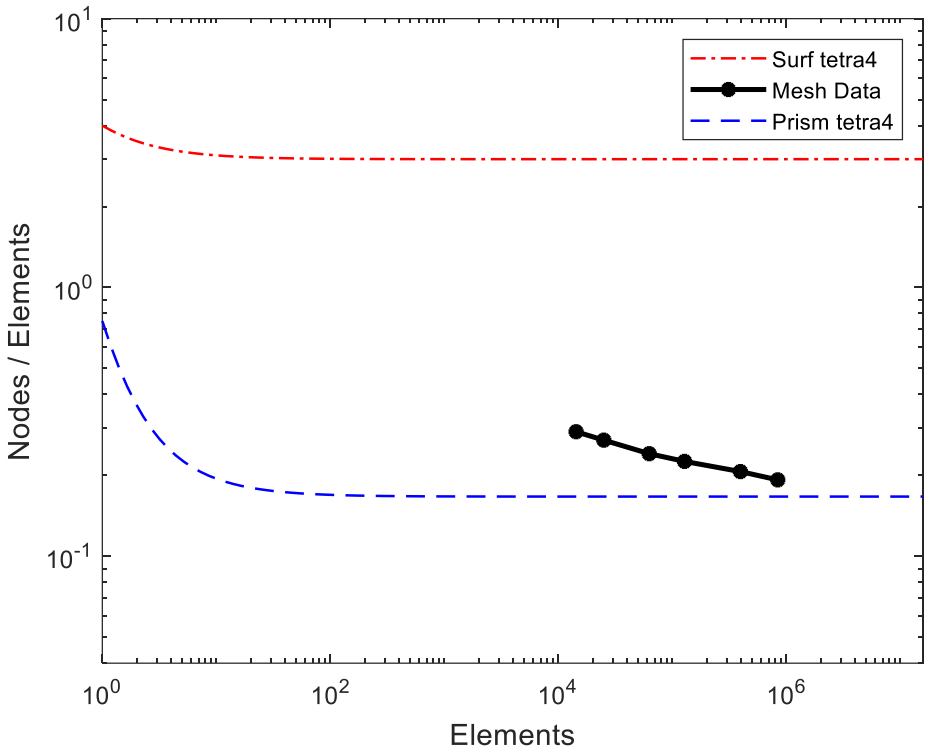

Figure 1.2.1.1 – H-convergence for Nodes/Elements.

As can be seen, the ratio approaches the Prism tetra4 curve when the number of the elements grows. Moreover, the amounts corresponding to SW mesh are compatible with the theoretical range of values. In addition to that, it is worth to note that, only after a severe refining of the mesh, the point representing the three triangulations, become near the Prism tetra4 curve. The reason of that might be the strong two-dimensionality of the assembly, which forces the structure to not assume a mesh with the densest volume of the elements.
A further confirmation of this is the difference between two radiuses regarding the geometry of the components. The first one can be calculated using the data in Figure 1.2.1.2 and is the radius that the structure will have if it was a sphere: from the inverse formula of the volume over the surface we get that the radius should be about 6 mm.

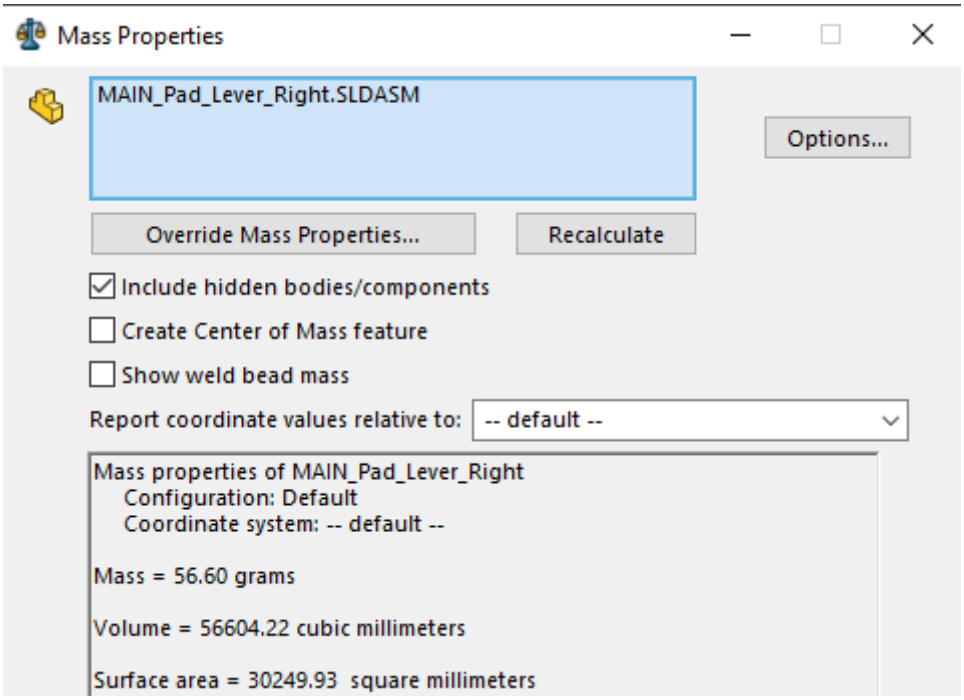

Figure 1.2.1.2 – Volume and surface of the assembly.

While the latter is equal to 80 mm and is the mean value between the radius of the smallest inscribed sphere (*dY*/2 in Figure 2.1.3) and radius of the largest circumscribed sphere (*Dist*/2 in Figure 1.2.1.4).

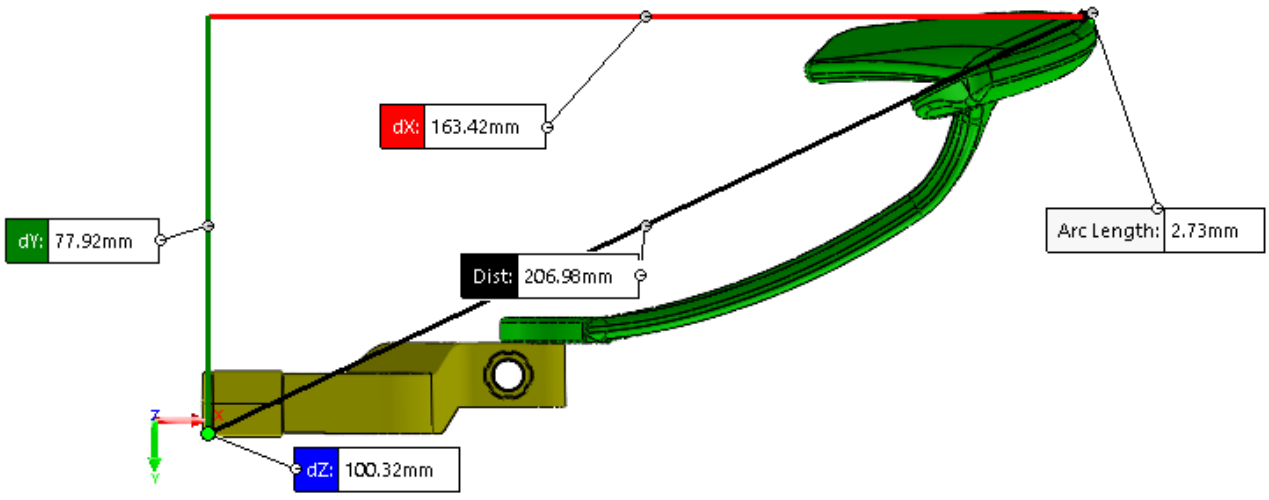

Figure 1.2.1.3 – Diameter of the smallest inscribed sphere.

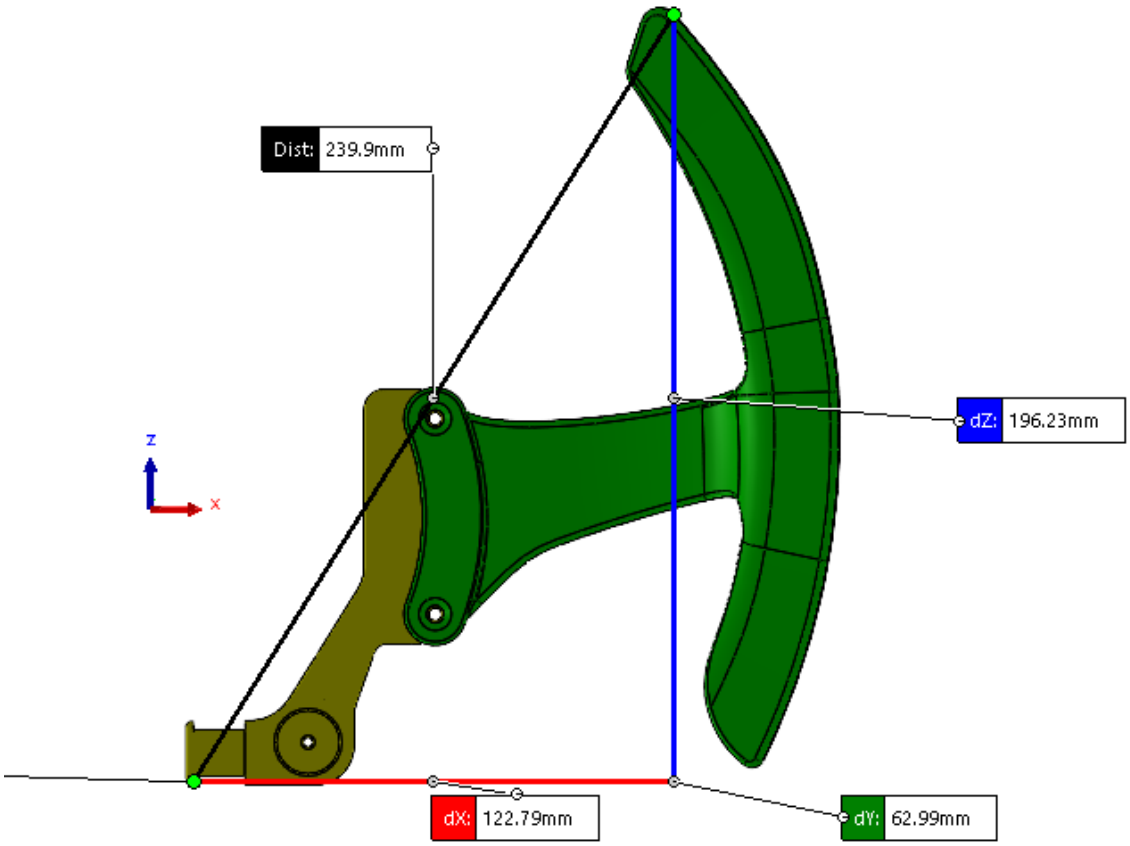

Figure 1.2.1.4 – Diameter of the largest circumscribed sphere.

The diversity of these two values gives a sort of quantification of how strong the bidimensionality is.
Another grade of the planarity of the assembly could be given by comparing the logarithmic distance between the two asymptotes and the distance between the mesh data and the prismatic curve. The results are shown in Table 1.2.1.2: the former gap is called “D1” while the latter “D2”.

Table 1.2.1.2 – Six configurations of the mesh parameters and nodes.

Frequency study	Global size [mm]	D1	D2	D2/D1[%]
1	4	1.2553	0.2413	19.2239
2	3	1.2553	0.2099	16.7232
3	2	1.2553	0.1596	12.7168
4	1.5	1.2553	0.1309	10.4269
5	1	1.2553	0.0931	7.4128
6	0.5	1.2553	0.0622	4.9544

As can be seen from Table 1.2.1.2 and Figure 1.2.1.1, only by approaching a value of D2/D1 proximate to 10% the mesh data become close to the Prism curve asymptote.

It could be interesting to perform an h-convergence analysis comparing the eight natural frequencies for the three initial discretisations, as shown in Figure 1.2.1.3.

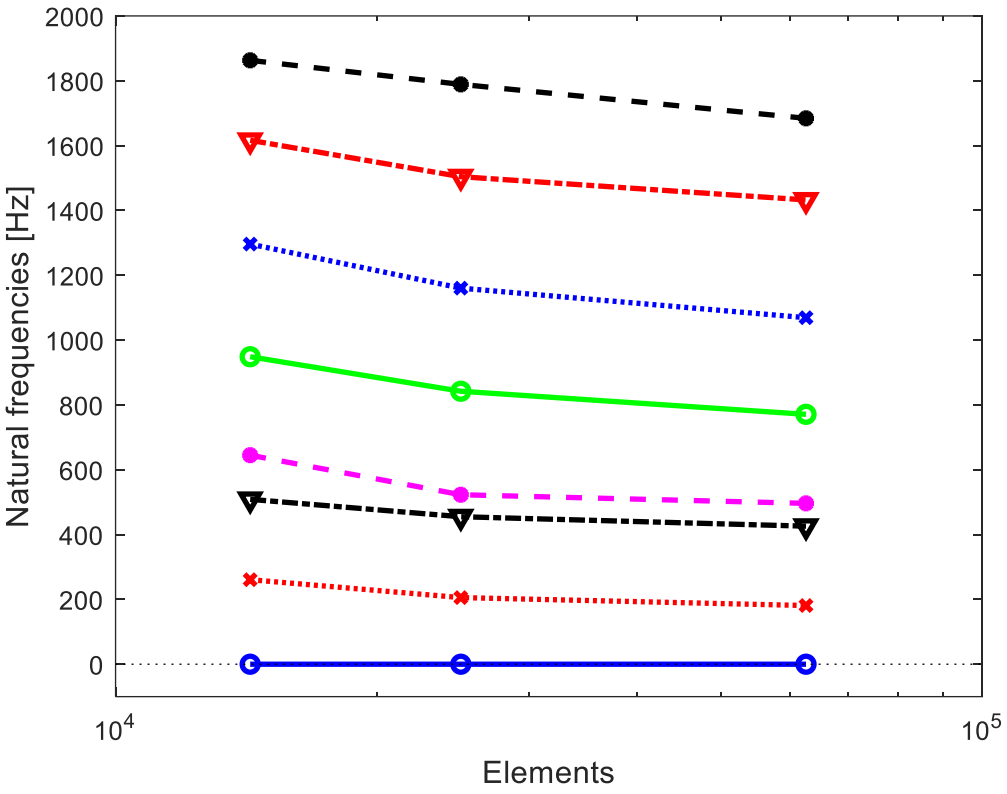

Figure 1.2.1.3 – H-convergence for natural frequencies.

Like one could expect, the trend is monotonous. The fact that values are decreasing as the number of the elements increases is related to the fact that stiffness of the assembly reduces while the mass remains constant.

1.2.2 Example of exported Nastran file

The following file (`MAIN_Pad_Lever_Right-Frequency 1.DAT`) is an example of exported Nastran file, corresponding to the meshed CAD model in the first frequency analysis in SolidWorks.
As can be seen, the document part where are described the element only contains tetra4, according to what it is written in § 1.2.

```
$     Output from COS2NAS translator Version 2014
$     Date         :  4/13/2022     Time:   20:49:51
ID,NASTRAN,
TIME 3600
SOL 3
CEND
TITLE=
ECHO=NONE
DISP  =ALL
SPC=100
METHOD=400
BEGIN BULK
CORD2C  1       0       0.00000 0.00000 0.00000 0.00000 0.00000 1.00000 +C1
+C1     1.00000 0.00000 0.00000
CORD2S  2       0       0.00000 0.00000 0.00000 0.00000 0.00000 1.00000 +C2
+C2     1.00000 0.00000 0.00000
CORD2C  3       0       0.065994-.833-02-.0344150.065994-.833-020.965585+C3
+C3     1.06599 -.833-02-.034415
CORD2C  4       0       0.065994-.833-02-.0344150.065994-.833-020.965585+C4
+C4     1.06599 -.833-02-.034415
GRID    1       0       0.073569-.0143270.021223
GRID    2       0       0.072494-.0143270.020935
```

```
GRID    3       0       0.071369-.0143270.021137
GRID    4       0       0.073569-.014327-.028777
GRID    5       0       0.072494-.014327-.029065
GRID    6       0       0.071369-.014327-.028863
GRID    7       0       0.060060-.014327-.033915
GRID    8       0       0.064673-.014327-.033915
GRID    9       0       0.069285-.014327-.033915
GRID    10      0       0.065978-.014327-.031017
GRID    11      0       0.064794-.014327-.026917
GRID    12      0       0.064915-.014327-.025557
GRID    13      0       0.065334-.014327-.024084
GRID    14      0       0.066990-.014327-.019321
GRID    15      0       0.068242-.014327-.014436
GRID    16      0       0.069082-.014327-.946-02
...
GRID    2783    0       0.155487-.064407-.056632
GRID    2784    0       0.153446-.064551-.064027
GRID    2785    0       0.130055-.0667860.104686
GRID    2786    0       0.123709-.0660180.114909
GRID    2787    0       0.150239-.049041.6444-02
GRID    2788    0       0.134744-.0356110.022064
GRID    2789    0       0.153291-.063154-.064731
GRID    2790    0       0.153344-.059539-.258-02
GRID    2791    0       0.109685-.023246.9317-02
GRID    2792    0       0.150499-.0533200.026129
CTETRA  1       1       1175    1190    1191    1192
CTETRA  2       1       1192    1193    123     116
CTETRA  3       1       1194    153     1193    1192
CTETRA  4       1       1191    1190    153     1192
CTETRA  5       1       1195    1191    1190    153
CTETRA  6       1       1196    1197    1198    1199
CTETRA  7       1       209     210     282     1196
CTETRA  8       1       1200    1201    1196    1202
...
CTETRA  9028    2       2596    2424    2434    2423
CTETRA  9029    2       2697    1655    1656    1661
CTETRA  9030    2       2699    2410    2411    2424
CTETRA  9031    2       2097    1904    1948    2662
CTETRA  9032    2       1904    2372    1903    2371
CTETRA  9033    2       2698    2597    2596    2424
CTETRA  9034    2       2632    2058    2054    2057
SPC     100     166     13      0.00000
SPC     100     167     13      0.00000
SPC     100     168     13      0.00000
SPC     100     169     13      0.00000
SPC     100     170     13      0.00000
SPC     100     171     13      0.00000
SPC     100     172     13      0.00000
SPC     100     173     13      0.00000
SPC     100     174     13      0.00000
...
SPC     100     746     13      0.00000
SPC     100     747     13      0.00000
EIGR    400     MGIV    0.0     1.0E+10 8       8                       +C5
+C5     MAX
PSOLID  1       1       0       2
PSOLID  2       2       0       2
MAT1    1       .7240+11.2800+110.3300002800.00 .2300-04298.000         +C6
+C6     .1850+09
MAT1    2       .7240+11.2720+110.3300002680.00 .2100-04298.000         +C7
+C7     .2280+09.1850+09
ENDDATA
```

1.3 Steps to real modal analysis simulation

According to Figure 1.13.1, frequency analysis, i.e. real modal analysis in SolidWorks is taken into account:

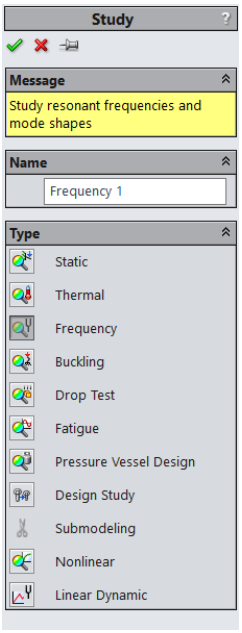

Figure 1.3.1 – Frequency simulation of SolidWorks.

1.3.1 Inputs of real modal analysis simulation

The following inputs for the assembly are utilised:

- materials for every part of the model, which it is chosen by clicking on `Part` in the simulation ambient, right click on the component whom the material should be applied, select `Apply/Edit Material` and finally decide it from a long list given by SW. In this case both the parts are made of Aluminium Alloy "EN AC 46100" in the reality. For this simple simulations, it is worth applying two different alloys for the components as similar as possible to the original material. Thanks to this, it is possible to easily change the colours of the meshed model in Lupos. In Table 1.3.1.1 and 1.3.1.2 are reported the parameters of the abovementioned part, where:

  - ρ is the density;
  - E is the Young modulus;
  - ν is the Poisson ratio;
  - G is the shear modulus, calculated as $G = \frac{E}{2(1+\upsilon)}$;
  - $R_{p0.2}$ is the yield strength.

Table 1.3.1.1 – Materials of the parts.

Real parts	Pad	Lever
EN AC 46100	356.0-T6 Permanent Mold Cast (SS)	2014-O

Table 1.3.1.2 – Aluminium alloy data.

Property	EN AC 46100	356.0-T6 Permanent Mold Cast (SS)	2014-O
ρ [kg/m^3]	2619	2680	2800
E [GPa]	74.56	72.40	72.40
ν [-]	0.33	0.33	0.33
G [GPa]	28.03	27.22	27.22
$R_{p0.2}$ [MPa]	170	152	95

- connections: make sure that the `Enforce common nodes between touching boundaries` is activated, as Figure 1.3.1.1 indicates. The screen in the just mentioned figure appears after a right click on `Global Interaction`, and selecting `Edit Definitions`;

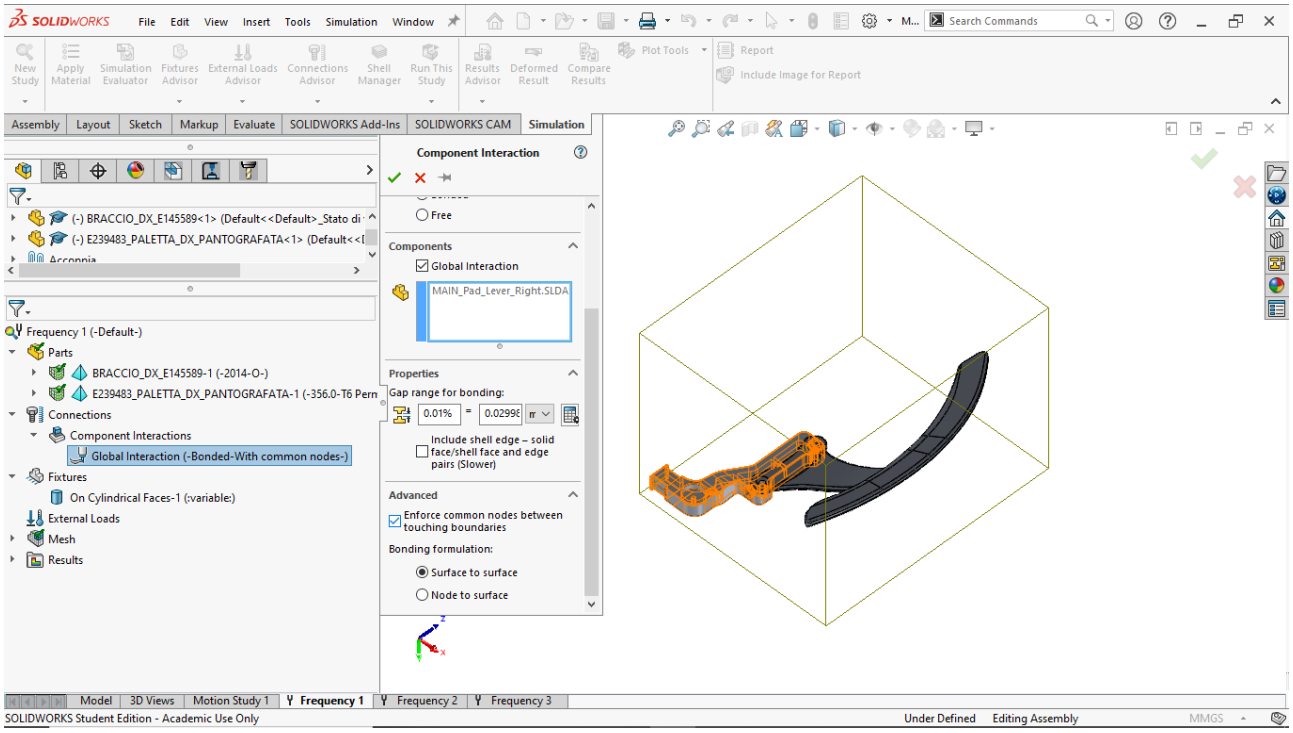

Figure 1.13.1.1 – Connection used in SolidWorks.

- fixtures applied: locking radial and axial displacements in the hole that houses the pin that allows the up-shift system to revolute around the z-axis of Figure 1.3.1.1. This means that there will be a rigid body mode in the results, in agreement with Figure 1.2.1.3;
- no external forces are applied;
- mesh discretisation, as shown in § 1.2.

1.3.2 Exporting the outputs of real modal analysis simulation

The frequency analysis can now be simulated in order to evaluate and export:

- natural frequencies, i.e. file `Frequency 1-Mode List-1.csv`, `Frequency 2-Mode List-2.csv` and `Frequency 3-Mode List-3.csv`;

- for each evaluated natural frequency, corresponding mode shape, i.e. modal displacement for each node, e.g. file `Frequency 1-7.csv` for mode #7 of the first simulation.

See the following figures for steps and parameters.
According to Figure 1.3.2.5, it is crucial to set in `Advanced Options`, `Range` (to export all nodes information) and choose, for each natural frequency, the corresponding number like Figure 1.3.2.2.

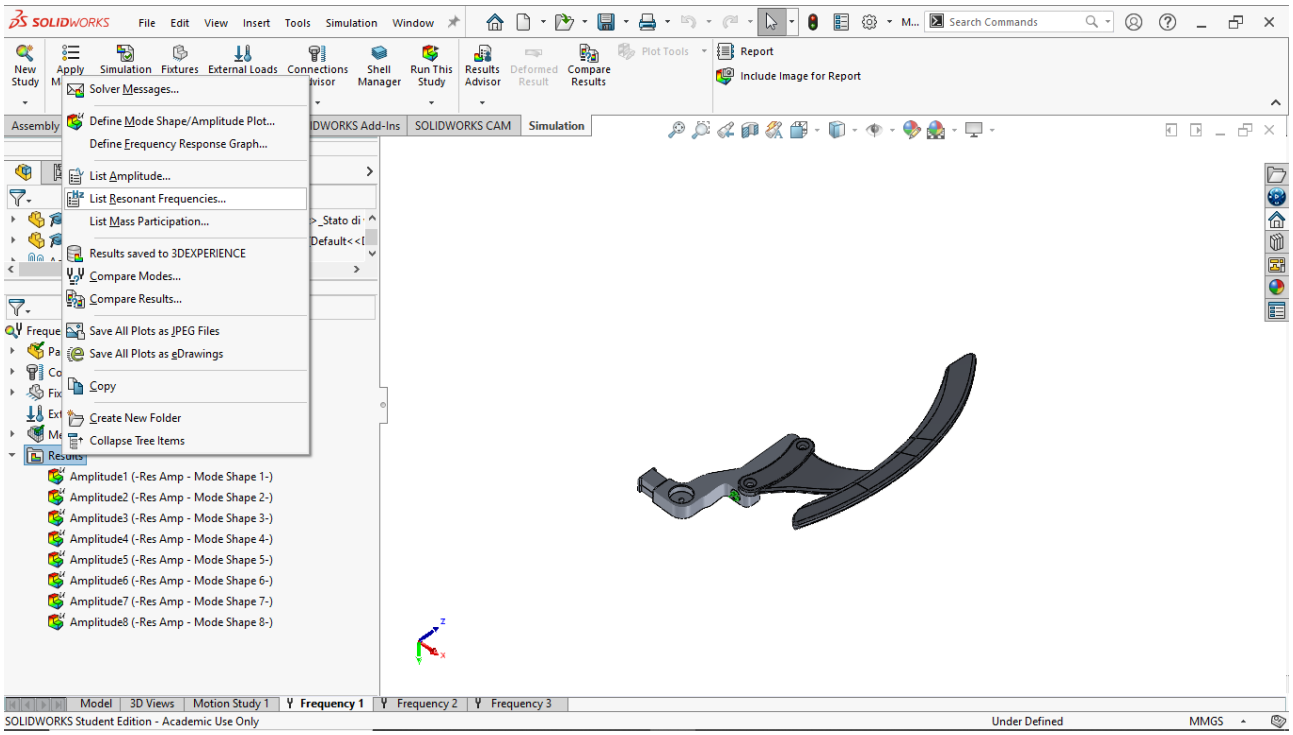

Figure 1.3.2.1 – Simulation frequency results export, step 1.

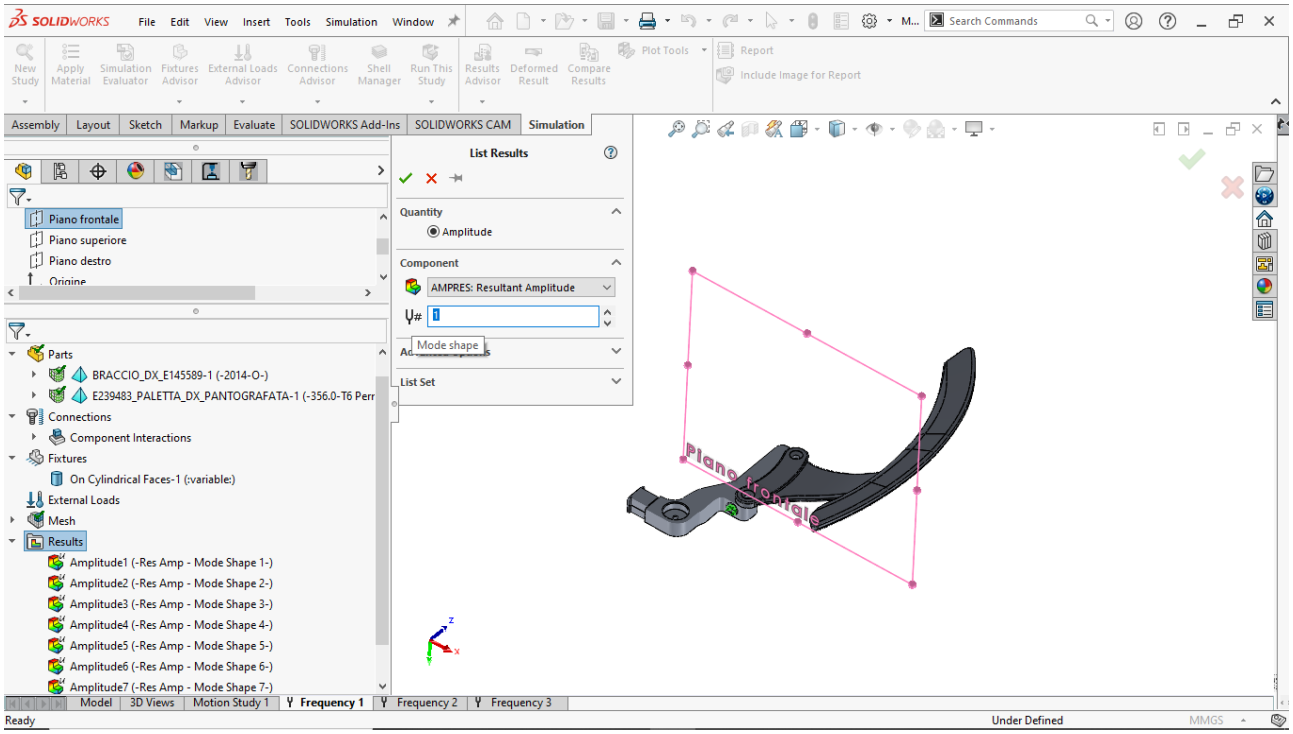

Figure 1.3.2.2 – Simulation frequency results export, step 2.

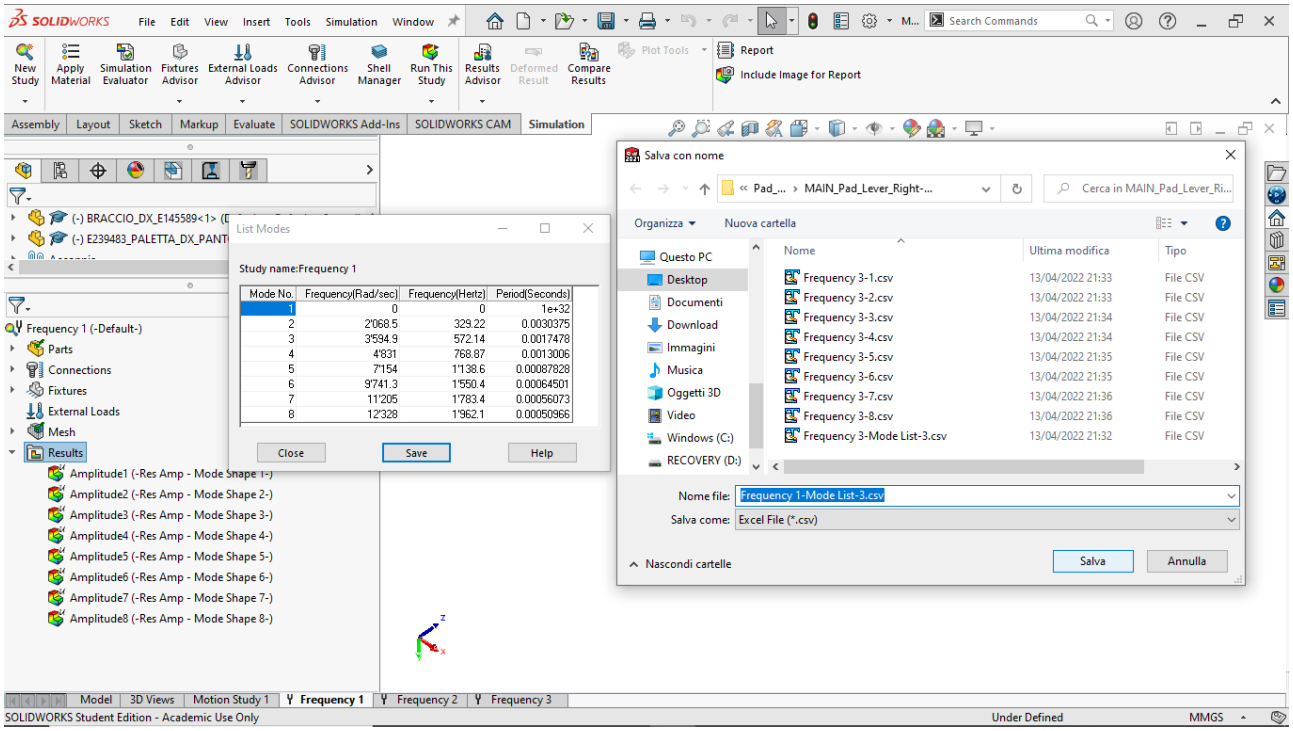

Figure 1.3.2.3 – Simulation frequency results export, step 3.

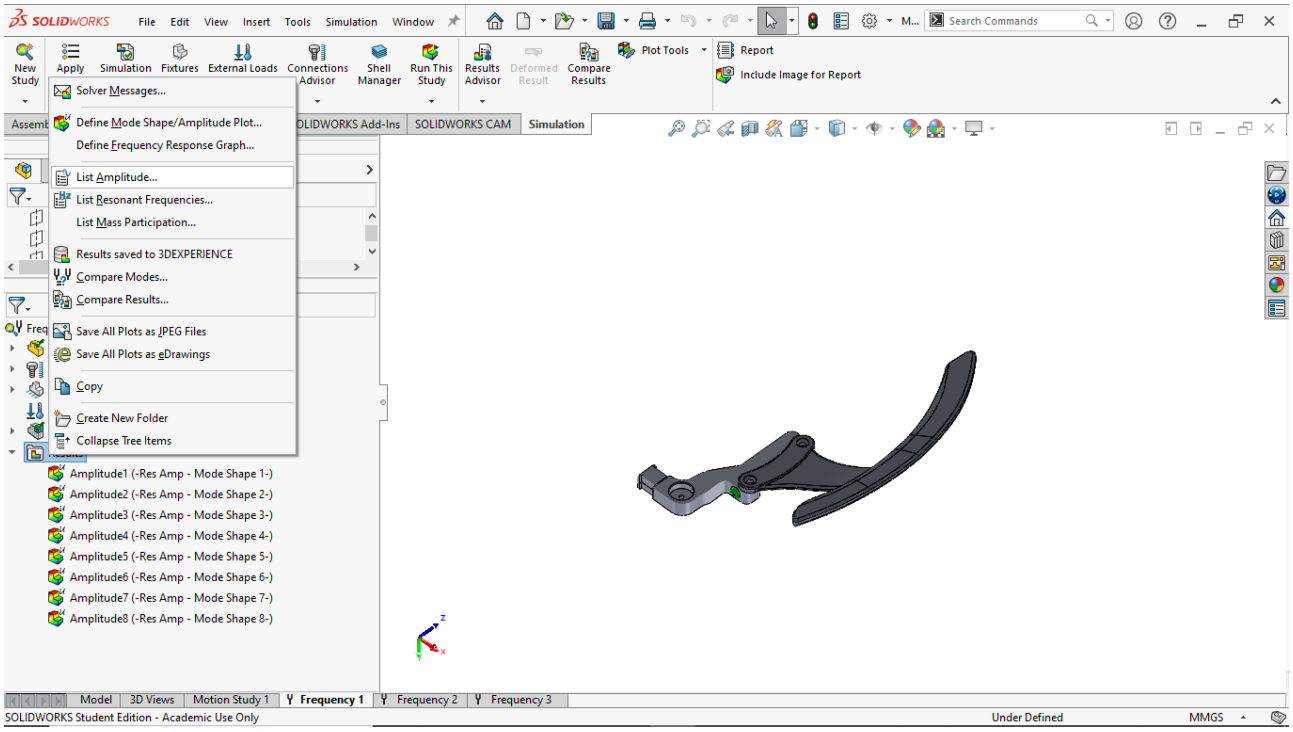

Figure 1.3.2.4 – Simulation mode shape results export, step 1.

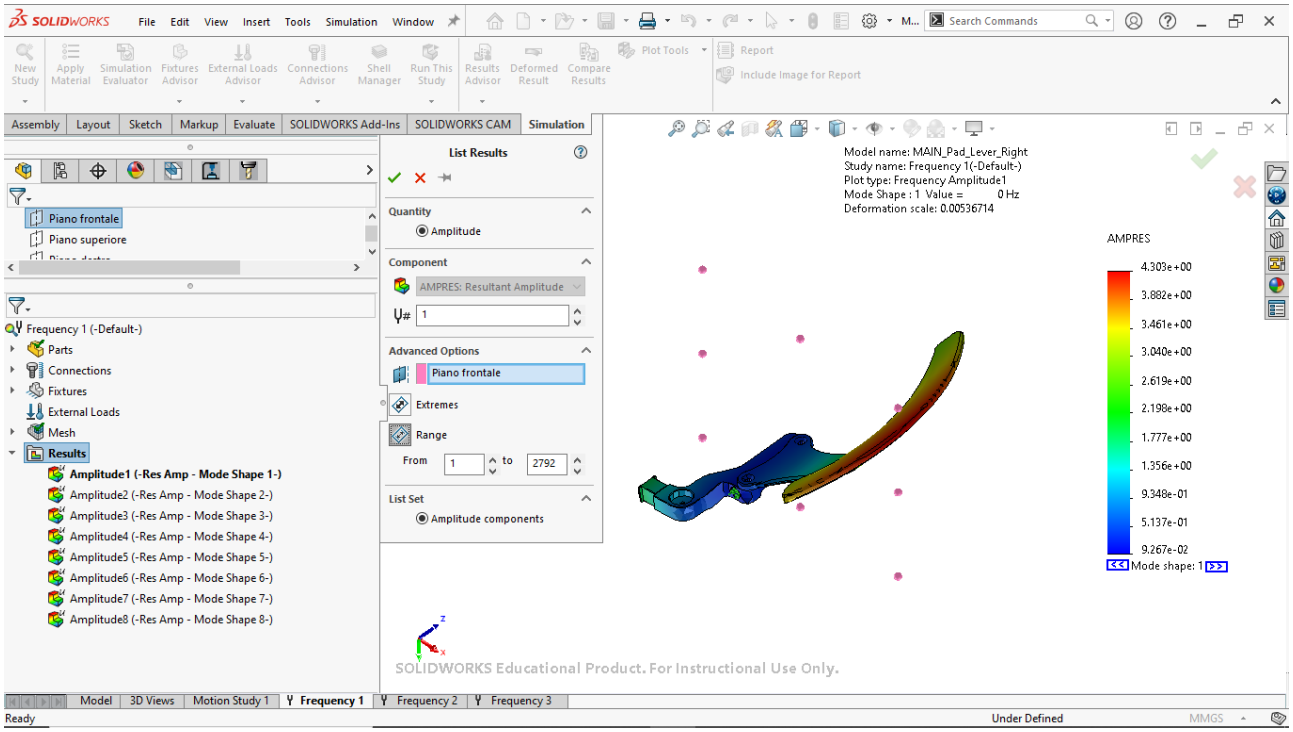

Figure 1.3.2.5 – Simulation mode shape results export, step 2: saving mode shape #1.

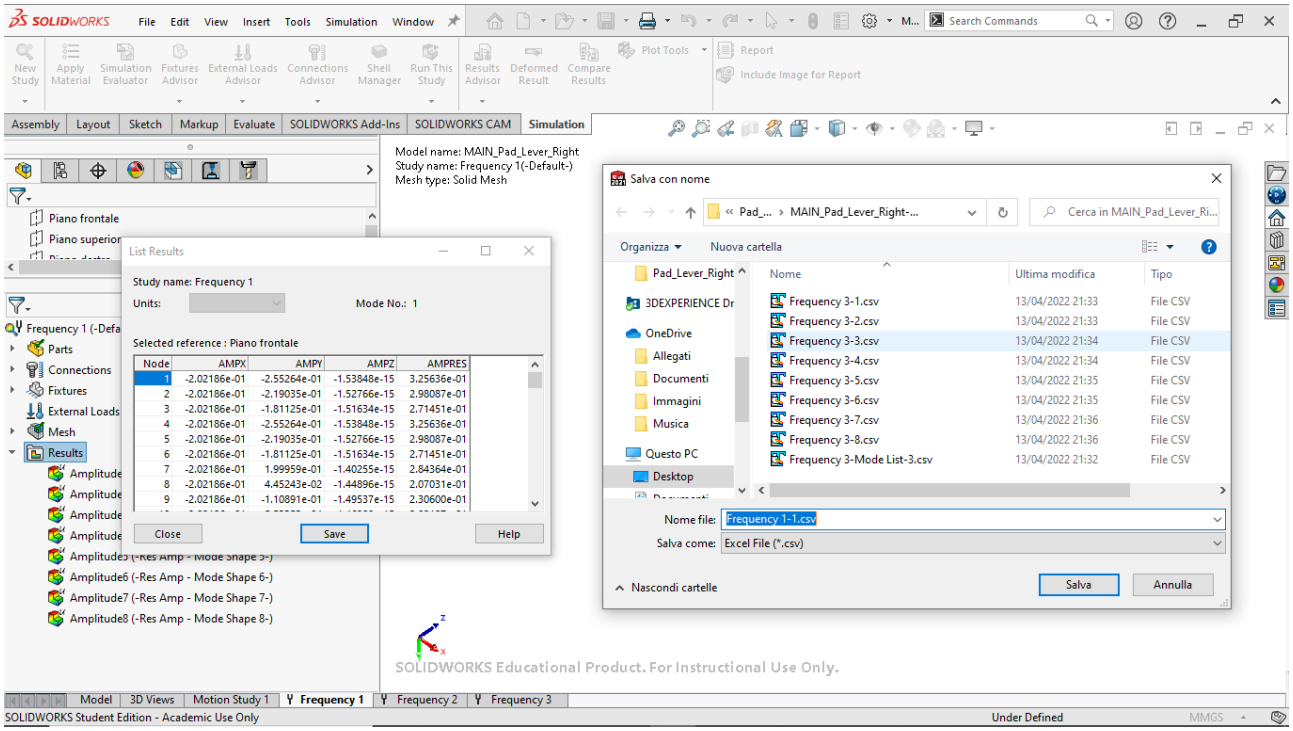

Figure 1.3.2.6 – Simulation mode shape results export, step 3: saving mode shape #1.

The last part of section§ 1.3.2 is dedicated to having a look of the files generated in the described process and writing down some suggestions to avoid futile mistakes.

The following file (`Frequency 1-Mode List-1.csv`) is an example of exported SolidWorks results about natural frequencies.

```
20:50, mercoledì, aprile 13, 2022
Study name:Frequency 1
Mode No.  ,Frequency(Rad/sec)  ,Frequency(Hertz)  ,Period(Seconds)
1  ,0             ,0             ,1e+32
2  ,2068.5        ,329.22        ,0.0030375
3  ,3594.9        ,572.14        ,0.0017478
4  ,4831          ,768.87        ,0.0013006
5  ,7154          ,1138.6        ,0.00087828
6  ,9741.3        ,1550.4        ,0.00064501
7  ,11205         ,1783.4        ,0.00056073
8  ,12328         ,1962.1        ,0.00050966
```

The following file (`Frequency 1-1.csv`) is an example of exported SolidWorks results about real mode shape #1 for the first simulation.

```
20:50, mercoledì, aprile 13, 2022
Study name:Frequency 1
Units:
Selected reference : Piano frontale
Node  ,AMPX  ,AMPY  ,AMPZ  ,AMPRES
1  ,-2.02186e-01  ,-2.55264e-01  ,-1.53848e-15  ,3.25636e-01
2  ,-2.02186e-01  ,-2.19035e-01  ,-1.52766e-15  ,2.98087e-01
3  ,-2.02186e-01  ,-1.81125e-01  ,-1.51634e-15  ,2.71451e-01
4  ,-2.02186e-01  ,-2.55264e-01  ,-1.53848e-15  ,3.25636e-01
5  ,-2.02186e-01  ,-2.19035e-01  ,-1.52766e-15  ,2.98087e-01
6  ,-2.02186e-01  ,-1.81125e-01  ,-1.51634e-15  ,2.71451e-01
7  ,-2.02186e-01  ,1.99959e-01  ,-1.40255e-15  ,2.84364e-01
8  ,-2.02186e-01  ,4.45243e-02  ,-1.44896e-15  ,2.07031e-01
9  ,-2.02186e-01  ,-1.10891e-01  ,-1.49537e-15  ,2.30600e-01
10  ,-2.02186e-01  ,5.53353e-04  ,-1.46209e-15  ,2.02187e-01
11  ,-2.02186e-01  ,4.04384e-02  ,-1.45018e-15  ,2.06191e-01
12  ,-2.02186e-01  ,3.63726e-02  ,-1.45139e-15  ,2.05432e-01
13  ,-2.02186e-01  ,2.22667e-02  ,-1.45560e-15  ,2.03409e-01
14  ,-2.02186e-01  ,-3.35469e-02  ,-1.47227e-15  ,2.04950e-01
15  ,-2.02186e-01  ,-7.57548e-02  ,-1.48487e-15  ,2.15912e-01
16  ,-2.02186e-01  ,-1.04061e-01  ,-1.49333e-15  ,2.27394e-01
...
2784  ,-1.89462e+00  ,-2.94690e+00  ,-1.53137e-14  ,3.50341e+00
2785  ,-1.96992e+00  ,-2.15869e+00  ,-1.56555e-14  ,2.92242e+00
2786  ,-1.94407e+00  ,-1.94485e+00  ,-1.53935e-14  ,2.74988e+00
2787  ,-1.37198e+00  ,-2.83884e+00  ,-1.12757e-14  ,3.15299e+00
2788  ,-9.19414e-01  ,-2.31670e+00  ,-7.65115e-15  ,2.49247e+00
2789  ,-1.84755e+00  ,-2.94169e+00  ,-1.49514e-14  ,3.47375e+00
2790  ,-1.72572e+00  ,-2.94350e+00  ,-1.40181e-14  ,3.41208e+00
2791  ,-5.02757e-01  ,-1.47228e+00  ,-4.20558e-15  ,1.55575e+00
2792  ,-1.51616e+00  ,-2.84761e+00  ,-1.23834e-14  ,3.22609e+00
```

Notes about `*.csv` files:

- Windows setting must be defined using symbol `.` (dot) as decimal separator and using the symbol `,` (comma) to separate columns, according to MATLAB settings;
- if `*.csv` files are generated using symbol `,` (comma) as decimal separator and using `;` (semicolon) to separate columns, software like `Notepad.exe` or `TextPad.exe` must be used to convert in this order `,` (comma) with `.` (dot), then `;` (semicolon) with `,` (comma).

1.4 Translation into Lupos using MATLAB

Next step is converting the Nastran file (`.DAT`) and the modal analysis results into Lupos by using two MATLAB routines: `BDFtoLUPOS` and `SW_CSVtoPhiW2`.

1.4.1 Example of script for real modal analysis simulation

The following MATLAB script can define the needed files for a real modal analysis and the following translation in Lupos format. As can be seen, the inputs are the results exported from SolidWorks. In particular, `BDFtoLUPOS` translates Nastran BDF (or DAT) file into Lupos files and `SW_CSVtoPhiW2` translate SolidWorks CSV files in `Phi`, `NodePhi` and `W2` files. According to § 1.2, three scripts were written in order to use the discretisations discussed in Table 1.2.1.

```
%Example of direct use of BDFtoLUPOS and SW_CSVtoPhiW2

%Pad and Lever from the right part are converted into Lupos by using a
%coarse mesh
datain = 'MAIN_Pad_Lever_Right-Frequency 1.DAT';
dataout = 'StructureRef_Freq1';
BDFtoLUPOS(datain,dataout)
 B
datain_Freq = 'Frequency 1-Mode List-1.csv';
datain_Phi = {...
    'Frequency 1-Mode 1.csv';...
    'Frequency 1-Mode 2.csv';...
    'Frequency 1-Mode 3.csv';...
    'Frequency 1-Mode 4.csv';...
    'Frequency 1-Mode 5.csv';...
    'Frequency 1-Mode 6.csv';...
    'Frequency 1-Mode 7.csv';...
    'Frequency 1-Mode 8.csv';...
    };
dataout = {...
    'StructureRef_Freq1_Phi.dat';...
    'StructureRef_Freq1_NodesPhi.dat';...
    'StructureRef_Freq1_W2.dat';...
    };
SW_CSVtoPhiW2(datain_Freq,datain_Phi,dataout)
```

1.5 Example of input/output files

1.5.1 CAD/FEM SolidWorks files

According to the simple example of Figure 1.1.1, some SolidWorks input files are:

- `MAIN_Pad_Lever_Right.SLDASM` (SolidWorks CAD assembly, shown in Figure 1.1.1);
- `E239483_PALETTA_DX_PANTOGRAFATA.SLDPRT` (SolidWorks CAD part, representing the pad);
- `BRACCIO_DX_E145589.SLDPRT` (SolidWorks CAD part, representing the lever);
- `MAIN_Pad_Lever_Right-Frequency 1.CWR` (CosmosWorks Result file for modal analysis, containing the meshed model and the mode shapes of the assembly);
- `MAIN_Pad_Lever_Right-Frequency 1.LOG` (ASCII simulation resume file, for checking the number of nodes of the model).

1.5.2 Exported FEM meshed and results model files

Independently from the kind of static or frequency analyses, the exported file provided following § 2 is `MAIN_Pad_Lever_Right-Frequency 1.DAT` (corresponding ASCII Nastran file of the meshed model of Figure 1.2.1);

Taking into account a real modal (frequency) analysis, the exported files provided following § 1.3.2 for the first simulation are:

- `Frequency 1-Mode List-1.csv` (corresponding ASCII natural frequencies [rad/s] file containing the first 8 values `(m = 8)` that requests the corresponding 8 mode shape files);
- `Frequency 1-Mode 1.csv` (corresponding ASCII mode shape #1 file of all the model nodes);
- `Frequency 1-Mode 2.csv` (corresponding ASCII mode shape #2 file of all the model nodes);
- `Frequency 1-Mode 3.csv` (corresponding ASCII mode shape #3 file of all the model nodes);
- `Frequency 1-Mode 4.csv` (corresponding ASCII mode shape #4 file of all the model nodes);
- `Frequency 1-Mode 5.csv` (corresponding ASCII mode shape #5 file of all the model nodes);
- `Frequency 1-Mode 6.csv` (corresponding ASCII mode shape #6 file of all the model nodes);
- `Frequency 1-Mode 7.csv` (corresponding ASCII mode shape #7 file of all the model nodes);
- `Frequency 1-Mode 8.csv` (corresponding ASCII mode shape #8 file of all the model nodes).

1.5.3 MATLAB/Lupos translated model and results files

In modal analysis, inside the example provided in § 1.4.1, through `BDFtoLUPOS.m` script, using as input file `MAIN_Pad_Lever_Right-Frequency 1.DAT`, the exported file provided following § 1.2 are:

- `Structure.geo` (ASCII Lupos file of the `N` model nodes and containing the number of the nodes and their corresponding coordinates in xyz reference system `(N x 4)`);
- `Structure.tet` (ASCII Lupos file of `T` model tetra4 elements `(T x 8)` and the nodes of each tetrahedron as well as a number representing the colour of the element in Lupos and the properties of the tetra4 material);
- `Structure.bcs` (ASCII Lupos file of the `V` model constraints `(V x 2)` and including the number of the constrained node and a number corresponding to degree of freedom locked as explained in Table 1.5.3.1 and described in [3]);

Table 1.5.3.1 – Dof and Id number.

Generalised dof	Id number
x, translation	1
y, translation	2
z, translation	3
x, rotation	4
y, rotation	5
z, rotation	6

- `Structure.fms` (ASCII Lupos file of model generalised forces elements `(F x 3)`).

Through `SW_CSVtoPhiW2.m` script and according to the input file `*.cvs` of the specific real modal analysis, the exported file provided following § 1.3 are:

- `Phi.dat` (ASCII Lupos file of model eigenvectors `(N x m = 13057*6 x 8 = 78342 x 8)` where `N` is the number of the nodes and the `m` is the number of the computed natural frequencies [-]);
- `NodesPhi.dat` (ASCII Lupos file of model nodes label `(N x 2)` [-]);
- `W2.dat` (ASCII Lupos file of the `m` model eigenvalues `(m x 1 = 8 x 1)` [$(rad/s)^2$]).

1.6 Example of Lupos figures

1.6.1 Visualisation of the assembly

Thanks to what it is explained in § 1.3.1, it is possible to easily change the colours of the meshed model in Lupos. Figure 1.6.1.1 shows how to do it. The method exploits the fact that the `.tet` file has the colour and the density of an element written in two consequent columns. Therefore, it is possible to choose green for the pad and red for the lever. The corresponding number for the just mentioned colour are: 3 for green and 2 for red ([3]). It is useful to remind that this simple modification can be done only because two slightly different materials has been selected for the parts of the assembly.

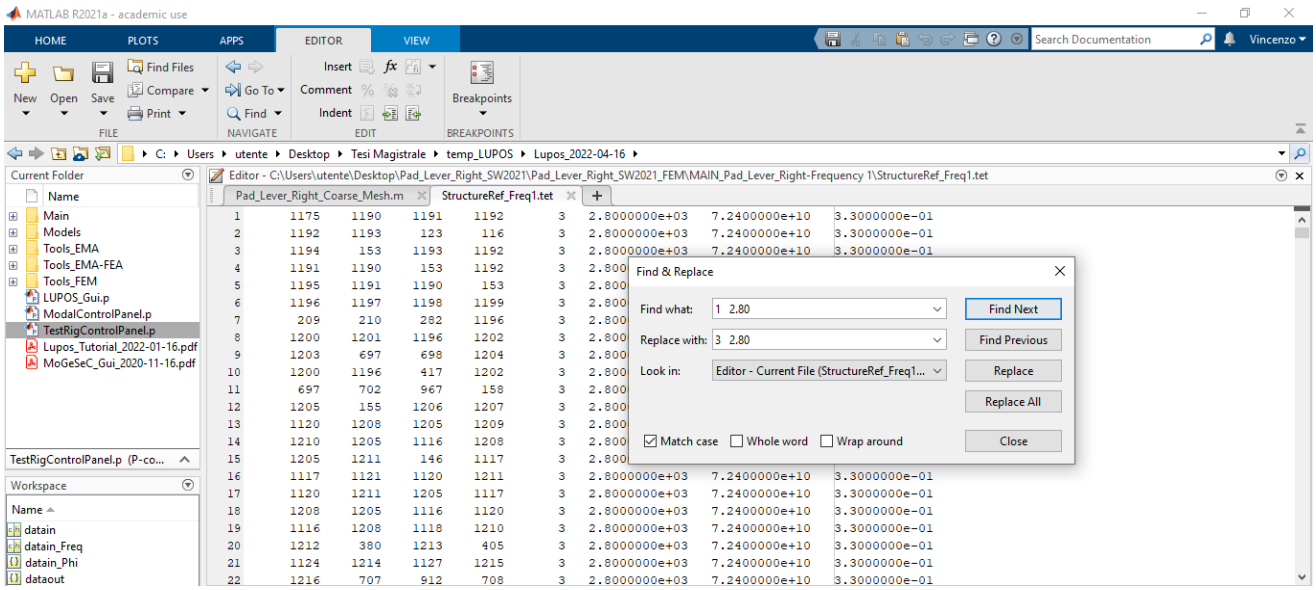

Figure 1.6.1.1 – Procedure of colour changing in MATLAB.

After loading the `.geo` file in TRCP ([3]), the model appears as shown in Figures 1.6.1.2-4. Each of these figures represents a model, according to Table 1.2.1.

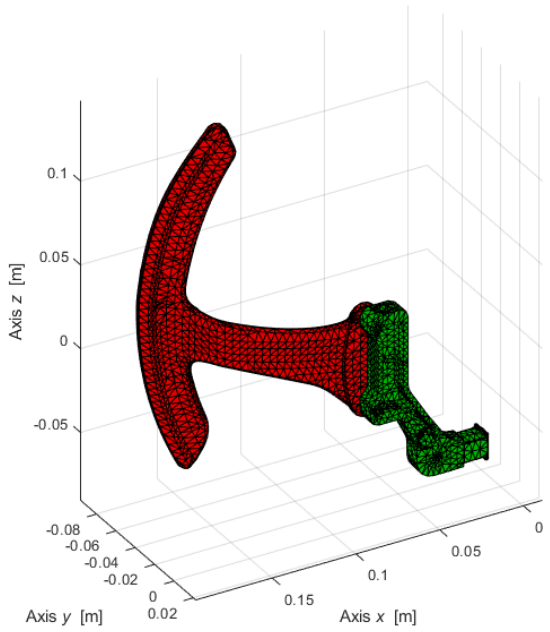

Figure 1.6.1.2 – First model with Tet.

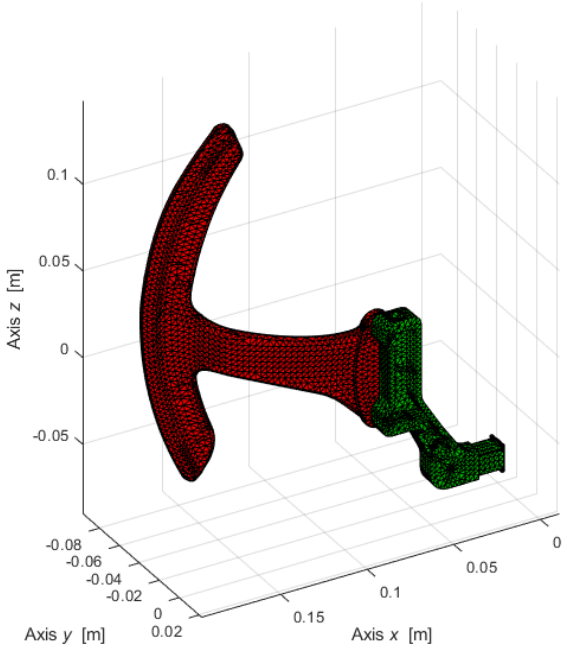

Figure 1.6.1.3 – Second model with Tet.

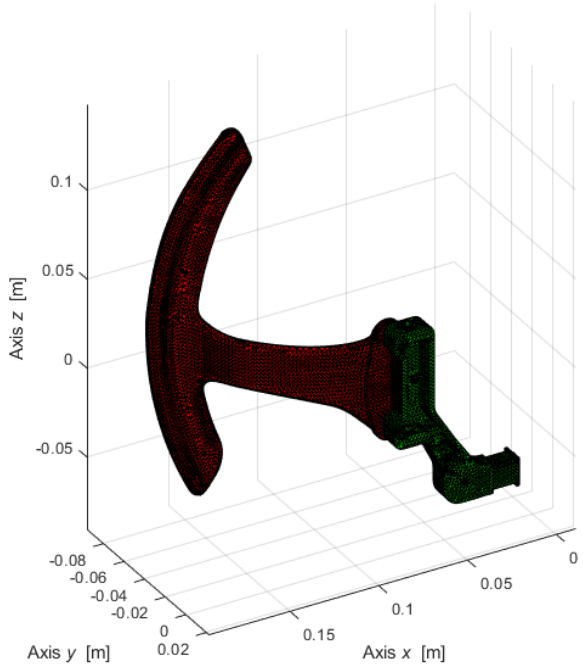

Figure 1.6.1.4 – Third model with Tet.

1.6.2 Visualisation of a mode shape

It is worth showing an animation in Lupos of the mode shape exported from SolidWorks. In order to do this, `.geo` and `*Phi.dat` files should be loaded in the appropriate cell in MCP. Figure 1.6.2.1 contains the mode shape for the first non-rigid body mode (i.e. the 2nd one) for the first simulation of the assembly.

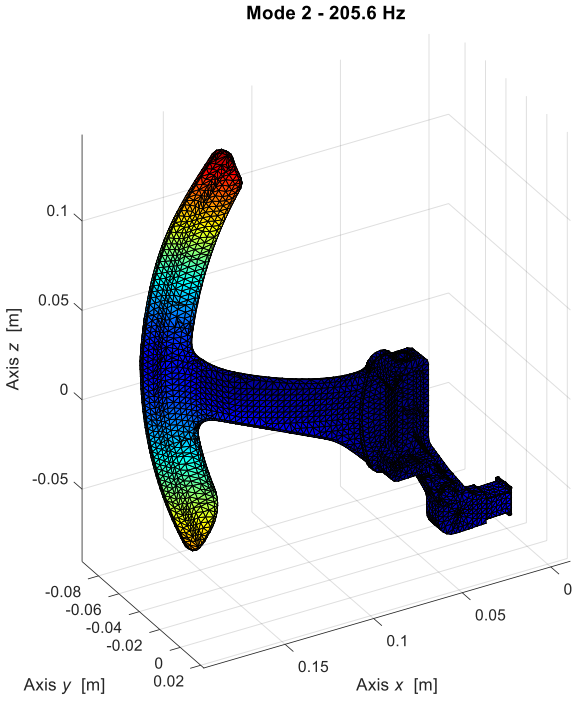

Figure 1.6.2.1 – 2nd mode shape.

1.7 Minecraft: from tetrahedrons to hexahedrons

This part of the report is devoted to the use of a Minecraft model, which is obtained by transforming the tetra4 mesh produced by SolidWorks into hexahedrons. In this particular case, the past elementary cubes are substituted with prisms, in the sense that the discretisation along the cartesian axis is different. The main advantage of this kind of model is certainly a lower number of the nodes and, consequently, a minor computational effort. In addition, the new mesh just needs the indication of the distances between the nodes in the three directions, and therefore the spatial dimensions of the elements.
The process of transformation is carried out, for each SolidWorks discretisation, in `Pad_Lever_Right_Prismatic_MINECRAFT.m` script, which is not fully reported here.
The structure of this main script is:

1. Define the desired dimensions of the hexahedrons, create an equispaced geometrical grid based on the real dimensions of the assembly and use this partitioning as the nodes of the prismatic elements.
2. Delete the non-existing nodes on the base of a nearness criterion with respect to the tetrahedral mesh.
3. Cancel the excessive prisms.
4. Attribute the proper material to the Minecraft discretisation.
5. Check of the mass and save the model.

In the following paragraphs some of these parts will be deepened and compared to the previous dedicated MATLAB routines.

1.7.1 Equispaced grid

In the initial approach of this Minecraft approximation, this part exploited a routine reported in [4], that created cubical elements utilising a grid that considered the sizes of the SW meshed assembly, i.e. the tetra4 mesh. Afterwards two main improvements have been made:

- The coordinates of the nodes of the parallelepipedal elements become multiples of the desired dimensions of the prisms, which are contained into a 1x3 vector, called `dist`.
- If the measured coordinates in a spatial dimension have discordant sign, there will surely be a node that has 0 as coordinate in that axis.

This portioning is performed in first lines of `PrismaticDiscretisation.m`, and is displayed in the next lines:

```
%% Partinioning of the prism containing parts
    %Definition of max size of a meshed box with hexahedrons and creating a
    %grid of equispaced nodes along x,y,z. The distance between the nodes in
    %one direction can be different from another direction
    disp('determining min/max geometrical dimensions...')
    %Dim [2x3] with min and max of x, y, z
    Dim = [min(Geo_ini(:,2:4)); max(Geo_ini(:,2:4))];
    num_cubes = round(diff(Dim)./dist)+2;
    x_mean = round(mean(Dim)./dist).*dist;
    x_min = zeros(1,size(num_cubes,2));
    x_max = zeros(1,size(num_cubes,2));
x = cell(1,size(num_cubes,2));
    for count = 1 : size(num_cubes,2)
        if rem(num_cubes(1,count),2)==1
```

```
            num_cubes(1,count) = num_cubes(1,count)+1;
        end
        x_min(1,count) = x_mean(1,count)-dist(1,count)*num_cubes(1,count)/2;
        x_max(1,count) = x_mean(1,count)+dist(1,count)*num_cubes(1,count)/2;
        x{1,count} = [x_min(1,count):dist(1,count):x_max(1,count)];
    end
    clear count
```

It is also worth, at this stage deleting possible in excess nodes in order to save time in part b). The strategy chosen is a loop where, for every axis, it is controlled if there the grid is unnecessary wide. It is not clever carrying out that in the previous part of the code since the randomness of the rounding shown before and the brevity of the adopted control.

```
%Deleting possible in excess nodes in order to reduce computation time in
Fea_simpler
    for count = 1 : size(num_cubes,2)
        if x{1,count}(1,1)+dist(1,count)<Dim(1,count)
            x{1,count} = x{1,count}(1,2:end);
            num_cubes(1,count) = num_cubes(1,count)-1;
        end
        if x{1,count}(1,end)-dist(1,count)>Dim(2,count)
            x{1,count} = x{1,count}(1,1:end-1);
            num_cubes(1,count) = num_cubes(1,count)-1;
        end
    end
    clear count x_min x_max x_mean Dim
    disp('... done!')
```

A further step is creating a `.geo` file where the nodes of the prisms are located. Before this application this was made by a loop. Now, instead, it is performed exploiting the just created grid and MATLAB logical indexing, and thus reducing computational time.

```
    disp(' ')
    disp('Grid creation...')
    num_nodes = num_cubes+1;    %nodes along the three dimensions [-]
    tot_nodes = num_nodes(1,1)*num_nodes(1,2)*num_nodes(1,3);

    %Knowing the size of the big box and the coordinates of the nodes it is now
    %much easier to create Model.Geo
    Model.Geo = zeros(tot_nodes,4);
    Model.Geo(:,1) = [1:1:tot_nodes].';
    Model.Geo(:,2) = repmat(x{1,1},1,num_nodes(1,2)*num_nodes(1,3));
    A = repmat(x{1,2},num_nodes(1,1),num_nodes(1,3));
    Model.Geo(:,3) = reshape(A,tot_nodes,1);
    B = repmat(x{1,3},num_nodes(1,1)*num_nodes(1,2),1);
    Model.Geo(:,4) = reshape(B,tot_nodes,1);
    clear tot_nodes x A B
```

In the last part of the script the prismatic elements are built. Unfortunately, this section could not be shortened. Moreover, it is decided arbitrary to firstly assign a generic Alluminium Alloy to the prisms. The right material will be applied in a separate function described in § 1.7.3.

```
    Model.Hex = [];
    h = waitbar(0,'Wait... ','Name','Hex');
    for count_z = 1 : num_cubes(1,3)
        for count_y = 1 : num_cubes(1,2)
            for count_x = 1 : num_cubes(1,1)
```

```
                waitbar((count_x+(num_cubes(1,1))*(count_y-
1)+(num_cubes(1,1))*(num_cubes(1,2))*(count_z-
1))/((num_cubes(1,1))*(num_cubes(1,2))*(num_cubes(1,3))),h,...
                    ['Wait: Hex ',num2str(count_x+(num_cubes(1,1))*(count_y-
1)+(num_cubes(1,1))*(num_cubes(1,2))*(count_z-1)),...
                    ' of
',num2str((num_cubes(1,1))*(num_cubes(1,2))*(num_cubes(1,3)))])
                Model.Hex = [ Model.Hex
                    count_x+num_nodes(1,1)*(count_y-
1)+num_nodes(1,1)*num_nodes(1,2)*(count_z-1) ...
                    count_x+num_nodes(1,1)*(count_y-
1)+num_nodes(1,1)*num_nodes(1,2)*(count_z-1)+1 ...

count_x+num_nodes(1,1)*count_y+num_nodes(1,1)*num_nodes(1,2)*(count_z-1)+1 ...

count_x+num_nodes(1,1)*count_y+num_nodes(1,1)*num_nodes(1,2)*(count_z-1) ...
                    count_x+num_nodes(1,1)*(count_y-
1)+num_nodes(1,1)*num_nodes(1,2)*count_z ...
                    count_x+num_nodes(1,1)*(count_y-
1)+num_nodes(1,1)*num_nodes(1,2)*count_z+1 ...

count_x+num_nodes(1,1)*count_y+num_nodes(1,1)*num_nodes(1,2)*count_z+1 ...

count_x+num_nodes(1,1)*count_y+num_nodes(1,1)*num_nodes(1,2)*count_z ...
                    5  2.8000000e+03  7.2400000e+10  0.33
                    ];
            end
        end
    end
    close(h);
    clear count_x count_y count_z tot_nodes num_cubes num_nodes h
    disp('... done!')
```

To be clearer, a demonstrating imagine is shown in Figure 1.7.1.1. The y coordinate of the highlighted node is caused by the MATLAB machine epsilon and should be 0, as the x coordinate.

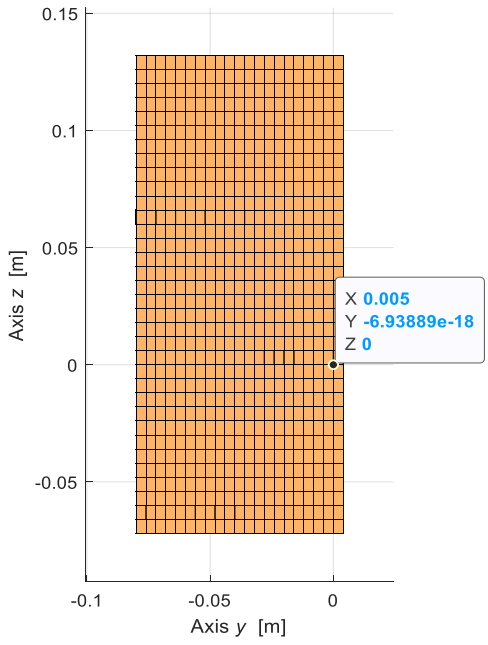

Figure 1.7.1.1 – yz view and node with 0 coordinates.

1.7.2 Simplification of the mesh

This paragraph deals with the elimination of the prisms nodes that are not near enough to the ones of the meshed assembly coming from SW. Indeed, the remaining ones are about 10% of the total nodes generated in § 1.7.1, that will be also called as "*Ema nodes*" The tet4, instead, are connected by the "*Fea nodes*".
This process is made into `FeaSimpler_Prismatic`, which needs four inputs:

1. `EmaGeo;`
2. `FeaGeo;`
3. `dist`: a modified version of the 1x3 vector discussed in § 1.7.1;
4. `wbar`: a logical input that specifies if a graphical visualisation of the process is requested.

The output is `EmaFea`: a `.geo` file that includes the coordinates of the survived nodes of the parallelepipedal elements.
As regards the condition that the surviving nodes have to satisfy, it is mandatory that at least one *Fea node* is located into a specific control volume. In particular, an ellipsoid centred in each *Ema node* and with semiaxis `dist(1,1)`, `dist(1,2)` and `dist(1,3)`, that are the desired sizes of the Minecraft elements, as examined before. Moreover, `dist` is multiplied by a coefficient, which will be called as "correction factor", "premultiplication factor" or "multiplication factor" in this chapter.
However there is an exception for this association criterion: if more than one node of the Hex mesh is going to survive thanks to the same *Fea nod*e, only the nearest *Ema node* keeps on living.
Figure 1.7.2.1 shows the working mechanism with a cubical mesh and `1*dist` for sake of simplicity.

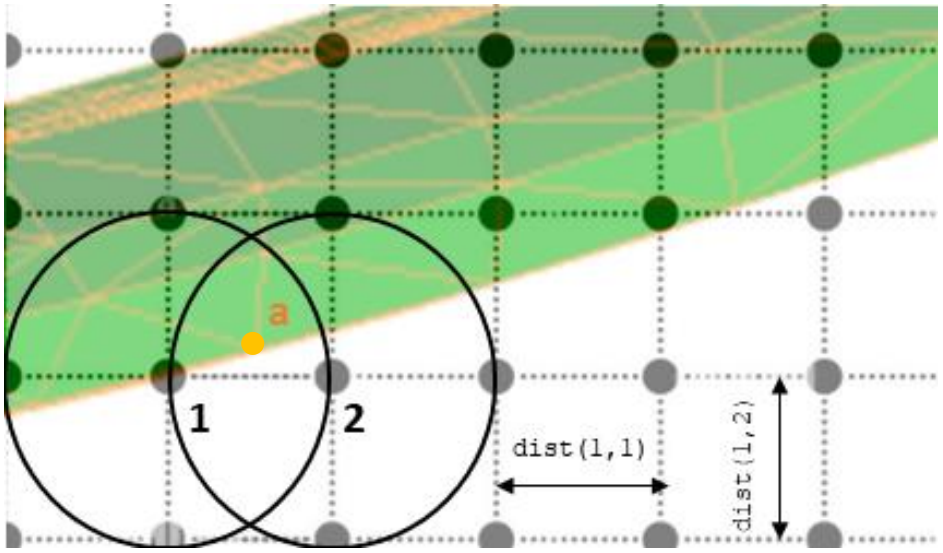

Figure 1.7.2.1 – Working mechanism of `FeaSimpler_Prismatic`.

As can be seen, in the background there is the SW mesh, whose elements have orange edges. The nodes of the Hex discretisation are symbolised with black dots. Moreover, a representation of the distance between the *Ema nodes* is presented using the parameters `dist(1,1)` and `dist(1,2)`. In the picture is explained the simplification applied to nodes 1 and 2, that would survive both because of the presence of node a, which is the closest *Fea nod*e contained in their control volume. But only node 2 is saved since it is the nearest to node a.

It is also crucial to acknowledge what happens if `dist` is multiplied by 0.5: in consequence of Figure 1.7.2.1, it can be easily understood that in this case a correspondance with two equal nodes is not anymore possible. That is because the control volumes of two adiacent Hex nodes just have a point in common and so the overlapping phenomena is not present. As Figure 1.7.2.2 (left) shows, the surviving prisms are very few also owing to a decrease dimensions of the control volumes. Therefore choosing a premultiplication factor minor than 1 is not a right strategy to have a correct parallelepipedal discretisation.

The more the factor grows, the more Hexs are saved because the control volumes become larger. Furthermore the number of the left nodes and prisms increase less than proportional with respect to the correction factor due to the elimination criterion related to the overlapping. This trend has a plateau after the premultiplication factor overcomes 2. Even if the remaining nodes after `FeaSimpler_Prismatic` keeps on increasing, the function `CheckModel`, which runs immediately after it, cannot save further prisms .
The explanation of this trend is related to the fact that a new survived *Ema node* is kept by `FeaSimpler_Prismatic` because a *Fea node* is contained in a prism that is not touching the Minecraft node at all.

In Figures 1.7.2.3-4 the effect of varying the multiplication factor is shown.

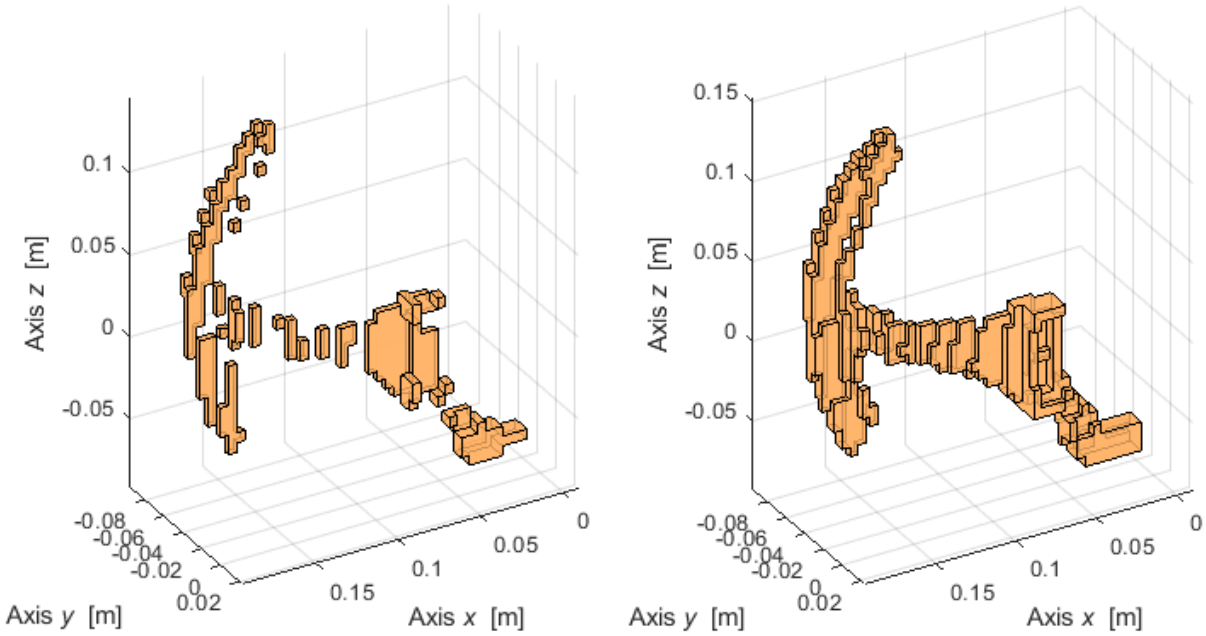

Figure 1.7.2.2 – Application of `FeaSimpler_Prismatic` to 2nd mesh with `0.5*dist` (left) and `0.8*dist` (right).

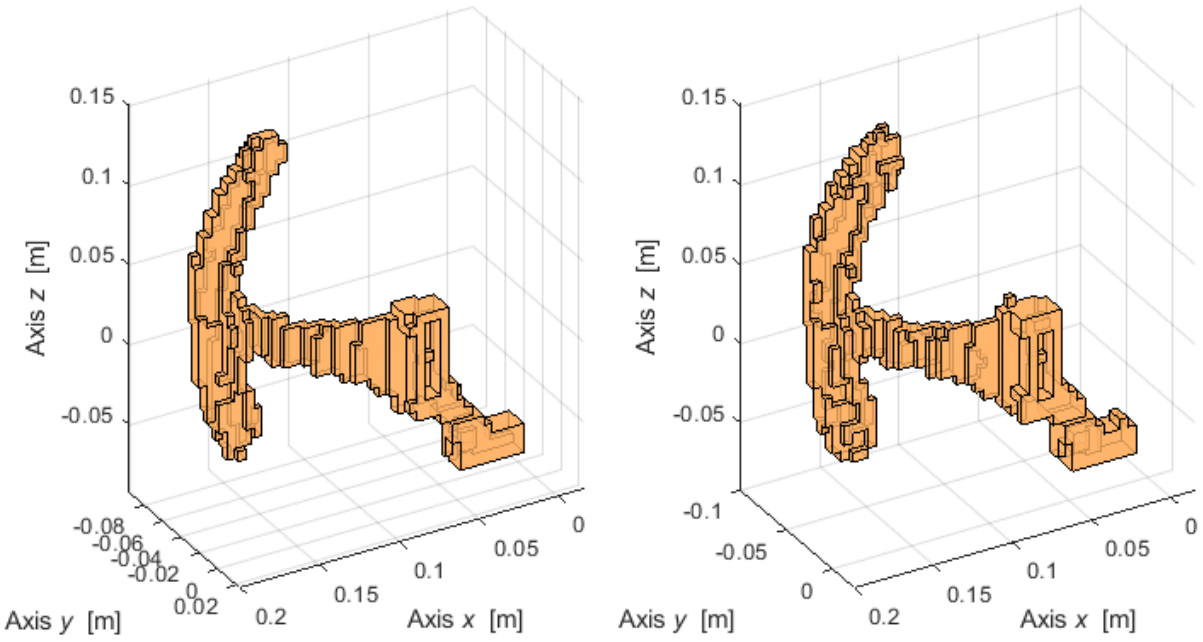

Figure 1.7.2.3 – Application of `FeaSimpler_Prismatic` to 2nd mesh with `1*dist` (left) and `1.5*dist` (right).

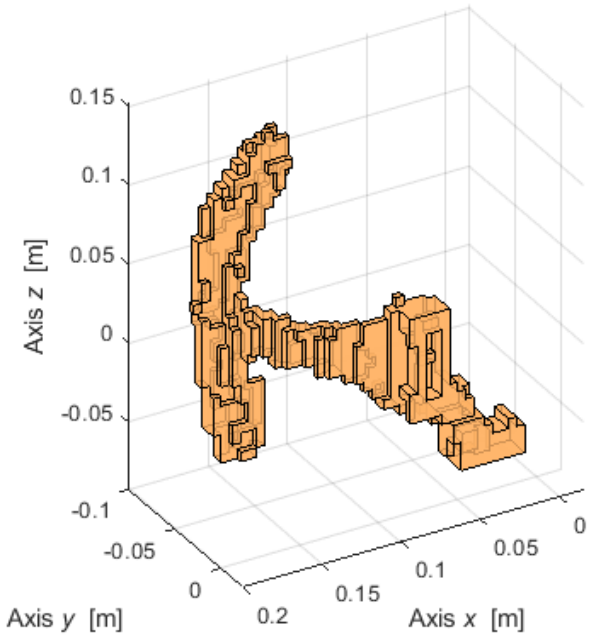

Figure 1.7.2.4 – Application of `FeaSimpler_Prismatic` to 2nd mesh with `1.9*dist`.

Figure 1.7.2.2 shows that the holes in the Minecraft model with `0.8*dist` are very lower with respect to the `0.5*dist` on foot of the bigger control volumes. Also the structure has a certain grade of regularity.

As can be seen in Figure 1.7.2.3, the left discretisation appears to be more uniform, while the right one and the one in Figure 1.7.2.4 have too many cubes and therefore an overestimation of the volume and the mass happens.

Eventually, Table 1.7.2.1. and Figure 1.7.2.5 show the trend of the survived nodes and prisms of the 2nd mesh in relation to the correction factor of `dist`.

Table 1.7.2.1 – Seven configurations of the mesh parameters, nodes and prisms.

Correction factor	# Survived nodes	# Survived prisms
0.5	998	250
0.8	1417	567
1	1653	709
1.5	2082	861
1.9	2290	901
3	2598	918
5	2716	918

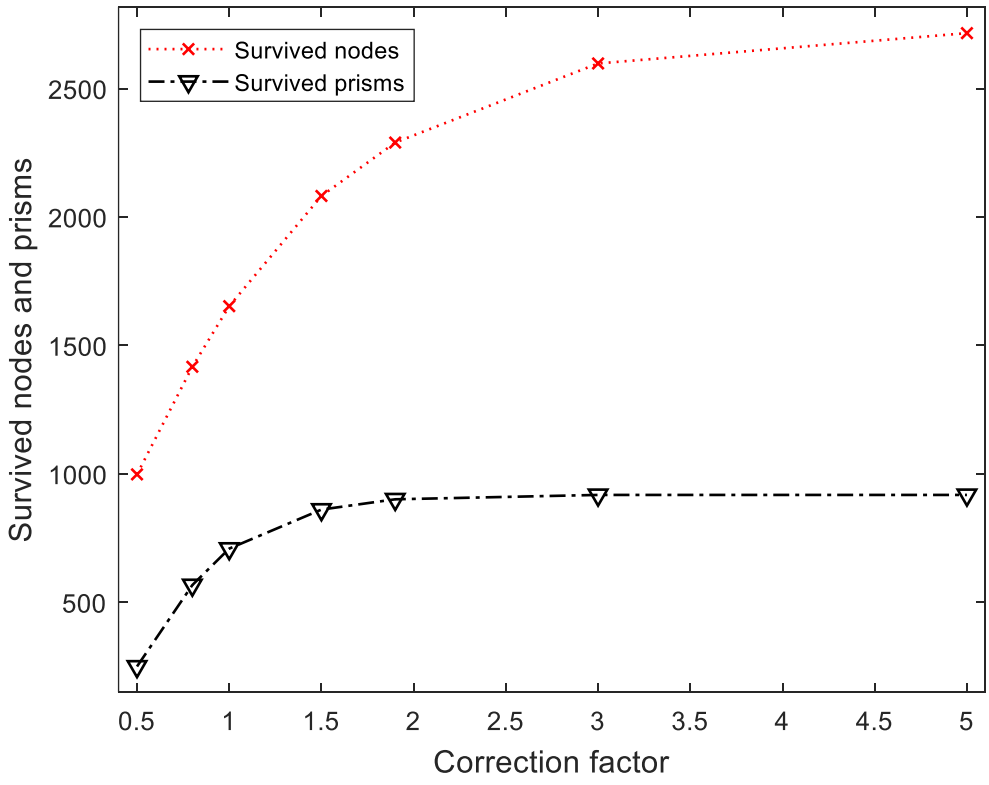

Figure 1.7.2.5 – Seven configurations of the mesh parameters, nodes and prisms.

1.7.3 Material assignment

After utilising `FeaSimpler_Prismatic` and `CheckModel` it is time to finally associate the proper material to the remaining prisms. The dedicated MATLAB function where this is done is `Hex_Mat_assign`. It has 5 inputs:

- `Hex_Geo`: contains the coordinates of the nodes of the survived prisms;
- `Hex_Hex`: contains the nodes that made up each prism. It will be modified and will become the only output of the function;
- `Tet_Geo`: contains the coordinates of the nodes of the initial tetra4;
- `Tet_Tet`: contains the nodes that made up each initial tetra4, as well as their properties;
- `Mats`: a structure that has the information about the material used in the assembly.

Basically, this routine is structured as follows:

1. Use of a modified Lupos routine called `CheckMass_TetHex_2`. The new part with respect to `CheckMass_TetHex` consists of the return of two new outputs, i.e. a matrix with 5 columns, containing respectively the volume, mass and centre of gravity for the Tets and another one for the Hexs.
2. A loop for each hexahedron, where its borders are found. Afterwards another inner loop is used to check, for every tetrahedron a COG condition and a node condition. The former checks if the barycentre of a Tet is contained in the Hex border, while the latter only actives if the first is not satisfied and verifies if a node of a Tet4 is located inside a prism. This section has the attention to not consider the mass of a surrounding Tet plural times if a tetrahedron has more than one node in a Hex.
3. The effective assigning of the appropriate material based on the mass of the neighbouring tetrahedrons. In particular, it attributes the right properties on the base of the majority of the material of the Tet related to a Hex by the criterions discussed in (2).
4. If `dist` is multiplied by 1.9 in `FeaSimpler_Prismatic` there will be some hexahedrons that will not find a single Tet node in it, so they will have not the proper material.

In order to solve this issue there are 3 strategies:

I. Use `FeaSimpler_Prismatic` without any factor applied to `dist`. The main drawback of this solution is that the number of the Hex making up the Minecraft model decreases about 10-20%. Nevertheless, this option makes to resulting structure to be more regular.

II. If a hexahedron is uncoupled at the end of the main loop, the properties of the last Hex analysed are assigned to it, knowing that some prisms could have the wrong properties and it is necessary to manually correct afterwards.

III. Correct them in another loop on the base of the properties of the neighbouring prisms, minding considering only the elements whose material has been correctly assigned. The schematic drawing in Figure 1.7.3.1 [5] can help to understand this strategy.

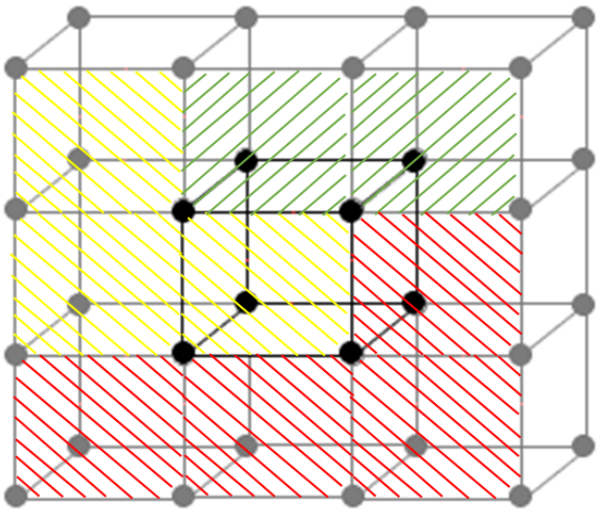

Figure 1.7.3.1 – 3rd solution – before.

As can be seen, Hex mesh has been represented with cubes instead of parallelepiped for sake of simplicity. It is shown the process of attribution of the element with darker edges on the base of its neighbouring cubes, which are:

- four red coloured;
- two green coloured;
- two orange coloured.

Since the 8 eight surrounding Hex include 2 uncoupled elements, the attribution of the property of the central one is only established on the remaining 6 prisms, therefore the material assigned to the Hex at issue is the red one, as shown in Figure 1.7.3.2. It is also worth to highlight that, if the number of valid neighbours had been 4 red and 4 green, it would have applied the green one, since has the minor density between the two.

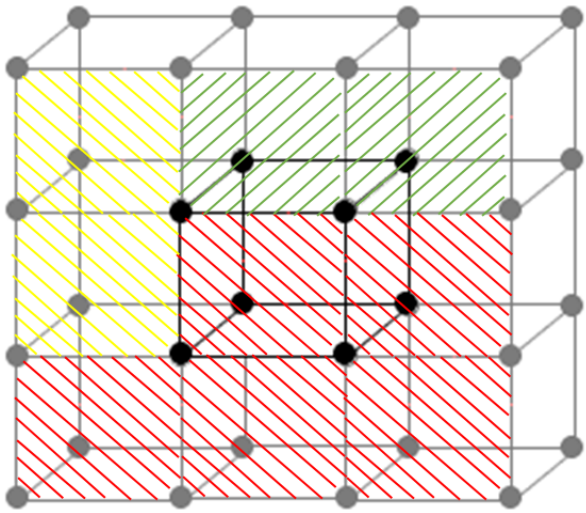

Figure 1.7.3.2 – 3rd solution – after.

The following pictures better explain part (4). All the imagines are made with `dist = [0.005 0.004 0.006] %[m]`. This choice of the dimensions of the cubes is the child of the overall sizes of the assembly. Indeed, it is clever, with this particular geometry, to decide for y-mesh density bigger than the x and z ones since the components have their minor dimensions along the y axis. Figures 1.7.3.3-5 concern the first solution for the three mesh of SW. Figures from 1.7.3.6-8, are related to the second strategy and `dist` multiplied by 1.9. Figures from 1.7.3.9-11 concern the comparison between the results with none of the solution applied and the ones with the third option and `dist` multiplied by 1.9. In addition to that it is useful to use the colour orange for the unassigned Hexs because the default colour for the Minecraft elements has always been this one.
It is evident, in the pictures concerning the 3rd solution, that the algorithm works well even in the regions where two materials are touching each other.

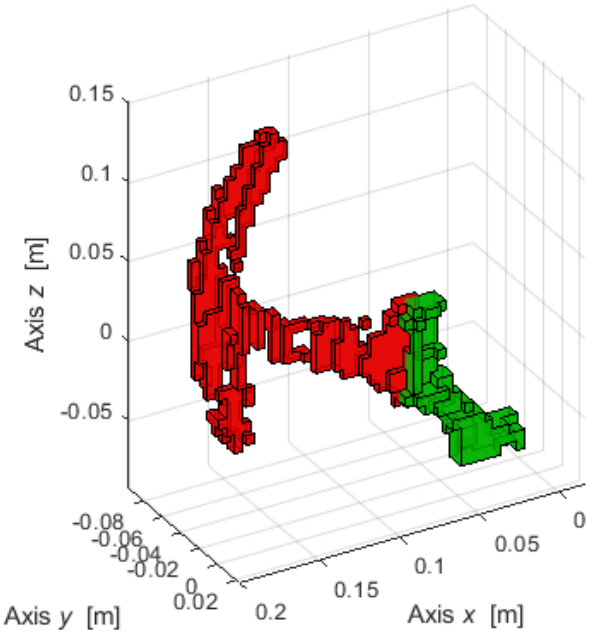

Figure 1.7.3.3 – 1st solution for 1st mesh.

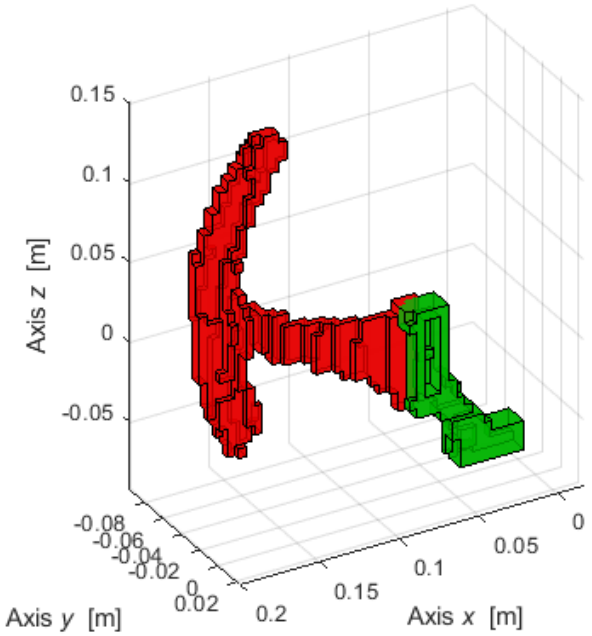

Figure 1.7.3.4 – 1st solution for 2nd mesh.

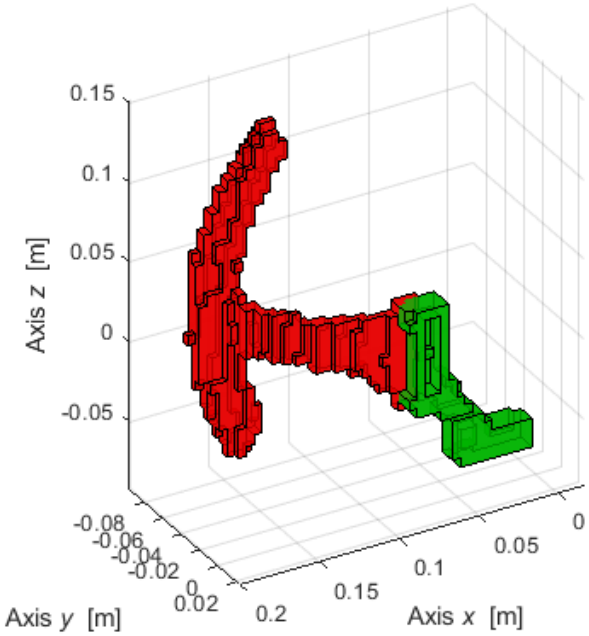

Figure 1.7.3.5 – 1st solution for 3rd mesh

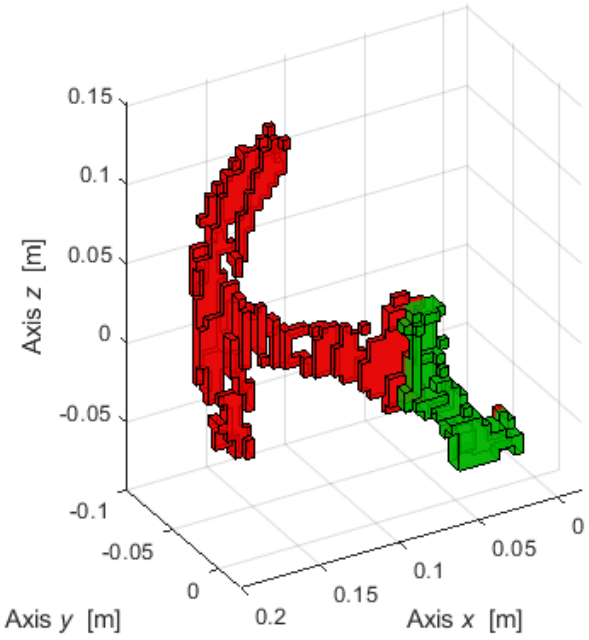

Figure 1.7.3.6 – 2nd solution for 1st mesh.

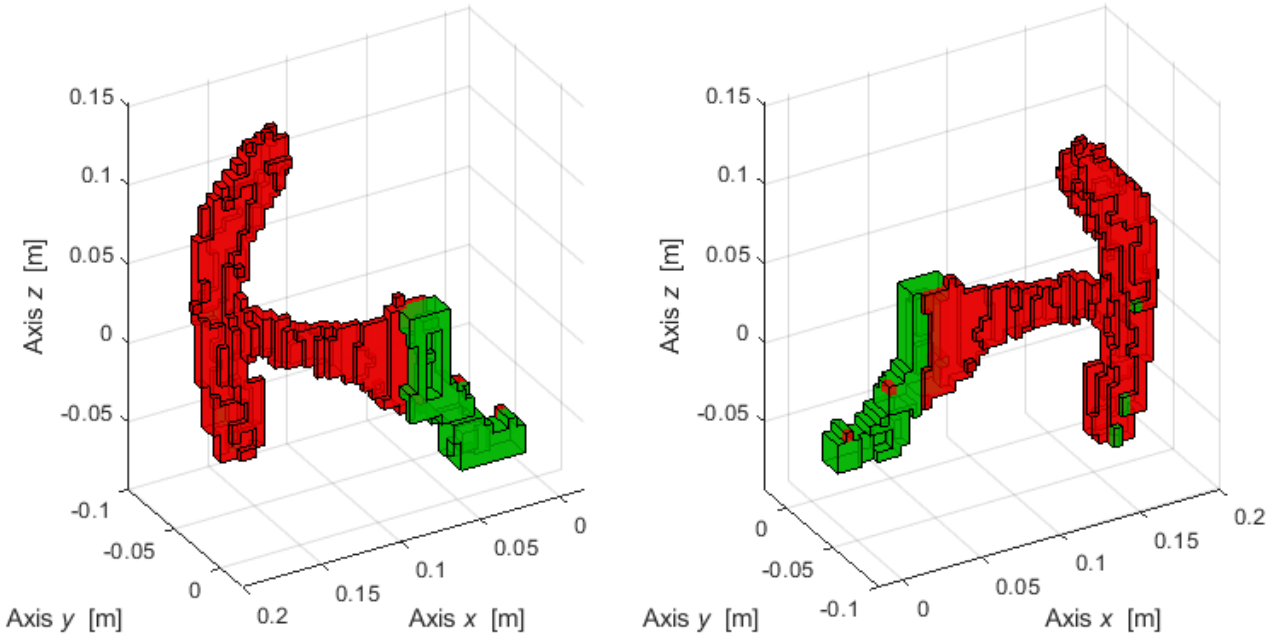

Figure 1.7.3.7 – 2nd solution for 2nd mesh front (left) and back (right).

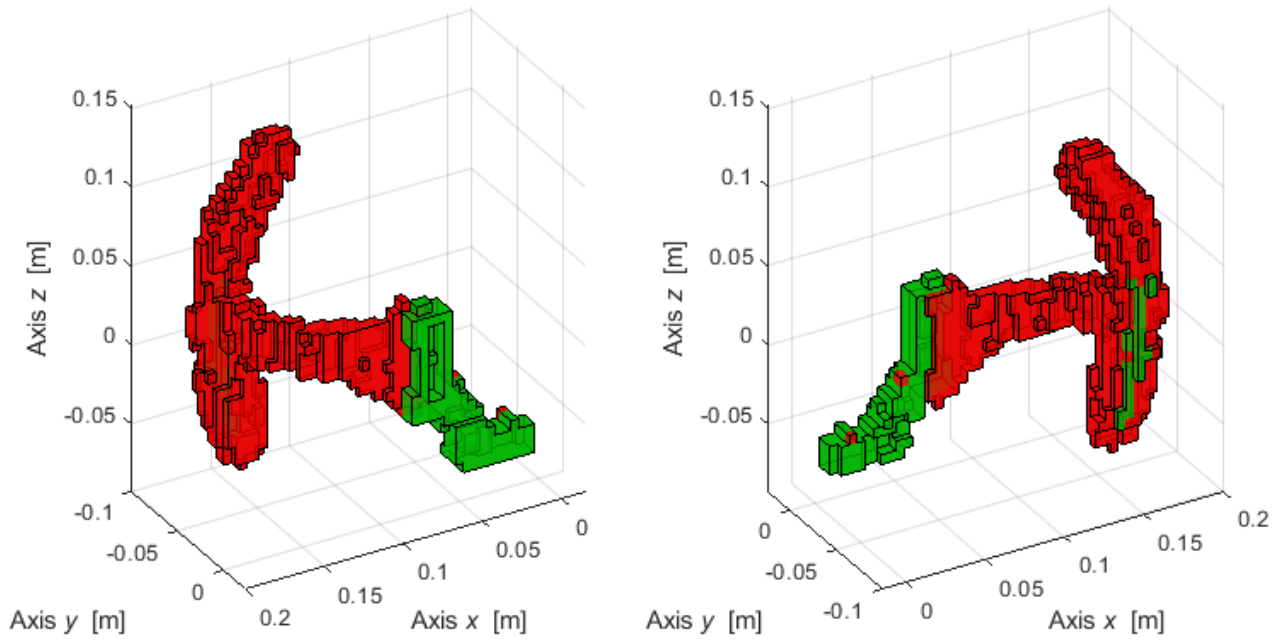

Figure 1.7.3.8 – 2nd solution for 3rd mesh front (left) and back (right).

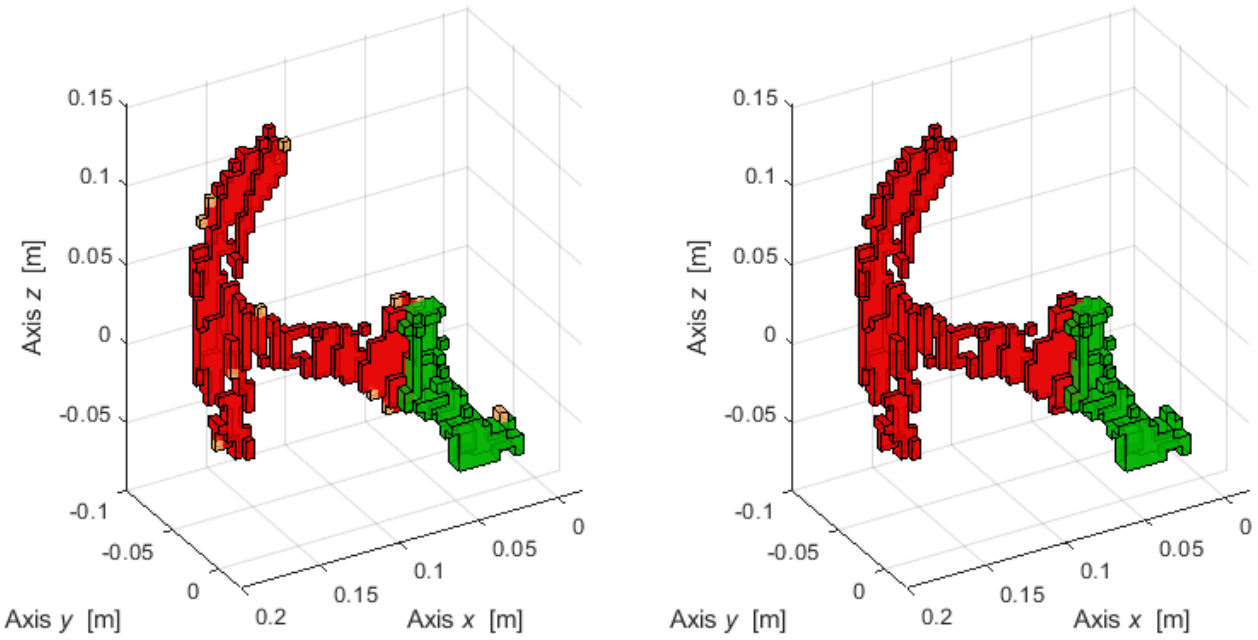

Figure 1.7.3.9 – Uncoupled Hexs for 1st mesh (left) and 3rd solution (right).

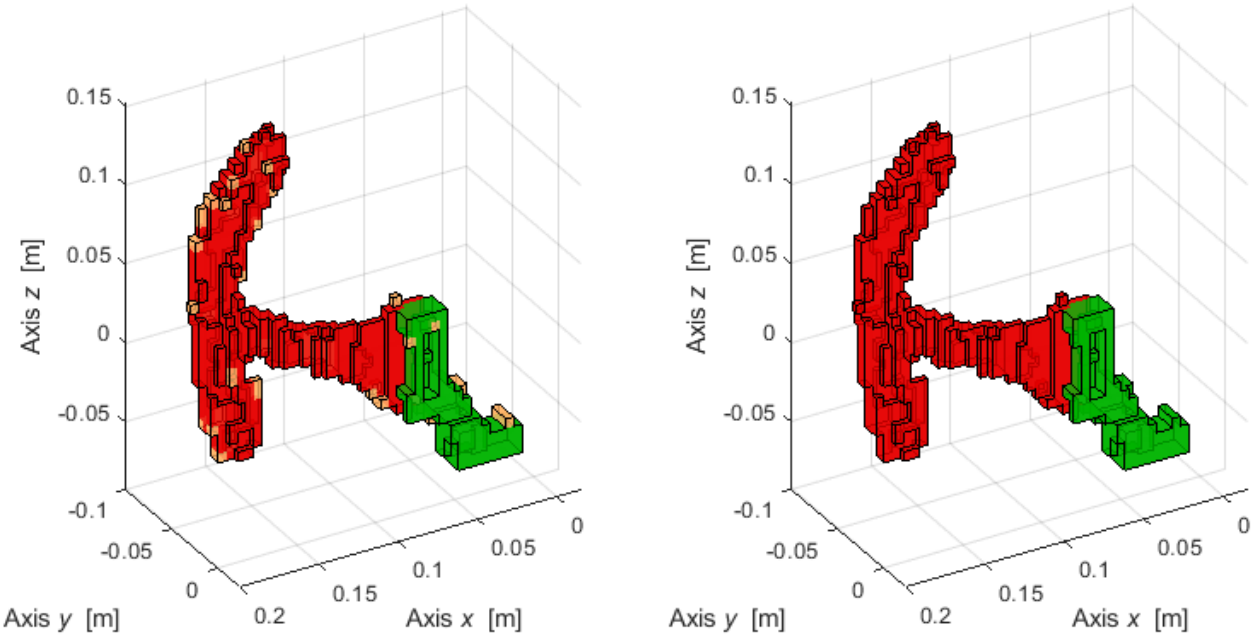

Figure 1.7.3.10 – Uncoupled Hexs for 2nd mesh (left) and 3rd solution (right).

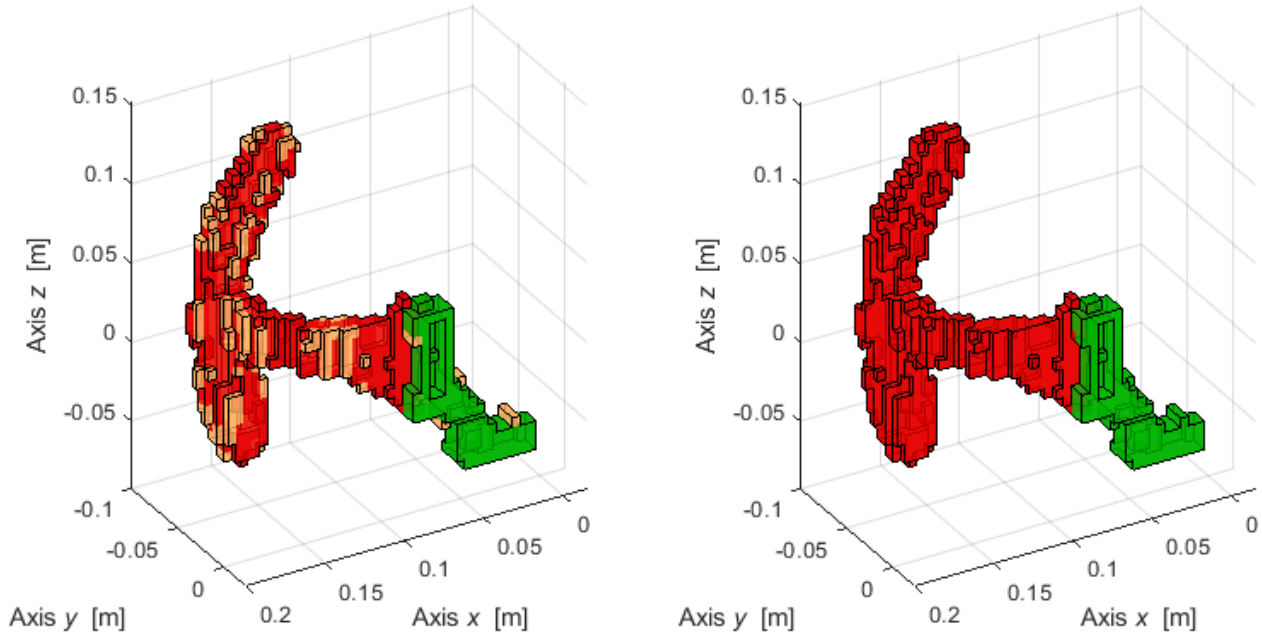

Figure 1.7.3.11 – Uncoupled Hexs for 3rd mesh (left) and 3rd solution (right).

It is also possible to use another function to assign the material to the prisms. This function has been developed by Professor Bonisoli and is called "`Converter_TetHex.m`". It evaluates for each Hex element its COG, then if at least one Tet and/or one Hex contain it, the Tet or the Hex

corresponding colour and material properties are assumed. The first found element that contains the Hex COG is assumed. If no element is found, nor colour, neither material properties are set.
There are three strategies to carry out the attribution:

1. check for each COG, if it is inside the same Tet;
2. check for all the COGs contemporaneously, they are inside the same Tet;
3. find for each COG the closest 10 nodes of Tets, for all the Tets using these nodes, if the COG is inside these Tets, from the closest node to each COG;

While the first two approaches are far more time-consuming than `Hex_Mat_assign`, the third one is similar to it.
Figures 1.7.3.12-13 show the comparison between the first solution of `Hex_Mat_assign` and the results of `Converter_TetHex.m`. Both the imagines are obtained with the second mesh simplified with `1*dist`.

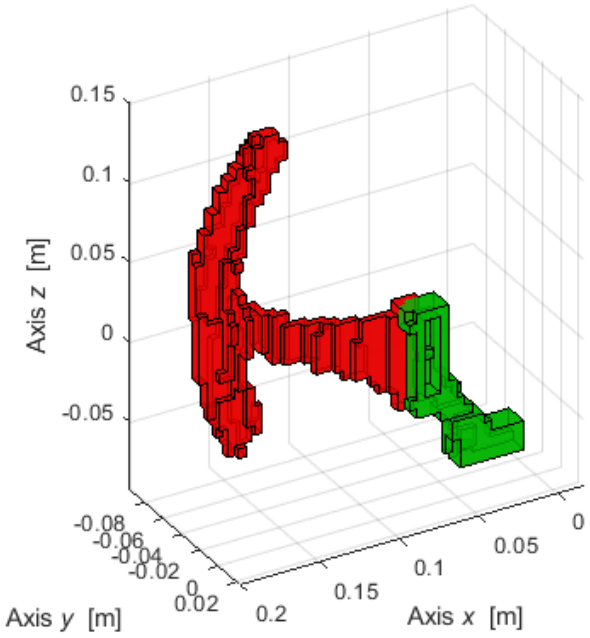

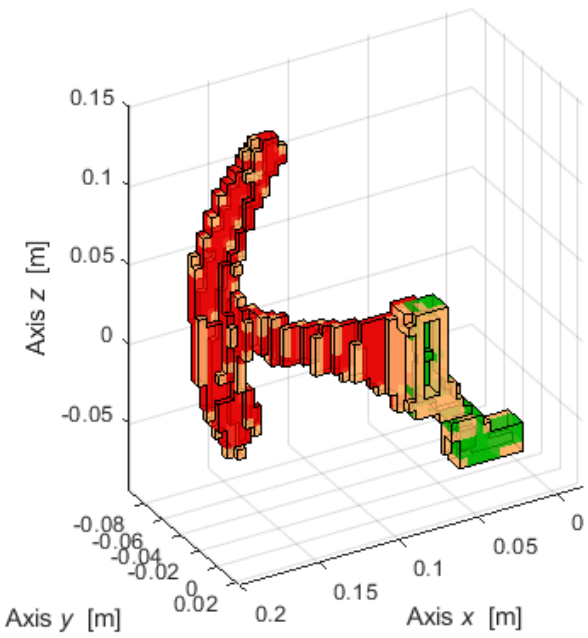

Figure 1.7.3.12 – `Hex_Mat_assign` to 2nd mesh. Figure 1.7.3.13 – `Converter_TetHex` to 2nd mesh.

It is evident that the second routine leaves many uncoupled hexahedrons because the condition to attribute the material is probably too strict. In addition to that, the complexity and tridimensionality of the assembly make a criterion like in Figure 1.7.3.12 to be more effective.
Even by changing the tolerance in `FeaSimpler_Prismatic` the results of the 2nd routine do not change, as shown in Figure 7.3.14. Moreover, the process of material attribution of Figure 1.7.3.12 lasted 13 seconds, as the one of Figure 1.7.3.13 for 16 seconds.

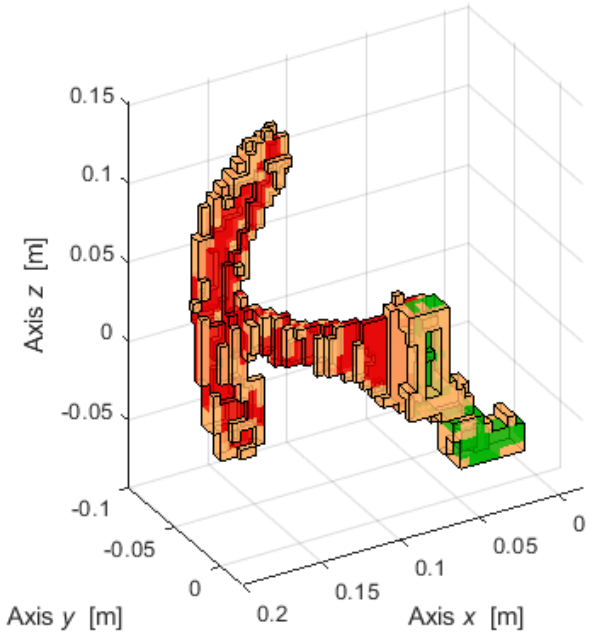

Figure 1.7.3.14 – `Converter_TetHex` to 2nd mesh with `1.9*dist`.

Eventually are presented some results obtained by setting `dist = [0.004 0.003 0.0035]; %[m]` and no premultiplication factor in `FeaSimpler_Prismatic` in the use of the third mesh, which is the finest.

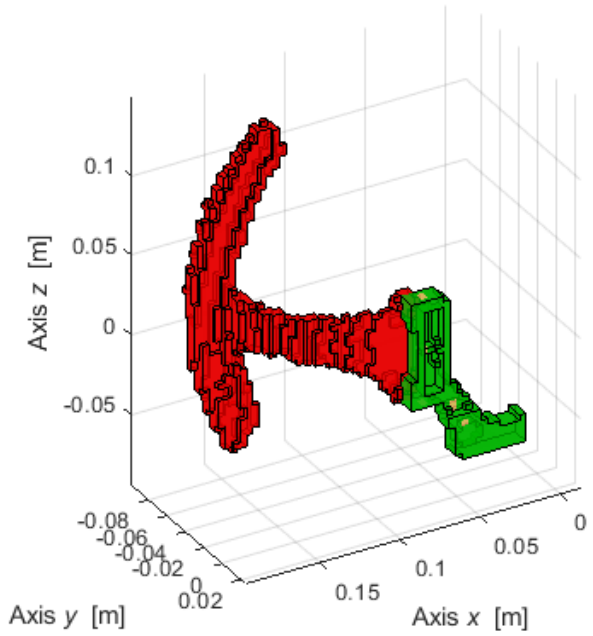

Figure 1.7.3.15 – 1st solution for 3rd mesh with `dist = [0.004 0.003 0.0035]`.

As expected, the increased number of prisms make the discretisation more complete, even if very few elements are not coupled to the right material.

The results become more precise if the 3rd solution is adopted.

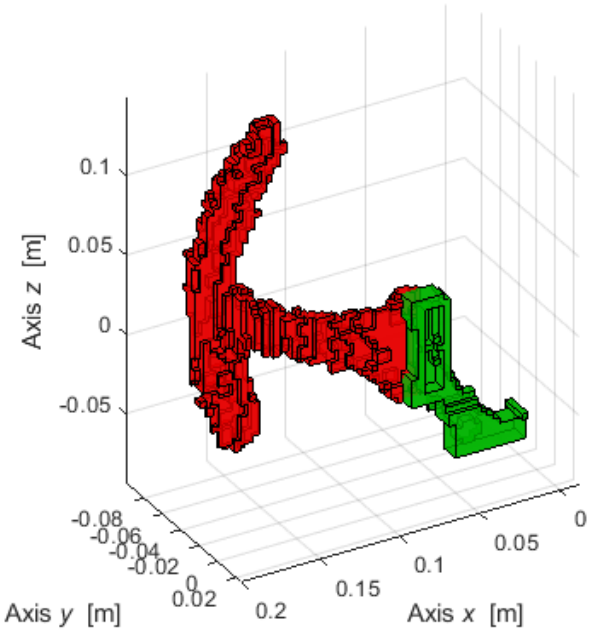

Figure 1.7.3.16 – 3rd solution for 3rd mesh with `dist = [0.004 0.003 0.0035]`.

It is also worth noting that a more cubical-shape elements seem to behave better in respect of the material attribution and the overall number of survived Hexs.

1.7.4 Mass check

The last part of this report is dedicated to confronting the mass of the Hex elements to the one of the undiscretised assembly of SW.
To carry out this operation the mass *massSW* of the components is computed directly in SW and it is 153.82 g, while the prisms mass is calculated by using `CheckMass_TetHex_2`.
The comparison of the mass is performed by the calculation of the percentual relative error *err* of the Hex mass with respect to the assembly weight. It is calculated with Equation 1.7.4.1.

$$err = \frac{massHex - massSW}{massSW} \cdot 100 \qquad (1.7.4.1)$$

where *massHex* is the measured mass of the Hexahedrons and *massSW* is computed by SolidWorks and is the real mass of the assembly. Therefore a positive error means an overestimation of the parts mass, while a negative one is an underestimation.
The results of the three main SW discretisation with `dist = [0.005 0.004 0.006]` and no correction factor in `Fea_Simpler` are reported in Table 1.7.4.1.

Table 1.7.4.1 – Results of the mass comparison.

Mesh	Percentual relative error
1	12.8 %
2	50.8 %
3	65.5 %

Like one would expect the cuboid mesh is an overestimation of the system mass and the big difference is justified by the fact that the structure is very tridimensional especially in the part of the Pads of the Levit. Indeed the thickness of these parts is 4 mm, and they are inclined to the x and y axis, so it is normal to discretise them with the use of two rows of Hexs instead of one when using `dist = [0.005 0.004 0.006]`.
An xy plane view of the Hex mesh and Tet mesh better explains this concept and is presented in Figure 1.7.4.1.

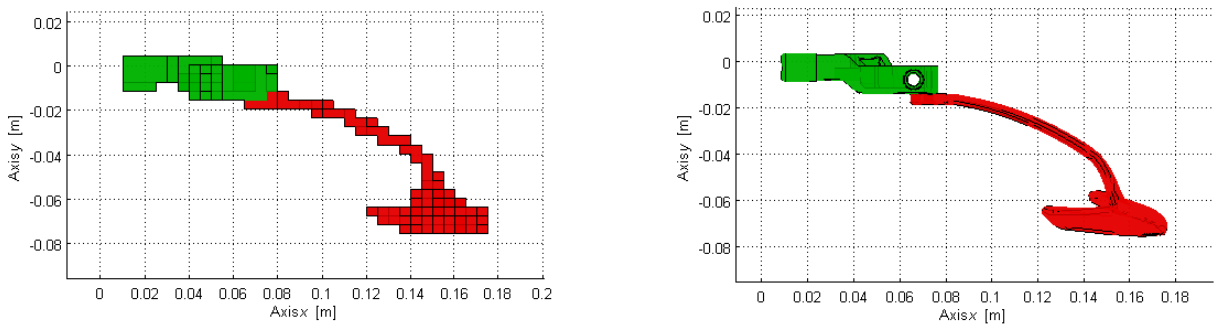

Figure 1.7.4.1 – xy plane view of the Hex (left) and Tet (right) discretisation of the 2nd mesh.

Moreover, it is also normal to have an increasing error as the mesh becomes finer because many more cuboids survive after the use of `Fea_Simpler_Prismatic` owing to the increasing presence of nodes of tetrahedrons in the original SW discretisation. This statement is in agreement with Figures 1.7.3.9-11 (right).
It is worth to analyse deeper the error of the second mesh: as a matter of fact the percentual becomes 17.6 % if the fourth mesh of Table 1.2.1.1 transform into Hex with `dist = [0.0025 0.002 0.003]`, i.e. half of the previous case. That is because the dimensions of the prisms allow to better reproduce the original shape of the assembly, as shown in Figure 1.7.4.2.

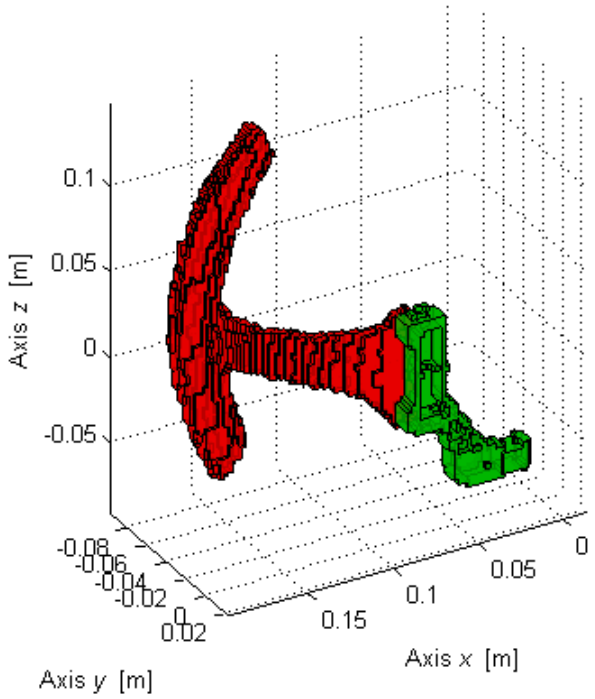

Figure 1.7.4.2 – Great improvement of 4th mesh with `dist = [0.0025 0.002 0.003]`.

1.8 Conclusions

This chapter has been created in order to avoid futile mistakes in the future in the procedure of exporting SolidWorks models into Lupos and re-discretise them. Moreover, two updates of Minecraft in terms of the elements and the materials are shown. The former is related to the fact that is now possible to discretise the structure into prisms and therefore not obligatorily in cubes; the latter concerns the automatic attribution of the material to the hexahedrons on the base of a nearness criterion of the original tetrahedrons.

2. Major distinctions between linear and nonlinear structures

This section has the purpose to highlight the major distinctions between the two models, using also some SDOF systems created in MATLAB/Simulink.
In particular, chapter § 2 deals with the free and forced behaviour of undamped and damped systems and the analyses of their frequency contents. Surely, the main reference of this first approach to nonlinear structures is the 'Duffing type' spring model [6]. The reason of that is the simplicity of the equation of motion and use of its parameters. Moreover, it allows to understand many aspects of nonlinear systems and it is widespread in the Vibration Mechanics.

2.1 Comparison of SDOF linear and nonlinear structures

In Table 2.1.1 are summarised the main differences between the two types of systems. Some of these aspects will be deepened in other paragraphs of this chapter, because they could be better understood with a use of proper models, imagines and contexts.
In the following table ω is excitation frequency, ω_n is the natural frequency of the system, n is a positive integer number, and IC stands for initial conditions, and bold for matrices.

Table 2.1.1 – Comparison of SDOF linear and nonlinear structures.

Linear systems	**Nonlinear systems**
Possibility of the use of superimposition of effects $\mathbf{K}(\alpha \mathbf{x}_1 + \beta \mathbf{x}_2) = \alpha \mathbf{f}_1 + \beta \mathbf{f}_2$ (*)	Incorrectness of the use of superimposition of effects
Maxwell theorem for reciprocity $\alpha_{j,k} = \frac{x_j(\omega)}{f_k(\omega)} = \alpha_{k,j} = \frac{x_k(\omega)}{f_j(\omega)}$ (*)	-
Only primary resonances $\omega = \omega_n$	Also subharmonic $\omega = \frac{1}{n}\omega_n$ and superharmonic resonances $\omega = n\,\omega_n$ (odd and even terms) with n positive integer
Analytical solution basically always possible; modal analysis, natural frequencies, mode shapes (*)	Deep use of numerical solutions, due to the extreme difficulty of carrying out analytical solutions; nonlinear normal modes (equivalent of modal analysis) (*)
Deterministic and sinusoidal behaviour (linear combination of frequencies/modes while using modal coordinates) (*)	Sinusoidal (linearisable),quasi-static, periodic and chaotic behaviour
Only an equilibrium point (stable or unstable), independent from the IC	Presence of multiple equilibrium points (stable or unstable); the effective steady-state solution depends on the IC
Closed elliptic orbits (conservative systems) in state space diagrams	Presence of the drift of the equilibrium point of the oscillation
-	Presence of stiffening and/or softening phenomena (stiffness coefficient), jump effect
-	Presence of progressive and/or regressive phenomena (equivalent of stiffening/softening for damping coefficient)
Participation factors are strictly constant	Internal resonances (energy path) (*)
-	Linear combination of resonances generating "Sidebands" $\omega_t = \omega_r \mp \omega_s$ (*)

The (*) marks the fact that the statement is valid for the MDOF systems.
It is worth to say that systems in nature are mostly nonlinear but can be linearised if the amplitude of the excitation is not too high.

2.2 Free behaviour of nonlinear systems

One of the most common sources of nonlinearity are the magnetic spring. They exploit the fact that two magnets oriented so that they repulse themselves, increase the modulus of the force in a nonlinear way. For example, a quantitatively way to express a magnetic spring force F_m is:

$$F_m = \frac{A}{\left(1+\frac{x}{B}\right)^n} \tag{2.2.1}$$

where A, B and n are coefficient that well reproduce the trend of F_m and are obtained experimentally and x is the gap between the ferromagnetic elements.
Figure 1.1.1 shows the trend of a normal magnetic spring with:

- $A = 1.5*10^{-3}/0.02^3$ N = 187.5 N;
- $B = 0.02$ m;
- $n = 3$.

Moreover, it is presented a linearisation around the system static equilibrium point x_e, which corresponds to coordinate where $F_m = F_0 = mg$. In this way the weight of the mass is excluded from the equation of motion. This operation permits to write, using the polynomial expansion stopped to the term of first power:

$$F_m = F_0 - k\left(x - x_e\right) \tag{2.2.2}$$

where k is the first derivative of the (2.2.1) calculated in x_e.

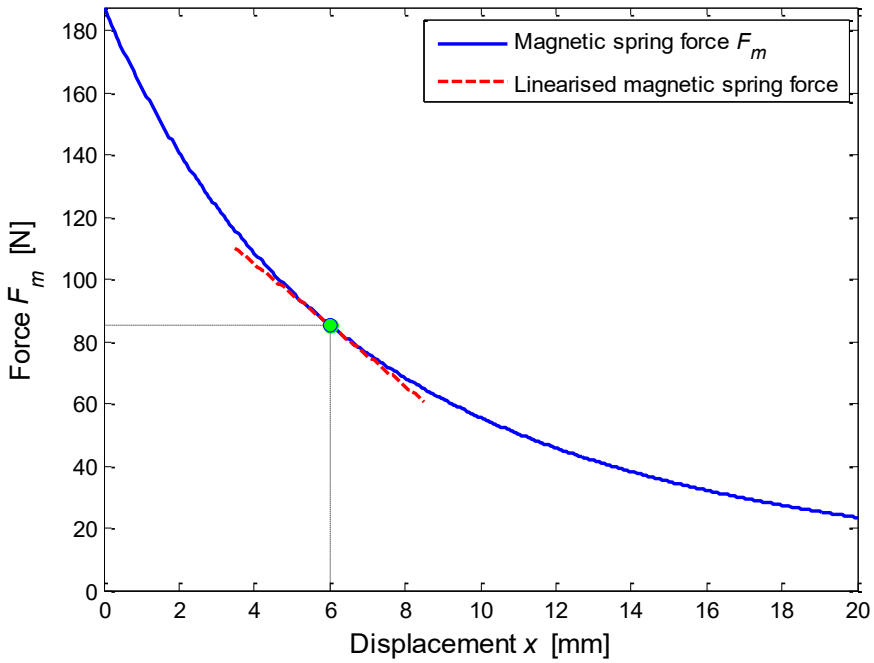

Figure 2.2.1 – Example of a magnetic spring characteristic and linearisation around $x_e = 6$ mm.

For example, for a mass of 0.06 kg and the parameters shown right after (2.2.1), the equilibrium point and the coefficient for a polynomial expansion of the third power like (2.2.3) can be computed with (2.2.4) and (2.2.5), that make reference to [7]:

$$F_k = F_0 - k_1 (x - x_e) - k_2 (x - x_e)^2 - k_3 (x - x_e)^3 \tag{2.2.3}$$

$$x_e = B\left(\sqrt[n]{\frac{A}{mg}} - 1 \right) = 0.11 \text{ m} \tag{2.2.4}$$

$$F_0 = \frac{A}{\left(1 + \frac{x_e}{B}\right)^n} = 0.5886 \text{ N};\ k_1 = \frac{n\frac{A}{B}}{\left(1 + \frac{x_e}{B}\right)^{n+1}} = 13 \text{ N/m};$$

$$k_2 = -\frac{n(n+1) A B^n}{2(x_e + B)^{n+2}} = = \text{-189 N/m}^2;\ k_3 = \frac{n(n+1)(n+2) A B^n}{6(x_e + B)^{n+3}} = = 2.3 \cdot 10^3 \text{ N/m}^3 \tag{2.2.5}$$

Another type of nonlinearity is the Duffing type spring. Its main feature is to have a spring force F_k related to the cube of the displacement x. Its complete formulation is structured as follows:

$$F_k = k_1 x + k_2 x^2 + k_3 x^3 \tag{2.2.6}$$

where k_1 is the classic linear positive stiffness, k_2 is the negative quadratic term and k_3 is the typical Duffing term. k_2 is negative because it reproduces the softening behaviour owed to the decreasing force that two magnets carry out of the distance between them is increased.
The sign of the cubic term causes a great distinction between the spring behaviour:

- $k_3 > 0$: hardening behaviour because its stiffness increases with the displacement modulus;
- $k_3 < 0$: softening behaviour because its stiffness decreases with the displacement modulus.

In Figure 2.2.2 are reported the characteristics of the two kinds of Duffing springs obtained with $k_1 = 1500$ N/m, $k_2 = 0$ N/m^2, $k_3 = \pm 10^8$ N/m^3. As can be seen, the softening curve has a relative minimum near 17 mm. If the system presents a displacement that overcomes this value, it will become unstable.

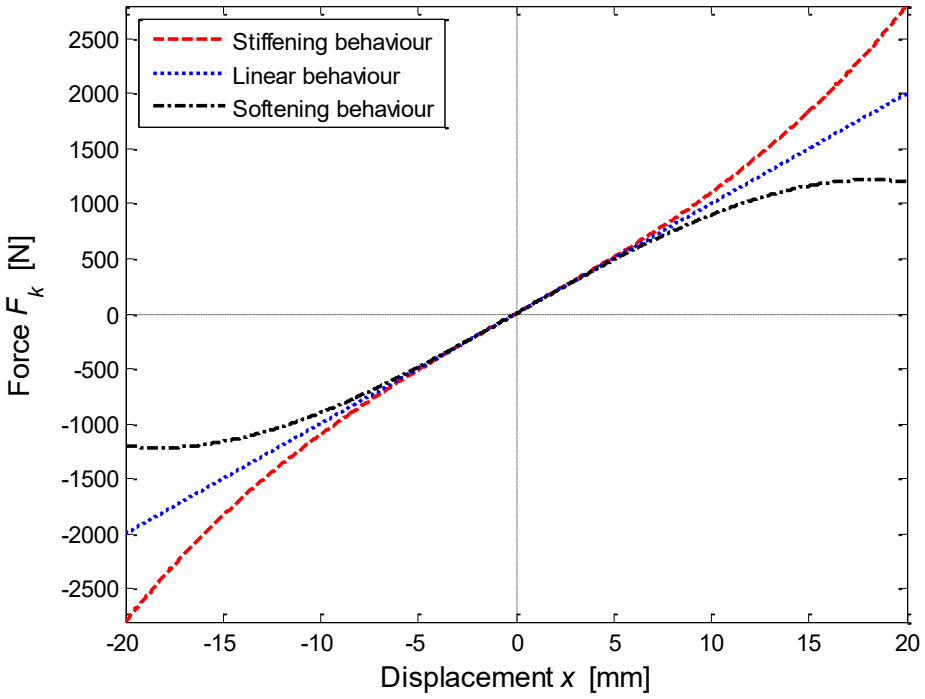

Figure 2.2.2 – Duffing cubic springs.

Similarly, it can exist a nonlinearity concerning damping, like follows:

$$F_c = c_1 \dot{x} + c_2 \dot{x}^2 + c_3 \dot{x}^3 \tag{2.2.7}$$

where c_1 is the classic linear positive damping, c_2 and c_3 are the quadratic and cubic terms.
In particular, its sign causes a great distinction between the spring behaviour:

- $c_3 > 0$: progressive behaviour because the dissipative force increases with the displacement modulus;
- $c_3 < 0$: regressive behaviour because the dissipative force decreases with the displacement modulus.

In Figure 2.2.3 are reported the characteristics of the two kinds of nonlinear dashpots obtained with c_1 = 1500 N/(m/s), c_2 = 0 N/(m/s)^2, $c_3 = \pm 10^8$ N/(m/s)^3.

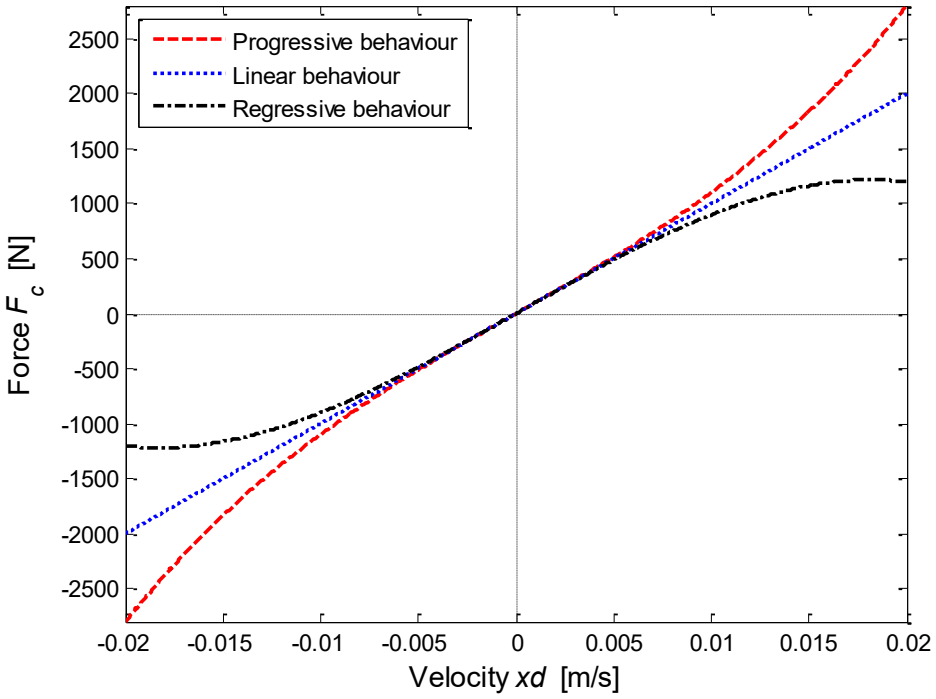

Figure 2.2.3 – Nonlinear cubic dashpots.

2.2.1 Free behaviour of conservative nonlinear systems

The analysed SDOF system has the parameter reported in Figure 2.2.1.1

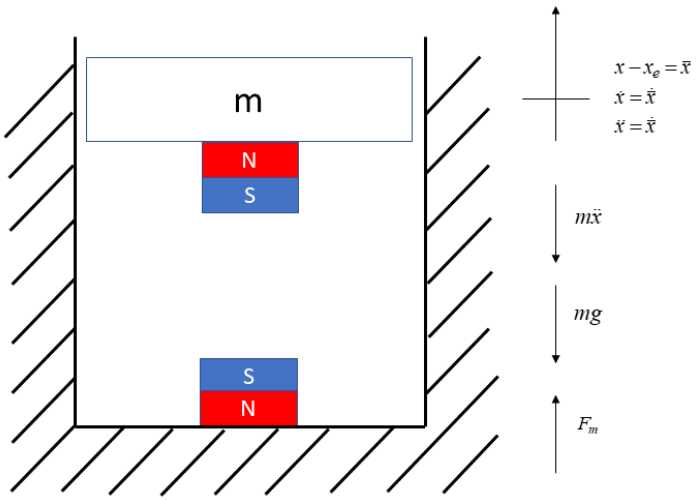

Figure 2.2.1.1 – Conservative SDOF nonlinear system.

It is made up by a mass connected to a magnetic spring with the same characteristic of Figure 2.2.1. The equation of motion is the following:

$$m\ddot{\bar{x}} - F_m + mg = 0 \qquad (2.2.1.1)$$

where $\bar{x} = x - x_e$ and x_e is the static equilibrium point of the same spring. F_m can be written as:

$$F_m = \frac{\bar{A}}{\left(1 + \frac{\bar{x}}{\bar{B}}\right)^n} \tag{2.2.1.2}$$

where $\bar{A}$ and $\bar{B}$ are different from the coefficients of (2.2.1) because the spring force is now described through a relative coordinate and not an absolute one. The spring can be described, after a polynomial development, as:

$$F_m = F_0 - k_1 \bar{x} - k_2 \bar{x}^2 - k_3 \bar{x}^3 \tag{2.2.1.3}$$

F_0 is equal to $mg = F(x = x_e)$. In this way the equation of motion is:

$$m\ddot{\bar{x}} + k_1 \bar{x} + k_2 \bar{x}^2 + k_3 \bar{x}^3 = 0 \tag{2.2.1.4}$$

The chosen parameters are listed in Table 2.2.1.1, while the chosen initial conditions are shown in Table 2.2.1.2.

Table 2.2.1.1 – Analysed SDOF system.

Parameter	Value
Mass m	0.06 kg
Linear stiffness k_1	1500 N/m
Quadratic stiffness k_2	-10^4 N/m^2
Cubic stiffness k_3	10^8 N/m^3

Table 2.2.1.2 – Initial condition for the analysed SDOF system.

Parameter	Value
x_0	0.002 m
$\dot{x}_0$	0 m/s

Note that the chosen initial displacement is compatible with the fact that a simulation using only k_1 and negative k_3 does not highlight instability phenomenon since the characteristic of a spring of this kind would be as shown in Figure 2.2.1.2. Thus it is evident that a system like this would become unstable if the initial condition was about $x_0 = 2.5$ mm.

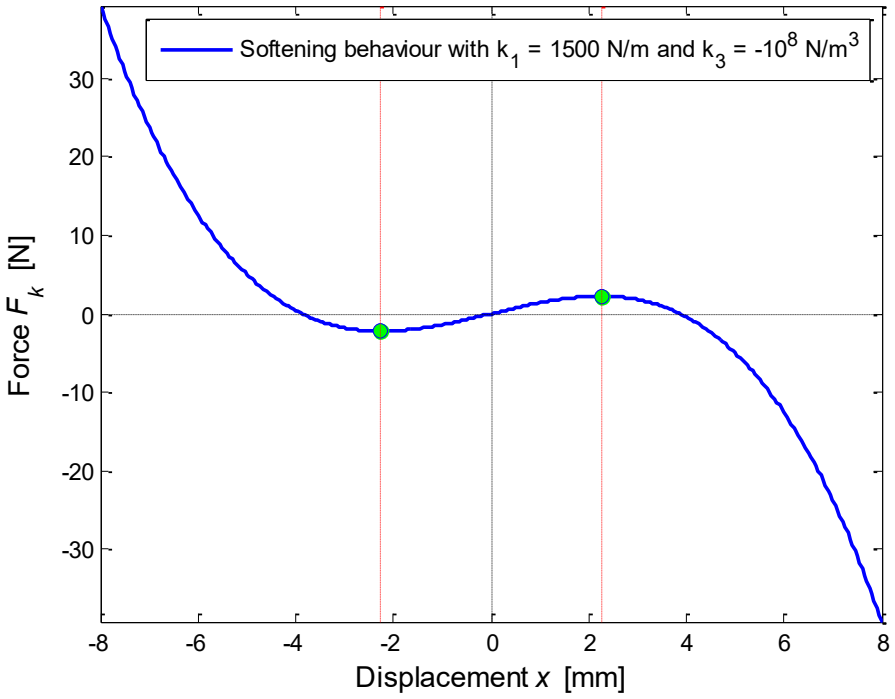

Figure 2.2.1.2 – Spring characteristic with k_1 = 1500 N/m and k_3 = -10^8 N/m^3 and its stability region.

The effects of nonlinearity can be spotted in the so called 'state plane', a graph that shows the velocity and the displacement of a mass respectively in y-axis and x-axis.
Some simulations results are shown in Figures 2.2.1.3-5, which are parametrised on the base of the nonlinearity level.

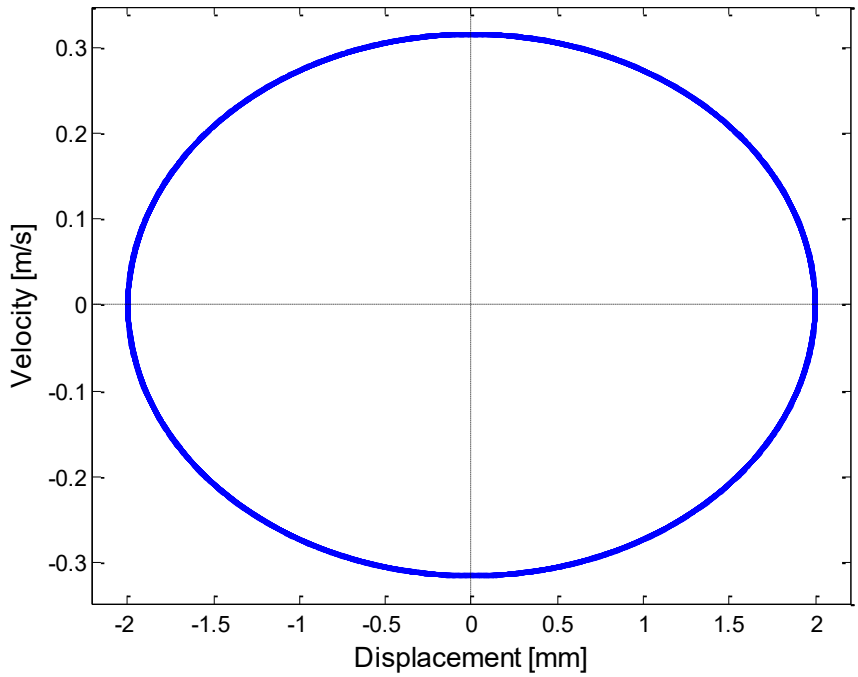

Figure 2.2.1.3 – State plane with linear spring k_1 = 1500 N/m.

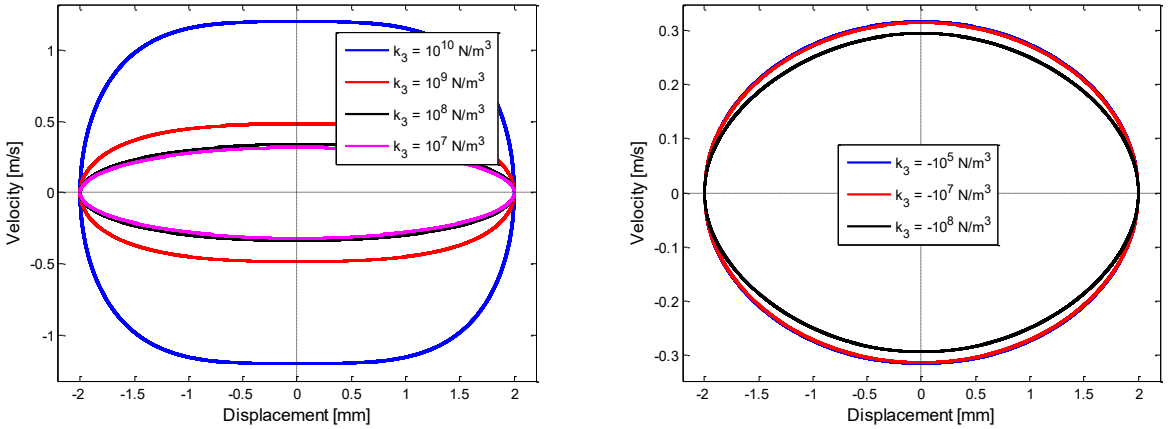

Figure 2.2.1.4 – State plane with linear and
various hardening cubic spring (left) and various softening cubic spring (right).

An increasing absolute value of the nonlinear terms produce a progressively deformed state plane.

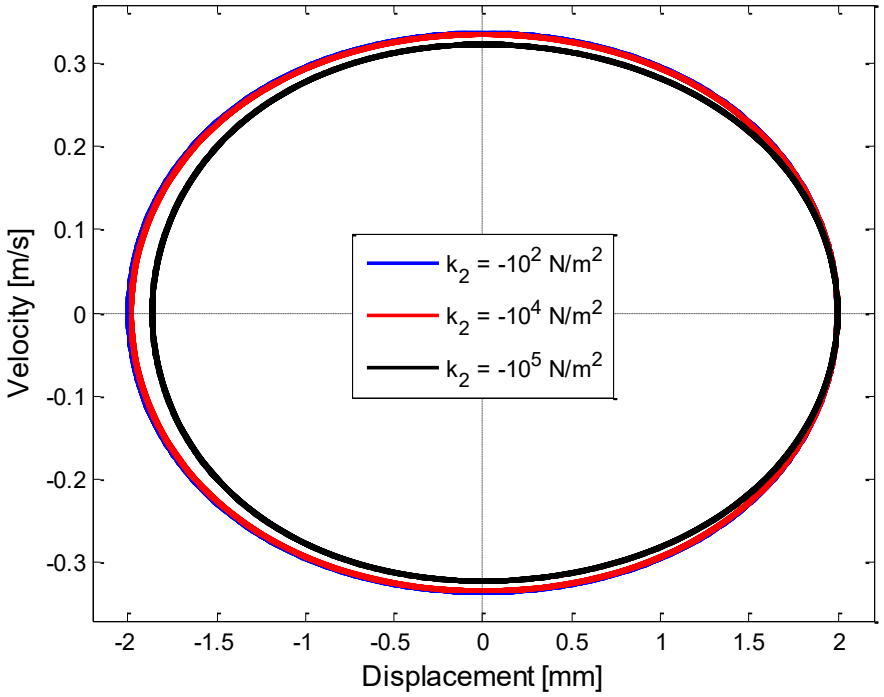

Figure 2.2.1.5 – State plane with linear, various quadratic and positive cubic springs.

An increasing absolute value of the nonlinear quadratic term produces a progressively unsymmetric state plane.

As can be seen, the imagines show the typical state plane shapes for the 3 analysed system:

- symmetrical elliptical shape for linear system;
- symmetrical pseudo-elliptical shape for nonlinear cubical systems;
- asymmetrical elliptical shape for nonlinear quadratic and hardening cubic systems.

2.2.2 Free behaviour of damped nonlinear systems

Briefly, what happens if a dissipative term is introduced into a nonlinear system is shown in Figure 2.2.2.1.

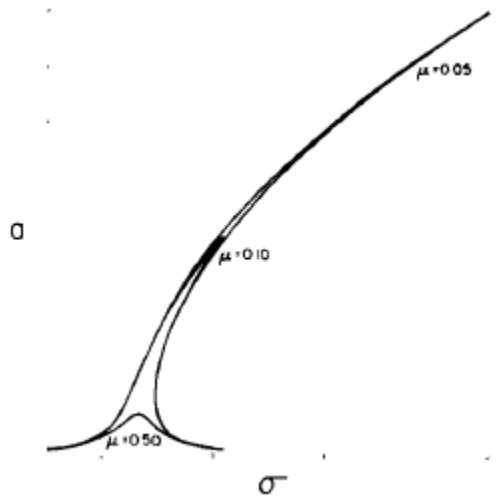

Figure 2.2.2.1 – Damping in nonlinear structures.

As can be seen, the typical nonlinear backbone disappears when damping (indicated with the 'μ' parameter) increases and the system seems to be linear, just like what takes place whether the excitation amplitude is too low.
Moreover, in the presence of damping, the phase shift of the response is altered and cannot be only 0° or 180° out of phase with the excitation, as occurs in nonlinear conservative structures.

For the system of Figure 2.2.1.1 is now introduced a low dissipative term modelled with the relative parameter ζ so that the damping term itself is calculated as $c = 2\zeta\,\omega_n\,m$. $\omega_n = \sqrt{\frac{k}{m}}$ is the linearised natural frequency of the system. The equation of motion becomes:

$$m\ddot{\bar{x}} + c\dot{\bar{x}} + k_1\,\bar{x} + k_2\bar{x}^2 + k_3\,\bar{x}^3 = 0 \qquad (2.2.2.1)$$

It is worth displaying the results of the state plane with various values of damping of the free-response of the system for 5 seconds.

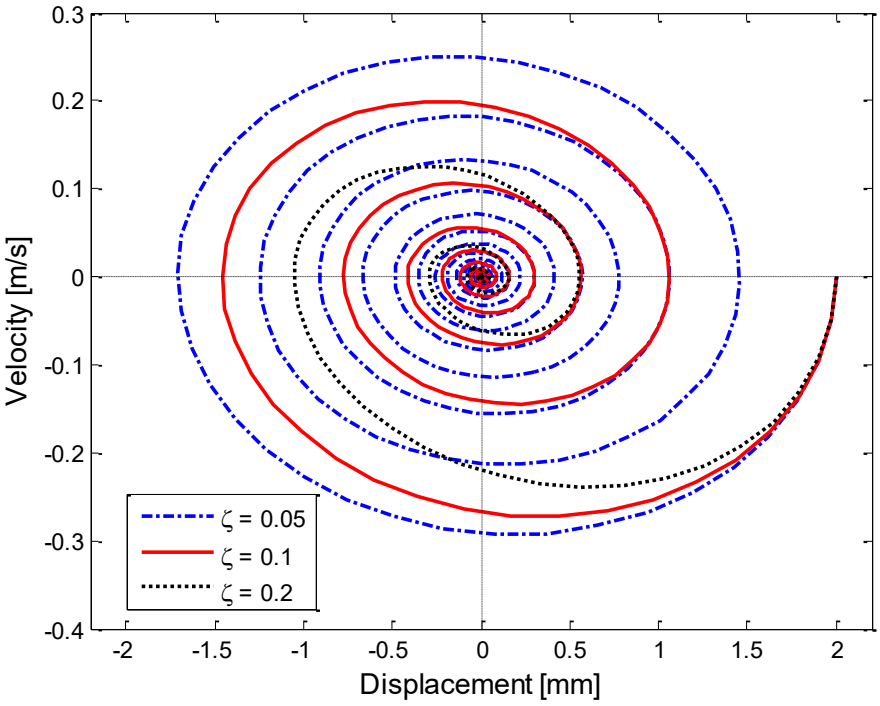

Figure 2.2.2.2 – State plane with linear spring and various values of damping factor.

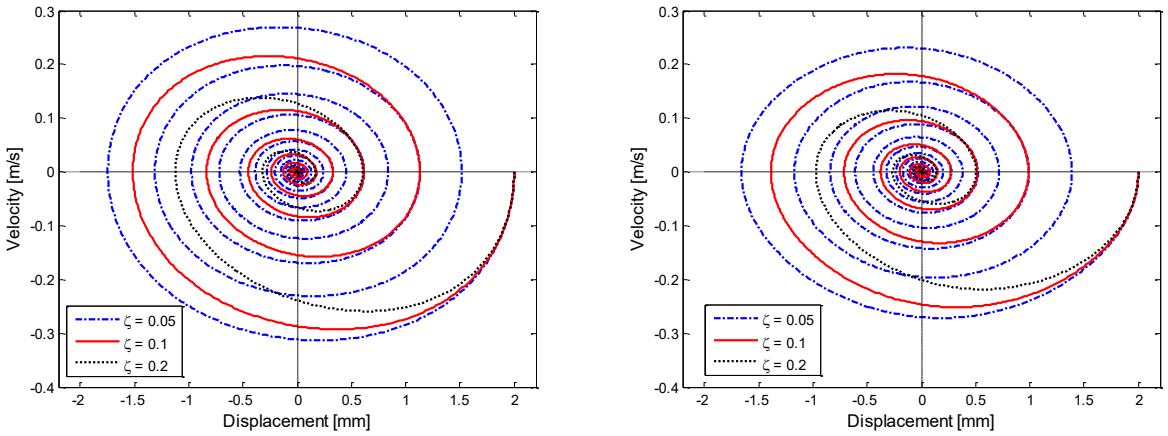

Figure 2.2.2.3 – State plane with linear, damped,
hardening cubic spring (left) and softening cubic spring (right).

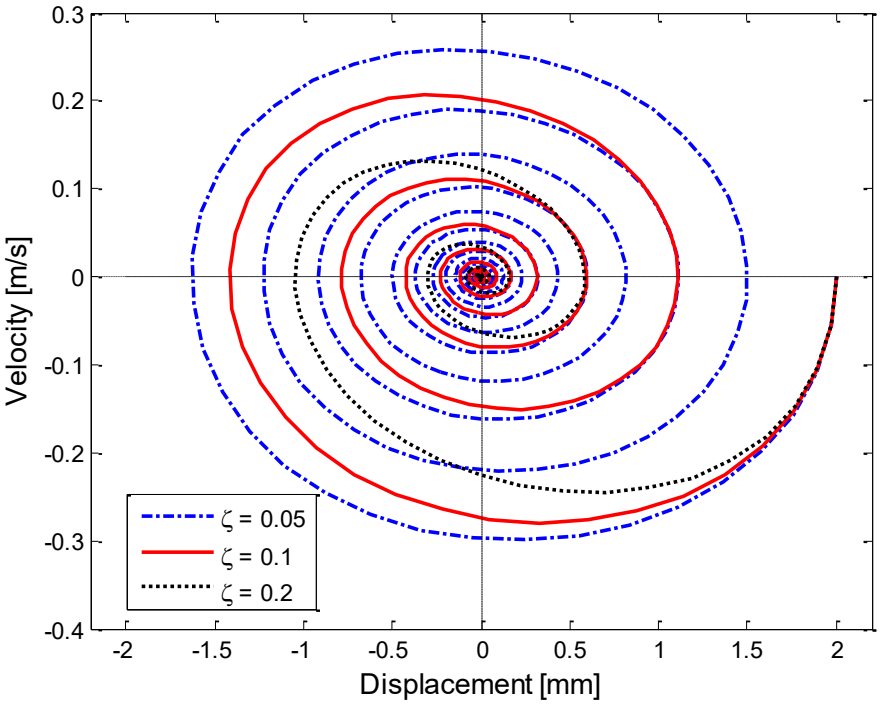

Figure 2.2.2.4 – State plane with linear, damped, quadratic and positive cubic springs.

Here the considerations that can be made are the same for Figures 2.2.1.2-4 with the difference that the dissipative term forces the system to run out of its energy.
Considering damping, it is partially visible in Figure 2.2.2.4 the drift phenomenon for $\zeta = 0.05$, which display the progressive shift of the centre of the orbit towards the right.
For high values of damping the differences of the graphs decrease, indeed it is worth producing Figure 2.2.2.5 in order to properly distinguish the orbits of the system with $\zeta = 0.05$.

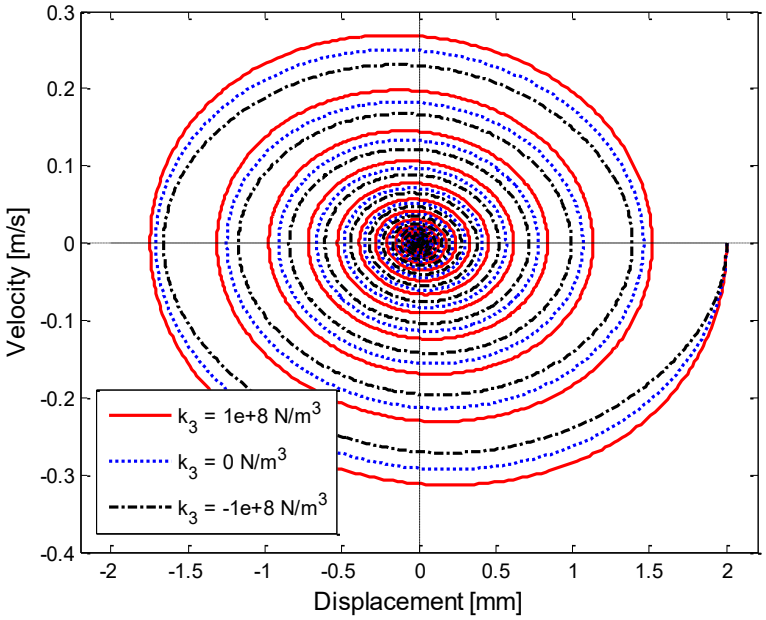

Figure 2.2.2.5 – Comparison between state planes of hardening cubic term (red), null cubic term (blue) and softening cubic term (black) with constant damping factor $\zeta = 0.05$.

As can be seen, the curves appear different only if they are in the same graph. This is a confirmation of the fact that non linearities are difficult to be spotted if the dissipation sources are intense.
If the damping had been set on higher values (e.g. $\zeta = 0.3 \div 0.5$), Figures 2.2.2.2-4 would have shown a more rapid process of assuming the coordinates (0,0) and therefore, simulations like these are not included in this report for sake of brevity.

Another import aspect for these simulations is that Simulink step time has been decreased in order to avoid aliasing. Indeed, the regions of the graph with the bigger displacements are characterised by rapid velocity changes so that the vertical part of the path appeared under sampled before the intensification of the measured points.
Eventually, it is important to create Figure 2.2.2.6, because the trajectory of the SDOF in the involuting pseudo-ellipses in the damped cubic system have identical shapes of the fundamental trajectory of the equivalent conservative system.

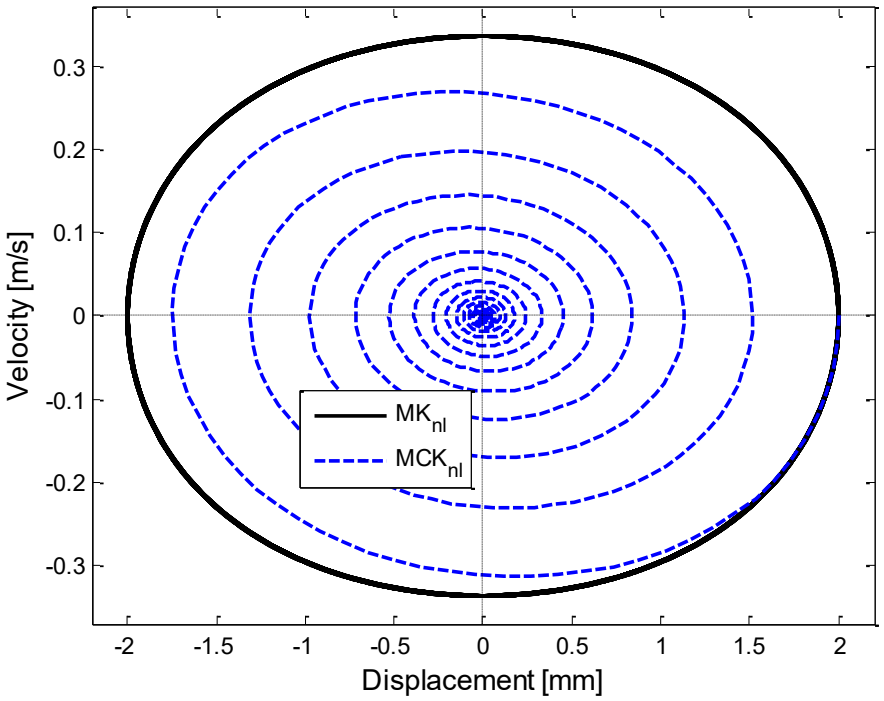

Figure 2.2.2.6 – Comparison between state planes of conservative system with linear and cubic springs and damped system with linear and hardening cubic springs $\zeta = 0.05$.

2.3 Forced behaviour of damped nonlinear systems

One of the main tools used to describe the Duffing springs is the 'frequency – response curve', where it is reported the amplitude of the response in relation to frequency of the harmonic excitation.
Figure 3.1 explains the difference between linear and nonlinear systems.

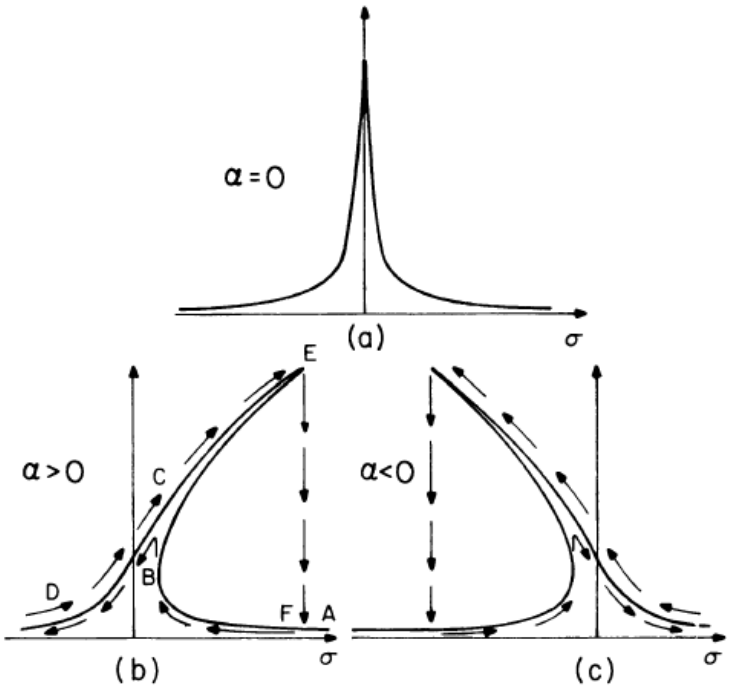

Figure 2.3.1 – Frequency – response curves
for a linear spring (a), hardening (b) and softening (c) Duffing springs.[8]

The x – axis in the imagine is tied to σ, which if it is equal to 0, means that is considered an excitation frequency corresponding to the natural frequency of the system. The α parameter is related to k_3, indeed Figure 2.3.1(b) concerns a hardening spring, as α is bigger than 0.
In these figures are presented the behaviour of the systems where a forward or backward frequency sweep is carried out.
In Duffing spring, can be seen the so-called backbones. In particular, the hardening one shows a jump phenomenon from the upper branch to the low one when the frequency excitation is increased quasi-statically. In fact the amplitude of the oscillations decreases, according to the definition of the hardening spring.

In addition to that, it is worth to have a look at the phase angle γ, defined as difference between the excitation phase angle and the response one.

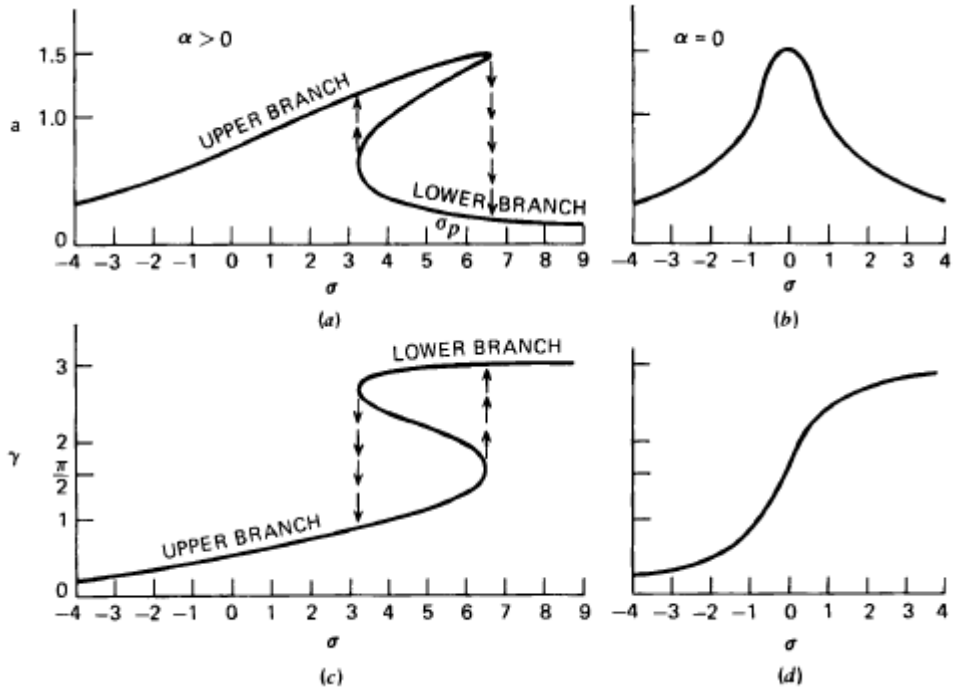

Figure 2.3.2 – Comparison of a hardening spring and a linear spring
for: (a) and (b) amplitudes; (c) and (d) phases. [10]

As known, the phase become 90° in correspondence of the resonance frequency in linear SDOF structures.
Instead, in nonlinear response curves the phase becomes 180° in the case of forward sweep test.

Moreover, according to what is written right after Table 2.1.1, Figure 2.3.3 shows how the backbones become more inclined if the amplitude of the excitation (symbolised with the '*k*' parameter) grows and how the system works as a linear one if it is under excited.

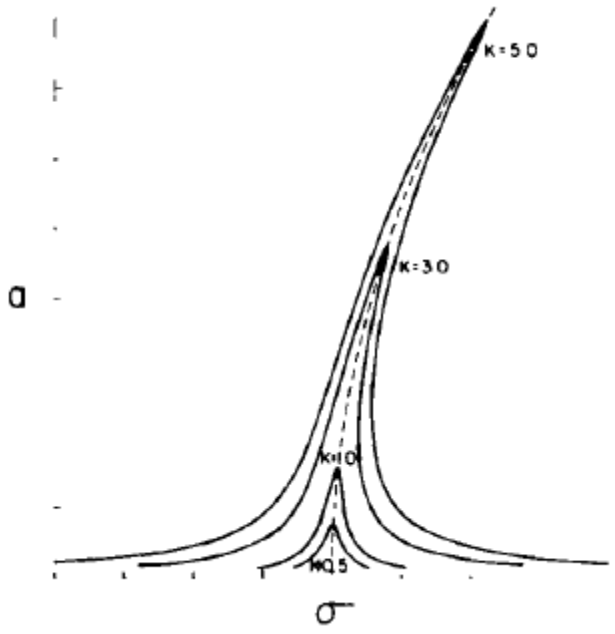

Figure 2.3.3 – Backbones and amplitude of the excitation.

2.3.1 Simulations of forward sweep

A system similar to the one of (2.2.2.1) is excited with a forward frequency sweep that covers 0 to 50 Hz in 50 s. The reason why these simulations were not performed with the same structure is that this kind of excitation made the mass to become unstable. More specifically, the oscillations resulted bigger than 3 mm and so, on the right of the relative minimum point shown in Figure 2.2.1.2 if the damping was not regulated to unrealistic high value and/or the initial displacement set to incredibly small amplitude.
Therefore the structure is now:

Table 2.3.1.1 – Analysed SDOF system.

Parameter	Value
Mass m	0.06 kg
Linear stiffness k_1	1500 N/m
Quadratic stiffness k_2	-10^4 N/m^2
Cubic stiffness k_3	10^6 N/m^3

While the chosen initial conditions are still:

Table 2.3.1.2 – Initial condition for the analysed SDOF system.

Parameter	Value
x_0	0.002 m
$\dot{x}_0$	0 m/s

What happens to the simulations is shown in Figure 2.3.1.1 to 2.3.1.4.

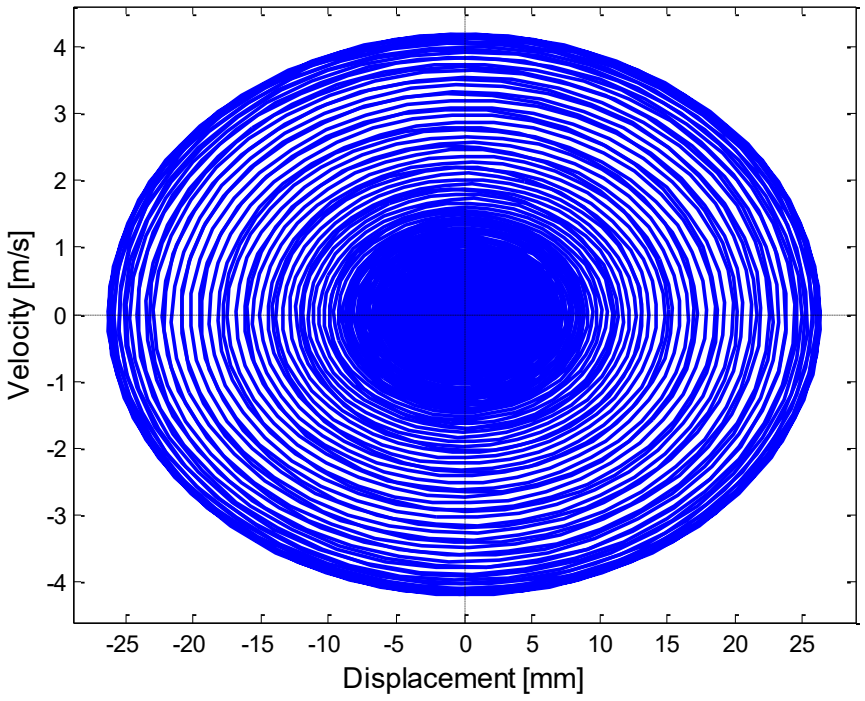

Figure 2.3.1.1 – State plane with linear spring with $\zeta = 0.01$

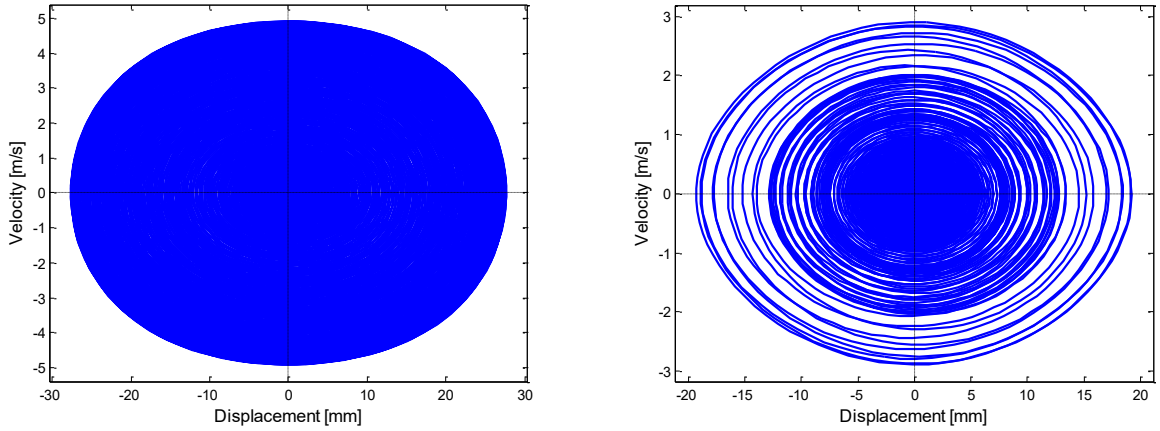

Figure 2.3.1.2 – State plane with linear, damped ($\zeta = 0.01$)
hardening cubic spring (left) and softening cubic spring (right).

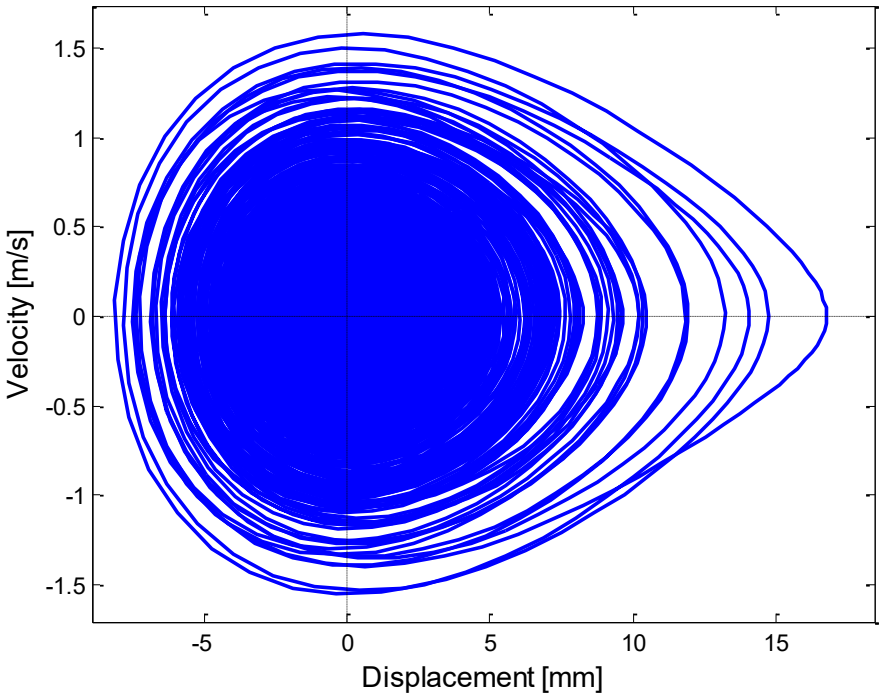

Figure 2.3.1.3 – State plane with linear, quadratic and positive cubic springs with $\zeta = 0.01$.

The same state plane can be obtained also for the SDOF system with a high dissipative term.
It is not reported the state plane for the system with the linear and cubic springs, since the only difference is that the oscillations expire in a faster way because of the damping.

2.3.2 Frequency response curves for damped SDOF

It is critical to analyse the frequency response function of the system with linear and cubic springs and variable damping in order to have the typical jump phenomenon displayed in Figure 2.3.2.1.

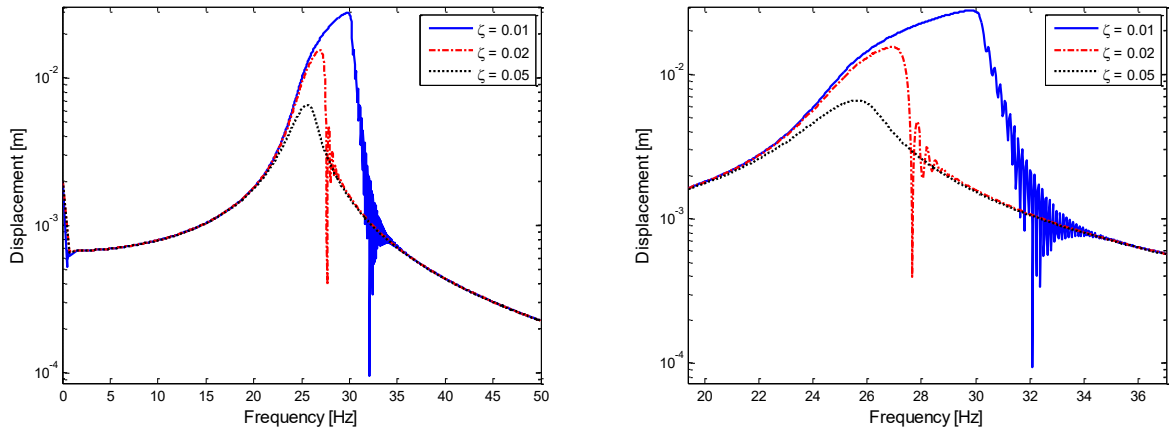

Figure 2.3.2.1 – Envelope of positive maximum displacements in time domain of stiffening cubical and damped system (left) and detail (right).

The jump phenomenon is much less evident as the damping factor grows, Furthermore, the oscillations after the jump are fewer than the blue one, while $\zeta = 0.05$ totally deletes the oscillations after the jump.
Note that the initial oscillations owed to solution of the homogenous associated are eliminated thanks to a damping 100 times bigger in the first second of simulation. Even the transitory after the jump could have been cancelled but is crucial to show how the dissipative terms deletes it, instead.
Another kind of visualisation of this issue is the one of Figure 2.3.2.2, which is the displacement time history. For the stiffening case the sweep is inverted in order to reproduce the typical backbone.

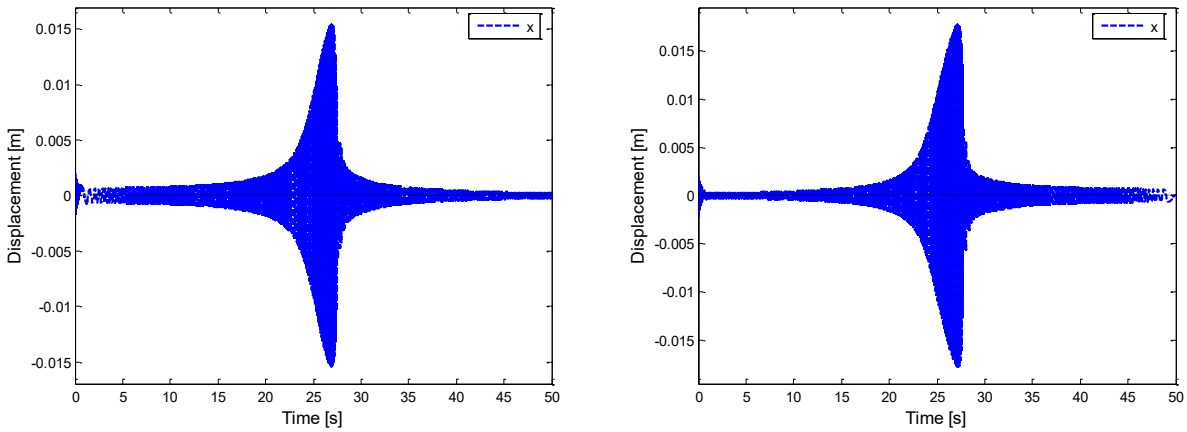

Figure 2.3.2.2 – Displacement time history of a damped ($\zeta = 0.02$) with cubic hardening spring (left) and cubic softening spring (right).

Note that the two graphs are almost the same with only the difference that the zone with slow oscillations caused by low frequencies is on the opposite side since the sweep is executed in opposed directions.

As regards the frequency response curves, it is legit to think that higher value of damping will totally cancel the backbones and the jump phenomena. This effect is verified in Figure 2.3.2.3.

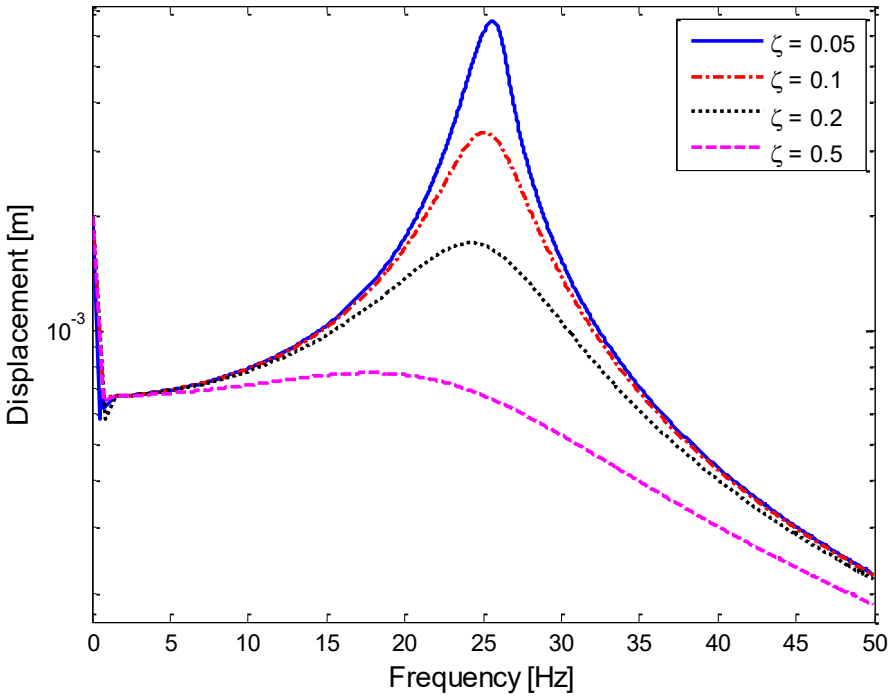

Figure 2.3.2.3 – Envelope of positive maximum displacements in time domain of a cubic stiffness system with various values of damping.

2.4 Time-frequency analysis of a damped SDOF nonlinear system

A further step is to analyse the time-frequency content of the free systems seen in § 2.2 with two approaches:

- use of the routine "`TimeFreq`", which is based on the Fast Fourier Transform (FFT);
- use of the wavelet approach.

Both the techniques have a 3D plot as output that is basically a succession of Frequency Response Functions in time. This can easily become a 2D explanatory plot in a plane that has time and frequency respectively as abscissa and ordinate whereas the intensity of the response is represented with a colour scale.
The main difference of the two methods is that the former has constant frequency sample f_s and delta-time sample Δt (because $\Delta t = 1/f_s$) while the latter, as the frequency increases, is able to decrease the delta-time sample Δt and therefore can catch more instantaneous phenomena.

The data analysed are obtained with a damping factor $\zeta = 0.005$, a simulation time $T = 10$ s and $f_s = 10^4$ Hz.
The first case is the linear system excited with $x_0 = 10$ mm and $\dot{x}_0 = 0$ m/s. In Figure 2.4.2 is displayed the comparison of the two approaches as well as the parameters to set in order to have a good graph using a tool called ACc, developed by Prof. Bonisoli and Paolo Cavallaro. From now on, every wavelet analysis will be accompanied by a screenshot of the ACc settings.

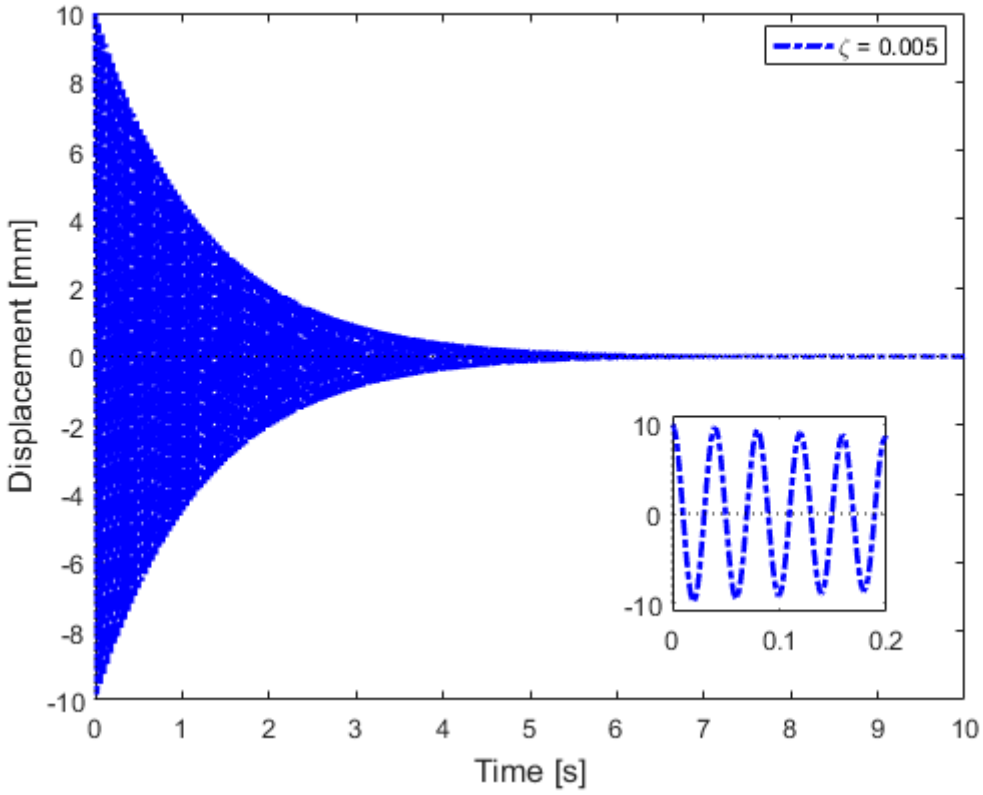

Figure 2.4.1 – Time-history for the linear system.

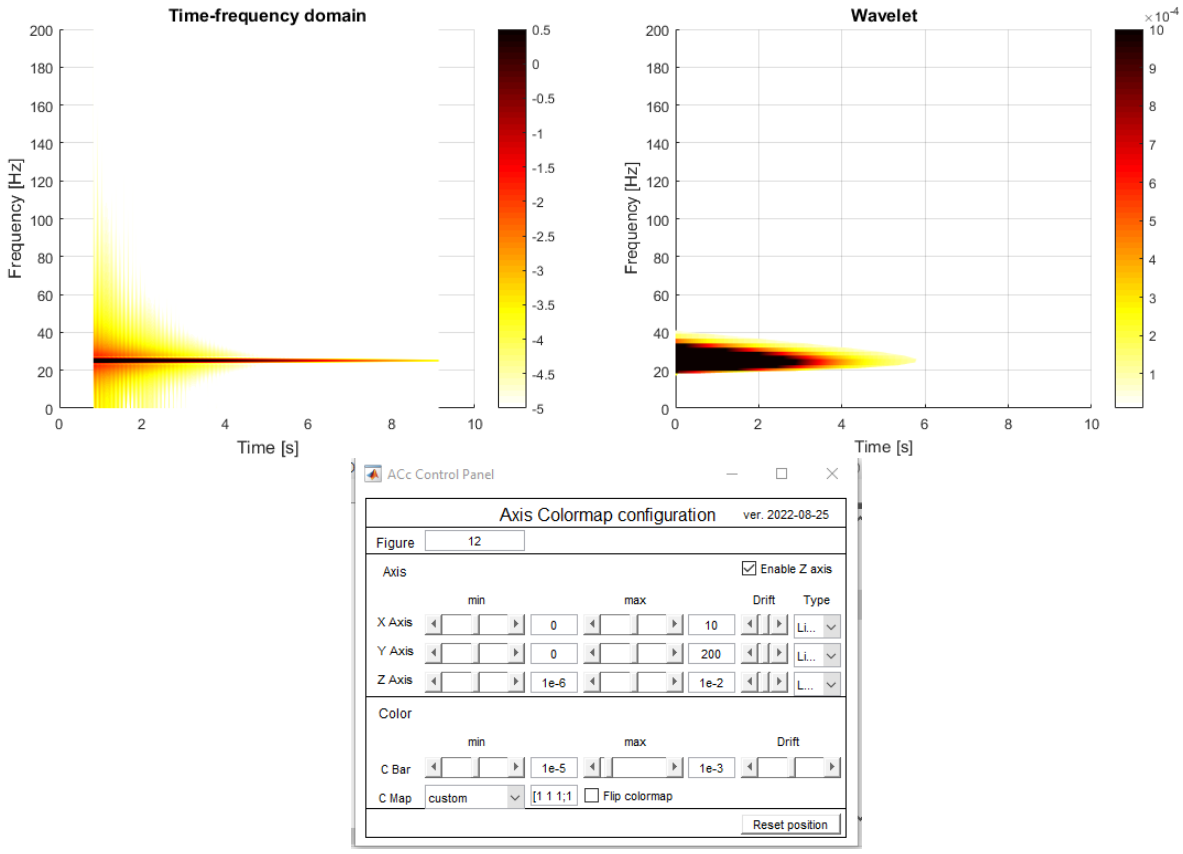

Figure 2.4.2 – Linear system: comparison between time-frequency content FFT (up-left) and wavelet (up-right) with ACc settings (low).

As can be seen, both the approaches highlight the natural frequency of the system, which is 25.16 Hz.

As regards the hardening system, it is excited with x_0 = 10 mm and $\dot{x}_0$ = 0 m/s and in Figure 2.4.3 is reported the time history and in Figure 2.4.4 are reported the results.

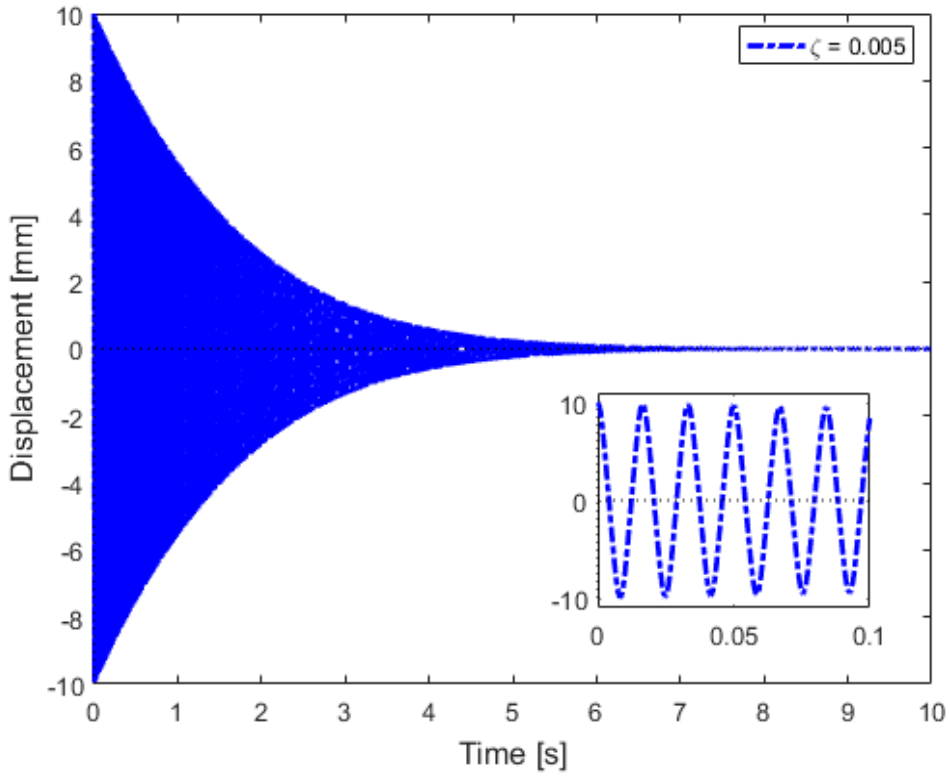

Figure 2.4.3 – Time-history for the hardening system.

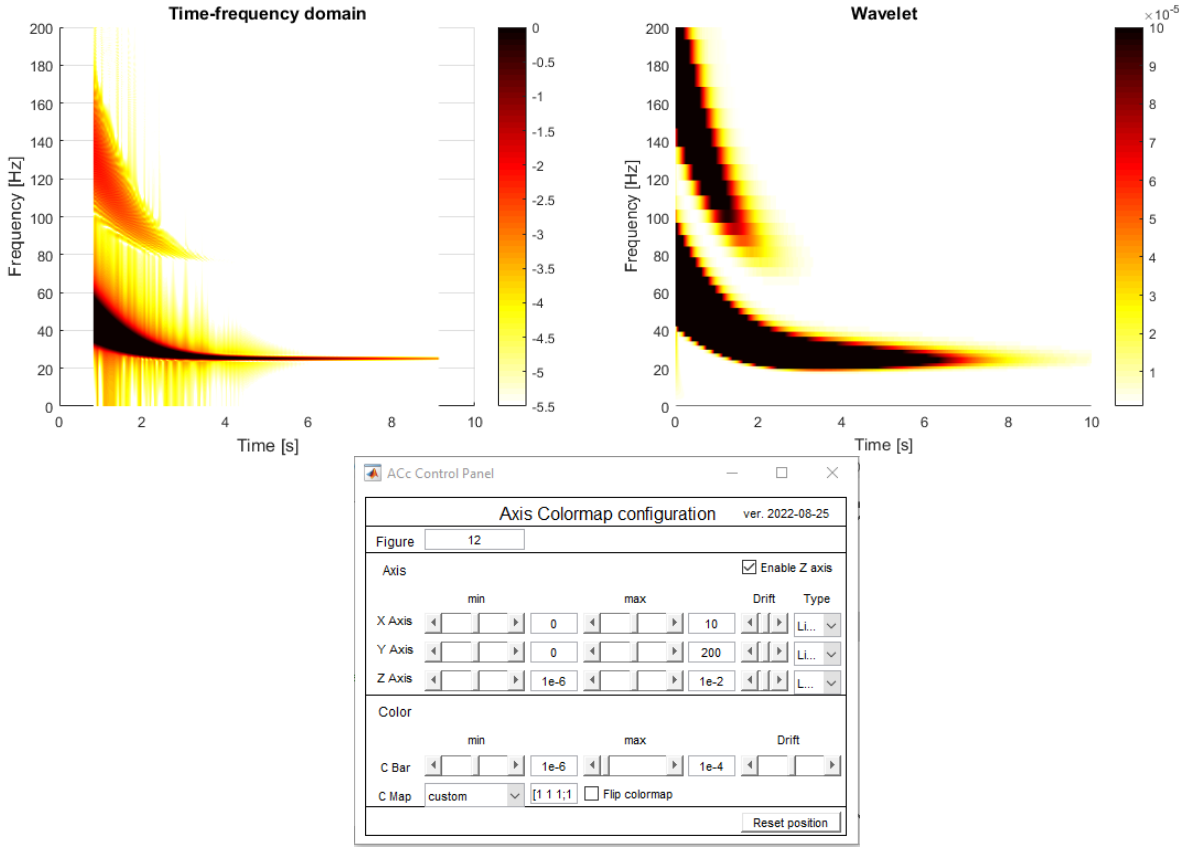

Figure 2.4.4 – Hardening nonlinear system: comparison between time-frequency content FFT (up-left) and wavelet (up-right) with ACc settings (low).

It is visible that the natural frequency decreases in time, as the oscillation amplitude reduces, showing a hardening behaviour. Since FFT analysis only captures a mean value of the instantaneous frequencies, it is not able to catch the gradual return to the fundamental frequency as precisely as the wavelet method does. For the same reason, wavelet approach is more accurate in detecting the initial oscillation frequency than FFT. Moreover, there is a distinction in the third superharmonic of the fundamental, which disappears after about 7 s in the left analysis and 5 s in the right one. That is because FFT is only able to catch the mean values of the oscillation frequencies in a T_w of 2 s therefore phenomena last more than the wavelet approach. Furthermore, for the same reason, the frequencies detected by FFT are always lower. At the end, it is logic stating that the wavelet approach is more appropriate to catch located-in-time phenomena.

The softening system is excited with $x_0 = 3$ mm and $\dot{x}_0 = 0$ m/s due to instability reason. The time-history is reported in Figure 2.4.5 and in Figure 2.4.6 are reported the results of the frequency analysis.

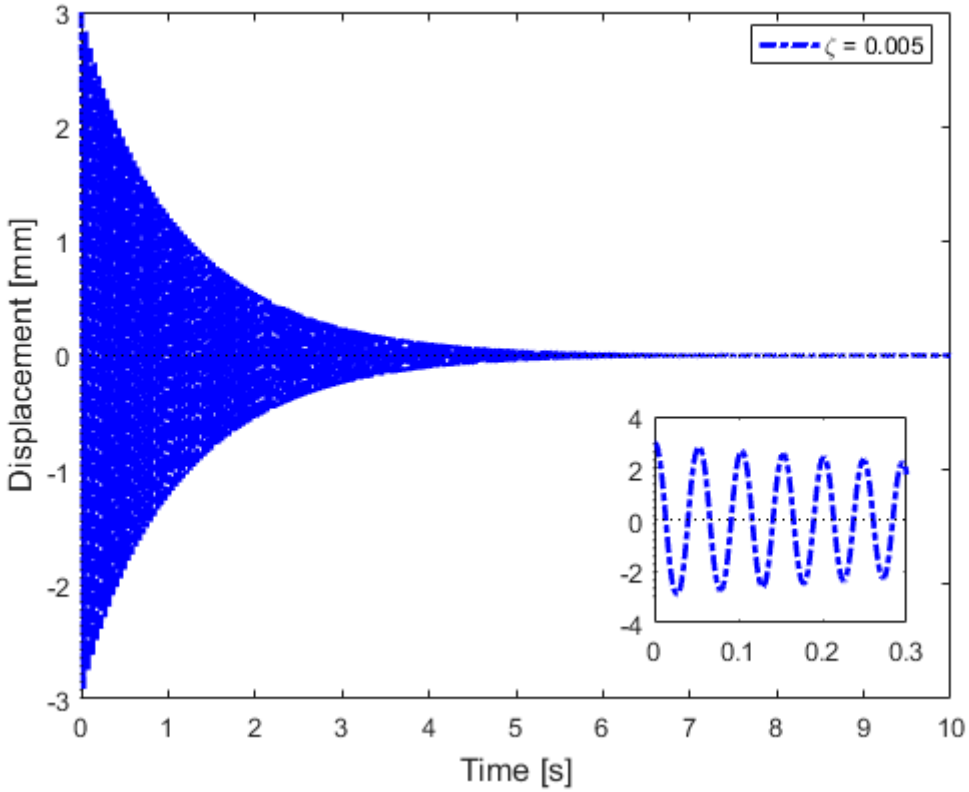

Figure 2.4.5 – Time-history for the softening system.

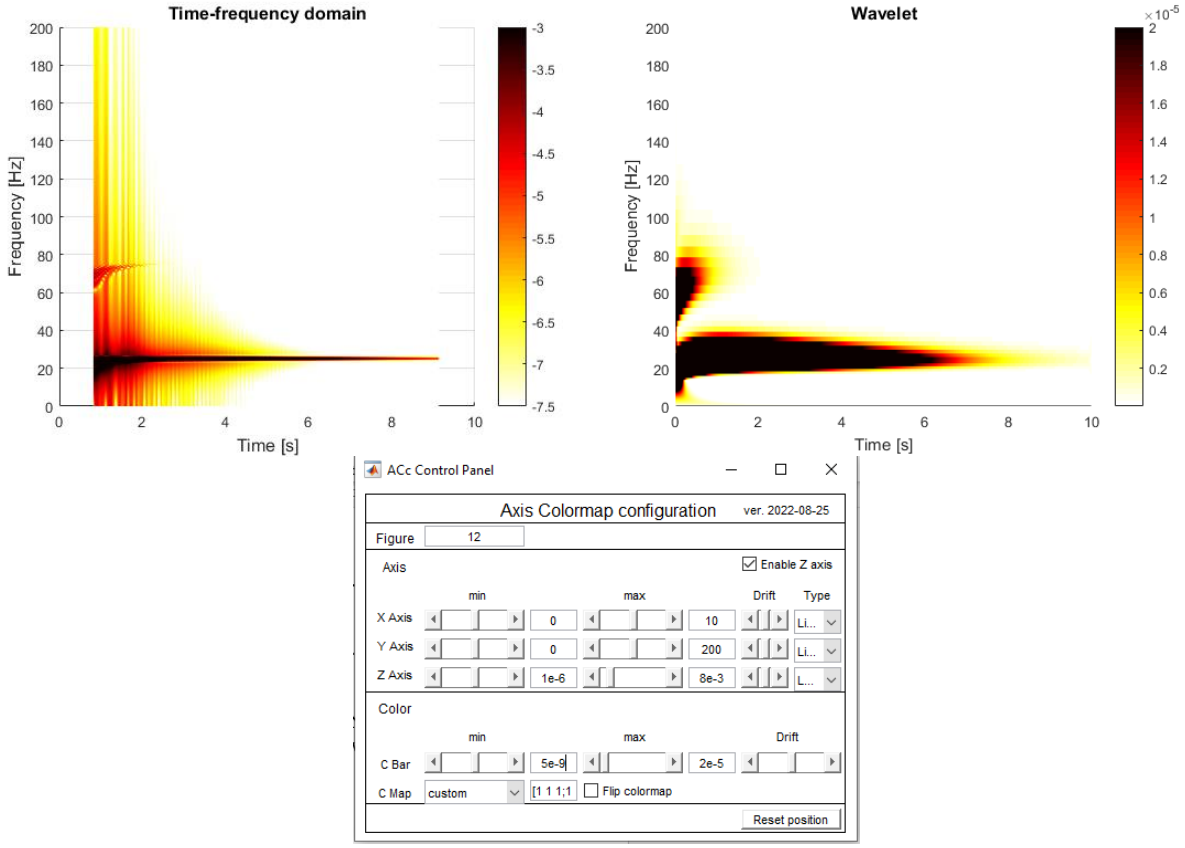

Figure 2.4.6 – Softening nonlinear system: comparison between time-frequency content FFT (up-left) and wavelet (up-right) with ACc settings (low).

Here it is clear a light softening behaviour in both the cases as well as the third superharmonic of the fundamental. Moreover, the frequency values in the wavelet method are higher than the ones of the spectrogram.

In the last configuration, i.e. a nonlinear quadratic system with $k_2 = -10^5 \text{N/m}^2$ and $k_3 = 10^8 \text{N/m}^3$ excited with $x_0 = 10$ mm and $\dot{x}_0 = 0$ m/s, time-history and the time-frequency contents are shown respectively in Figures 2.4.7-8.

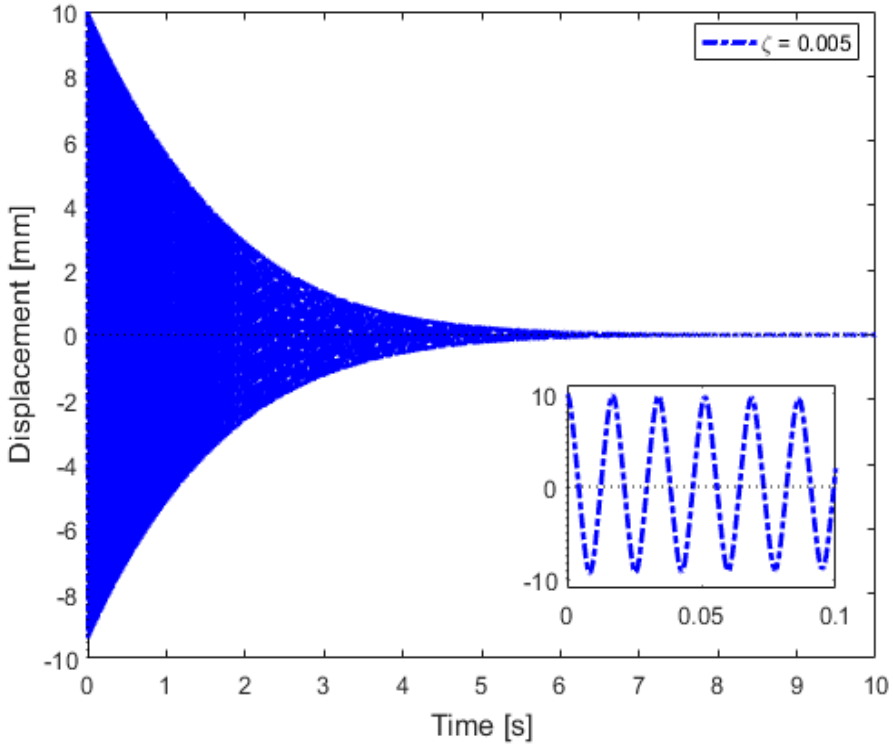

Figure 2.4.7 – Time-history for the quadratic system.

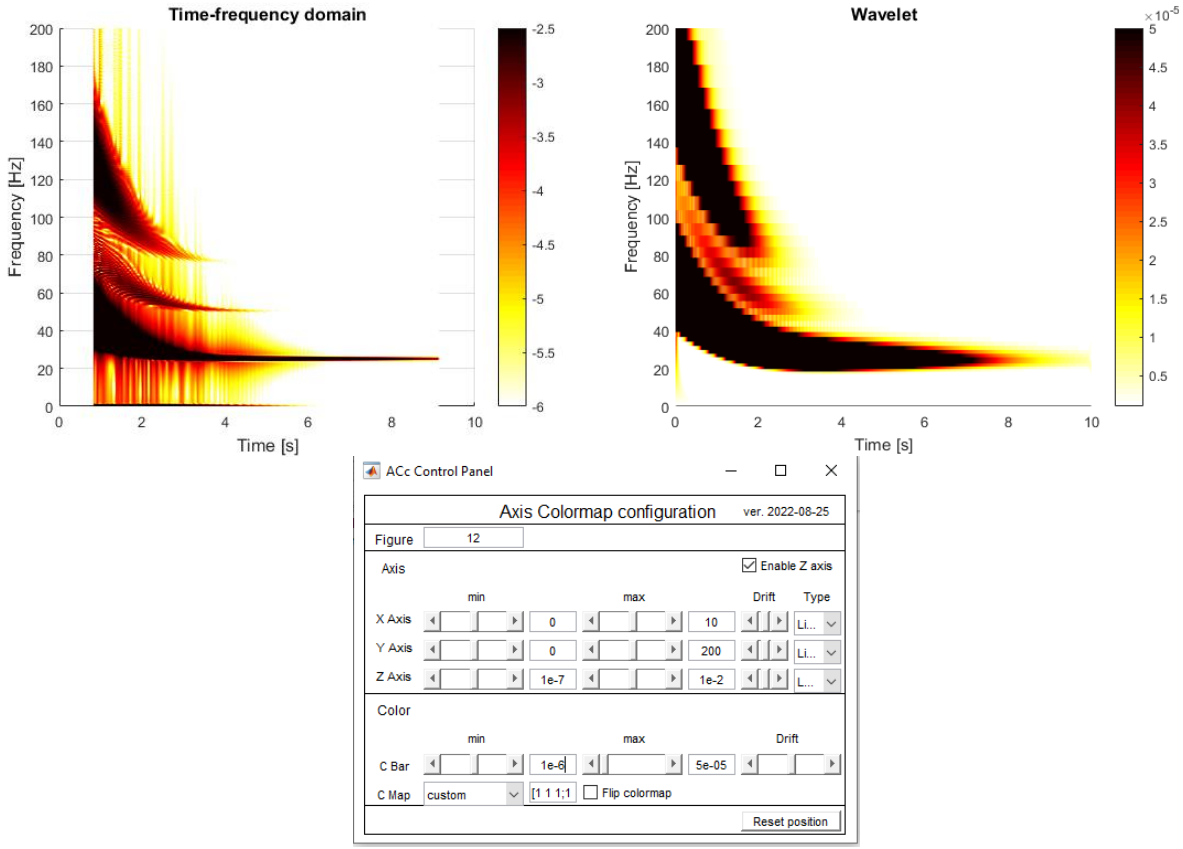

Figure 2.4.8 – Quadratic nonlinear system with positive cubic springs:
comparison between time-frequency content
FFT (up-left) and wavelet (up-right) with ACc settings (low).

The fact that there is a strong nonlinear contribution coming from positive Duffing spring makes the system behave in a hardening way. This fact is confirmed by the fact that the third superharmonic is much more evident than the second one. Even here can be done the same observations of Figure 2.4.2.

2.5 Conclusions

This chapter has the aim to introduce the theme of nonlinear properties of mechanical structures in the thesis. They are initially synthetically exposed in Table 2.1.1 and then are deepened with the help of books. Afterwards, a simple SDOF system is created in MATLAB and many simulations are performed in Simulink specifically to recreate and analyse the features debated in the previous pages.
This is preparatory for the final chapter of the work, where are carried out experimental tests on a beam system and several proofs of nonlinearities are present and examined.

3. Nonlinear beam dynamics

An example of nonlinear system is experimentally analysed in § 3. It is a cantilever Euler-Bernoulli beam with a lumped mass at one end. It has four configurations:

1. two pairs of two permanent magnets acting in repulsion. This introduces a nonlinearity owed to the unsymmetric characteristic of the force carried out by these elements;
2. two pairs of two permanent magnets acting in attraction. This introduces a nonlinearity owed to the unsymmetric characteristic of the force carried out by these elements;
3. a non-holonomic constraint that acts like a pin located at a certain distance from the clamp. This introduces a nonlinearity owed to the contact of the beam with the introduced new constraint;
4. the simple and typical clamped-free beam. Even here a nonlinearity can be present due to a big initial condition displacement which does not allow the small-oscillation simplification.

Therefore, the experimental activity on this component aims to characterise its vibrational properties in the all the configurations and duplicate what had been discovered in [9].

The experimental test was performed at Torino and post-processed until 2022-09-21 on which the main activity was concluded. Moreover, the experimental tests are divided into 2 campaigns on the base of the used lasers:

1. performed in 2022-06-27 with the use of two point-lasers of the type LK-H082 and LK-H152, and a laser profiler LJ-X8900 that has the possibility to monitor the displacement of more than ten points of the beam;
2. performed in 2022-07-05 with the use of three point-lasers of the type LK-H082 and LK-H152.

This report is mainly devoted to the 2nd campaign apart from section § 3.3, where are analysed 3 tests executed in 2022-06-27.

3.1 Experimental setup

The nonlinear analysis is performed adopting three conditions:

1. two pairs of two permanent magnets acting in attraction;
2. two pairs of two permanent magnets acting in repulsion;
3. a non-holonomic constraint that acts like a pin located at a certain distance from the clamp;
4. the simple and typical clamped-free beam.

In Figure 3.1.1 shows the setups of the system in the 2nd campaign because it is the most complex. The 1st and 2nd configurations are equal apart from the way the magnets are acting.

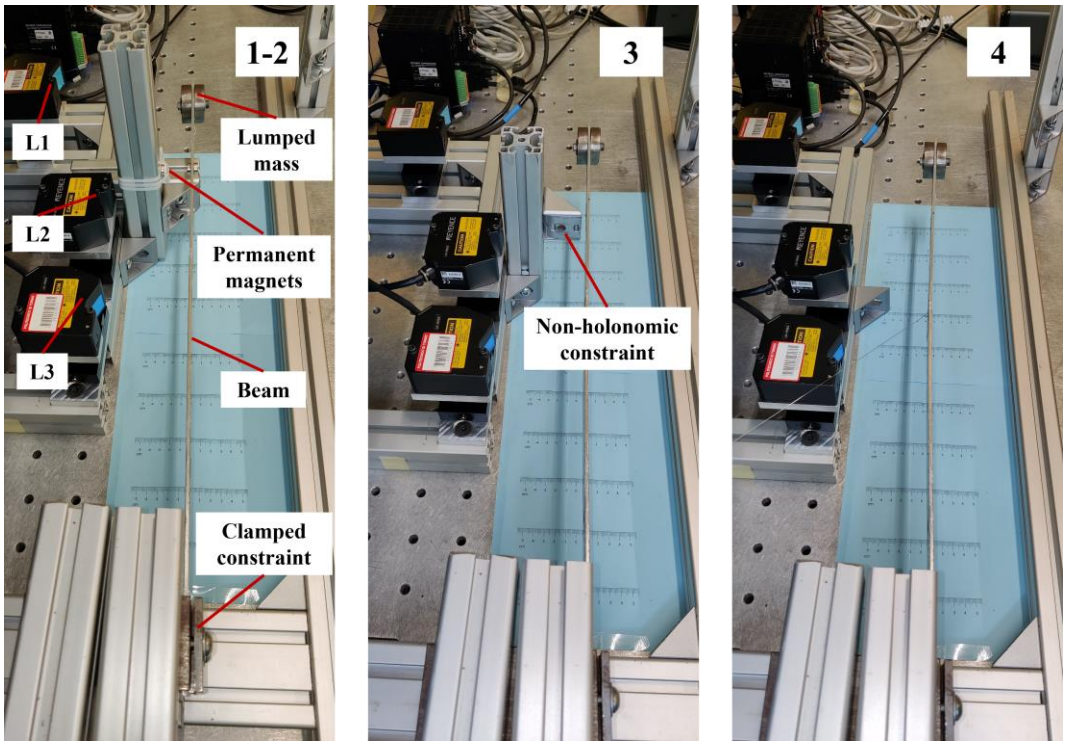

Figure 3.1.1 – Overview of the experimental setups of 2nd campaign.

The 1st set of tests differs from the 2nd for the absence of L3 and the position of the magnets with respect to the reference system.
In Figure 3.1.2 and Figure 3.1.3 are highlighted the most important dimensions of the test rig in conditions 1 (in configuration 2 the 30.5 mm dimension changes accordingly to Table 3.1.2.2) and 3 as well as the used reference system.

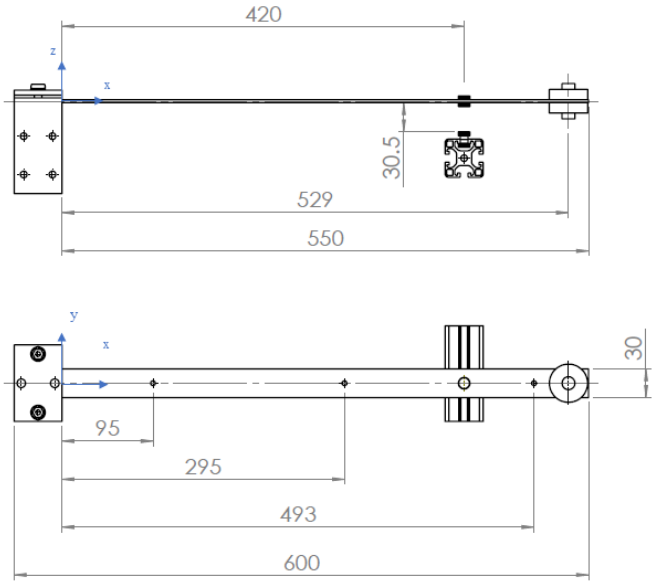

Figure 3.1.2 – Sketch of the nonlinear system in configurations 1 and 2 of 1st campaign, relevant dimensions are in millimeters.

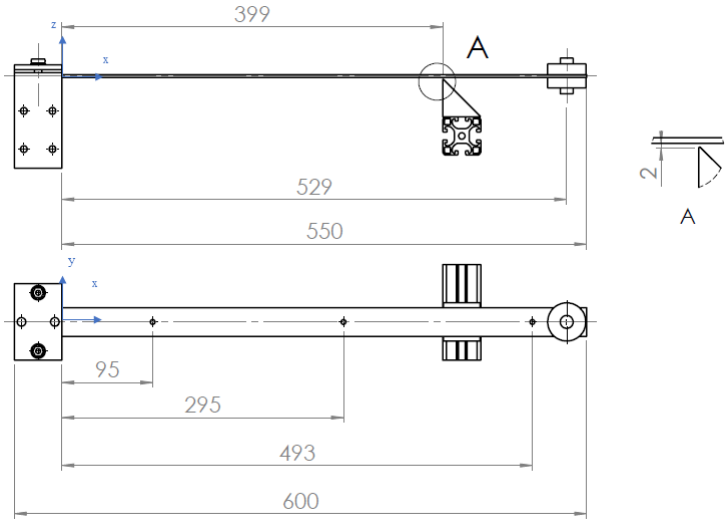

Figure 3.1.3 – Sketch of the nonlinear system in configuration 3 of 1st campaign, relevant dimensions are in millimeters.

As regards configuration 4, the system is the same with only the presence of the cantilever beam and the lumped mass at the right end. In Figure 3.1.4 there is a detail of the method used to fix the magnets to the support and a view from the top. Later these three magnets will be called as "Constraint magnets".

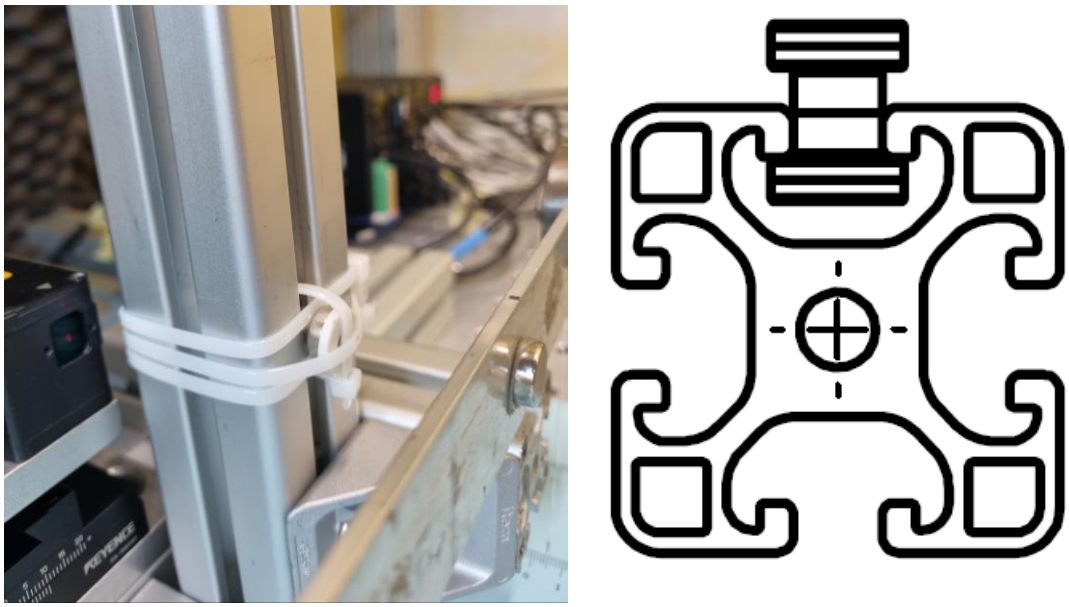

Figure 3.1.4 – Detailed views of the magnets used in configurations 1 and 2.

The excitation of the structure is performed with a wire that can be in two different positions:

- the hole near the lumped mass located at 493 mm from the clamp;
- the hole located at 295 mm from the clamp.

The reason of that is two excite separately the first two typical bending vibration modes of Euler beams: in particular the former introduces the system in a static deformation equivalent to the 1st mode shape and the latter to the one of the 2nd bending mode shape.
In order to excite the structure with only a non-null initial displacement the wire is tensed with one hand until the desired initial condition (IC) is reached with the help of the displacement of the laser L1 displayed in Test.Lab. Then the wire is locked and finally cut by a pair of scissors that permits to have null initial velocity thanks to the instantaneity of the action. Moreover, this choice has the advantage of being easily repeatable.
In addition to that it is important the tense the wire along the middle transversal plane of the beam, because in this way the torsional modes of the structure are not excited.
In Figure 3.1.5 is shown how the initial conditions are set.

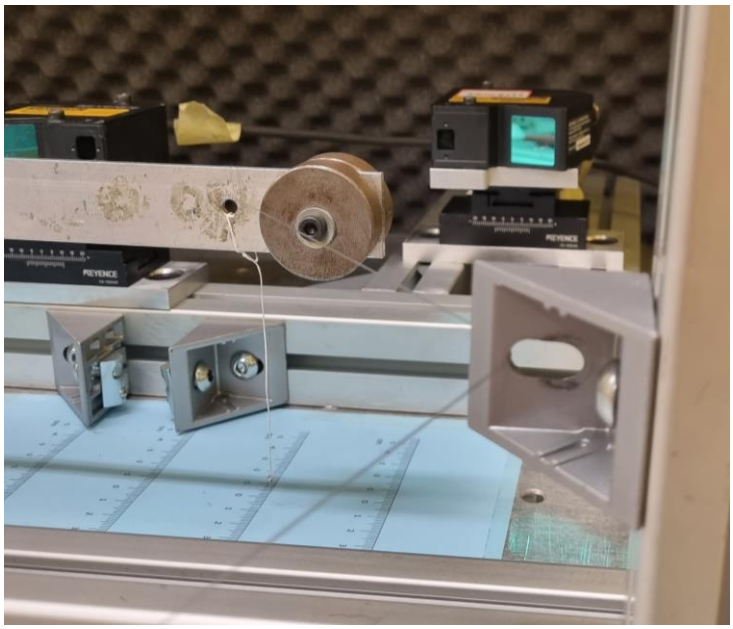

Figure 3.1.5 – View of the method to excite the system with the desired initial condition.

It is crucial to examine some aspects of the two used constraints.
As regards the clamp, it is made up by two steel parts secured by two screws. A great torsional stiffness is given by the four threaded rods that properly lock the system. Furthermore, the fact that the fastenings of the beam are located outside the area of the contact between the block and the extrusion bar makes the clamp more ideal and because the contact does not give more stiffness to the constraint.
While the non-symmetric constraint has the attention that the contact with the beam includes all the length of the rounded edge as shown in Figure 3.1.6.

Figure 3.1.6 – Clamp (left), non-holonomic constraint non in contact (centre) and in contact (right).

The lasers measure the displacement of three points, that are, according to the reference system shown in Figure 3.1.3:

1. a point between the two constraints (x = 210 mm);
2. a point right before the non-holonomic constraint or the permanent magnets (x = 390 mm);
3. a point at the end of the beam on the lumped mass (x = 545 mm).

As said before, also a laser profilometer LX-J8900 is utilised in the 1st campaign. It is positioned at distance of 980 mm and fastened with a specific support to a table near the TestRig. It monitors the displacement of 12 fixed points, like displayed in Figure 3.1.7.
When the profilimeter was used, the TestRig only contained L1 and L2, because L3 had been added in the 2nd campaign.

Figure 3.1.7 – Measured points of the blade laser highlighted with a yellow mark.

The 2nd node is 65 mm far from the 1st one, that represent the clamp. Point 1 was not set at the end of the steel block of the clamp because the constraint is not ideal and maybe during the beam oscillation a little variation of the z-displacement at x = 0 mm position could happen.
Point 2 to 11 are progressively separated by a 40 mm distance, while the last point measures the displacement of the same point were the laser LK-H152 is pointed and so has a distance from the 11th node of 65 mm.
These points will have a proper name with a progressive number in paragraph § 3.3.3.

3.1.1 Experimental test definition and hardware

The 1D laser used are called L1, L2 and L3 according to Figure 3.1.
They are of the type LK-H082 and LK-H152 and shown in Figure 1.1.1, in which the clamp is on the left side.

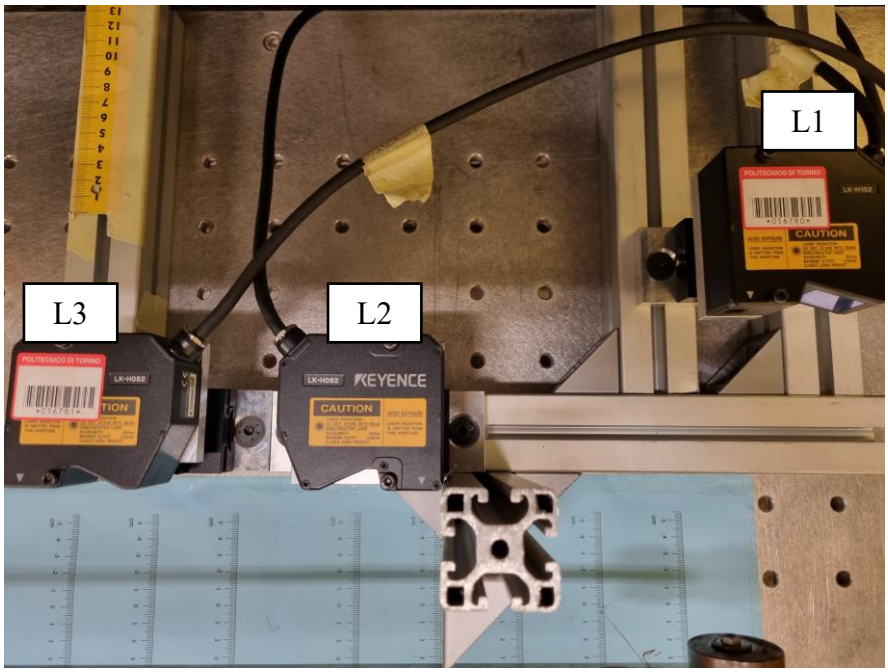

Figure 3.1.1.1 – Details of the lasers in configuration 3.

One crucial feature of these devices is that the range of motion of the measured points must stay within a certain range d indicated in the data sheet. Indeed their position has been decided on the base of the fact that the displacement of the point of the beam grows as the distance from the clamp increases.
The range of the measured motion of the lasers is described in Table 3.1.1.1.

Table 3.1.1.1 – Laser characteristics.

Label	Product name	Distance D [mm]	Range d [mm]	Sensitivity S [mV/mm]
L1	LK-H152	150	±40	250
L2	LK-H082	80	±18	555.56
L3	LK-H082	80	±18	555.56

The lasers are connected to a Siemens SCADAS and their sensitivity S must be set in the software Test.Lab in compliance to the margin of error $\Delta V = 20$ V of the output voltage, corresponding to ±10 V. Therefore the sensitivity is computed as:

$$S = \frac{\Delta V}{2\,d} \tag{3.1.1}$$

3.1.2 Geometry and weight of the used tools

When one has to deal with this experimental test should always remember to check the weights of the used objects.
In this case, they were measured with KERN ALJ 220-4NM and METTLER PM34-K DeltaRange and the results are shown in Table 3.1.2.1.

Table 3.1.2.1 – Weight and property of used object.

Item	Volume [mm^3]	Weight [g]	Material	Density [kg/m^3]	Young modulus [GPa]	Poisson ratio [-]
Constraint base	$38.147 \cdot 10^4$	2990.5	Steel	7800	200	0.3
Constraint plate	$2.4756 \cdot 10^4$	193.1	Steel	7800	200	0.3
Screws & washers	$0.2615 \cdot 10^4$	20.4	Steel	7800	200	0.3
Total Constraint	$40.884 \cdot 10^4$	3204.0	Steel	7800	200	0.3
Beam (600×30×3)	$5.3386 \cdot 10^4$	144.1	Aluminium	2699.2	69	0.33
Big disks	$2.4726 \cdot 10^4$	203.37	Steel	8225.0	200	0.3
Fasteners	$0.1219 \cdot 10^4$	9.51	Steel	7800	200	0.3
Total Lumped mass	$2.5945 \cdot 10^4$	212.88	Steel		200	0.3
Beam magnets (#2 Ø12h4)	904.779	7.1	NdFeB magnet	7800	200	0.3
Constraint magnets (#2 Ø12h4 and #1 Ø8h8)	1709.026	13.3	NdFeB magnet	7800	200	0.3

Notes:

- the volumes of “Constraint base”, “Constraint plate”, “Screws & washers”, “Fasteners” “Beam magnets” and “Constraint magnets” are computed indirectly from the weight and density;
- the volume of “Beam” is computed directly thanks to the dimensions reported in Figure 3.1.3 and considering 2 holes Ø5.5 and 1 hole Ø10.
- the volume of “Big disks” is computed directly thanks to the dimensions reported in Figure 3.1.2.1;

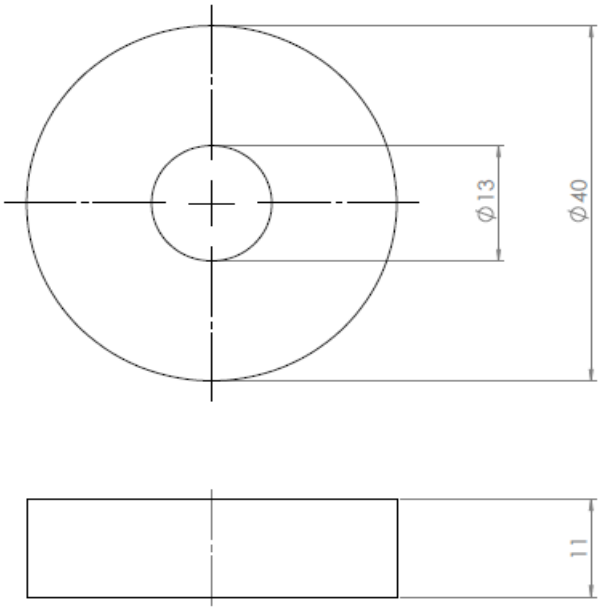

Figure 3.1.2.1 – Detail of one big disk making up the lumped mass.

- the volumes of “Total Constraint” and “Total Lumped mass” are calculated with the sum of their elements.

In Figures 3.1.2.2-4 are presented the photos of the weighings.

Figure 3.1.2.2 – Weighings of the clamp.

Figure 3.1.2.3 – Weighings of the beam.

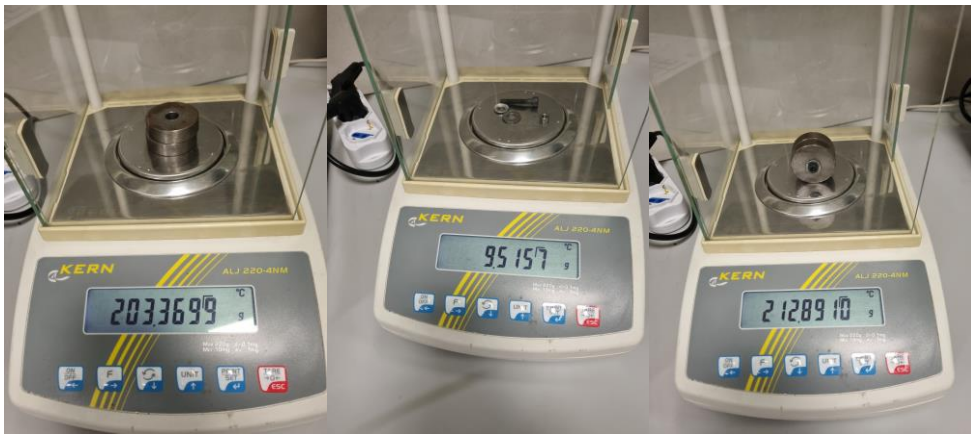

Figure 3.1.2.4 – Weighings of the lumped mass.

The dimensions of the used magnets are Ø12 h4 and Ø8 h8, where Ø stands for diameter and h for height.
Moreover, it can be useful to have a Table with every important point in terms of the Test Rig.

Table 3.1.2.2 – Geometry of I/O points.

Identifier	Exp. point	Model node	x [mm]	y [mm]	z [mm]
Lumped mass centre	P1	156	529	0	0
Non-holonomic constraint	P2	142	399	0	-3.5
Magnets centre in configuration 1	P3A	-	420	0	-30.5
Magnets centre in configuration 2	P3R	-	420	0	-34.23
Clamp	P4	100	0	0	0
Hole near lumped mass (1^{st} mode excitation point)	P5	near 152	493	0	0
Middle hole (2^{nd} mode excitation point)	P6	131	295	0	0
Laser L1 (mass)	L1	between 157 and 158	545	-2	-1.5
Laser L2 (contact, non-holonomic constraint, magnets)	L2	141	390	2	-1.5
Laser L3 (internal point)	L3	122	210	-7.5	-1.5

Model nodes come from the numerical simulations made in § 3.4.

3.1.3 Acquisition parameter settings

In LMS Test.Lab the parameters are displayed in Figure 3.1.3.1. The time acquisition changes at every experimental test and so it is not displayed.

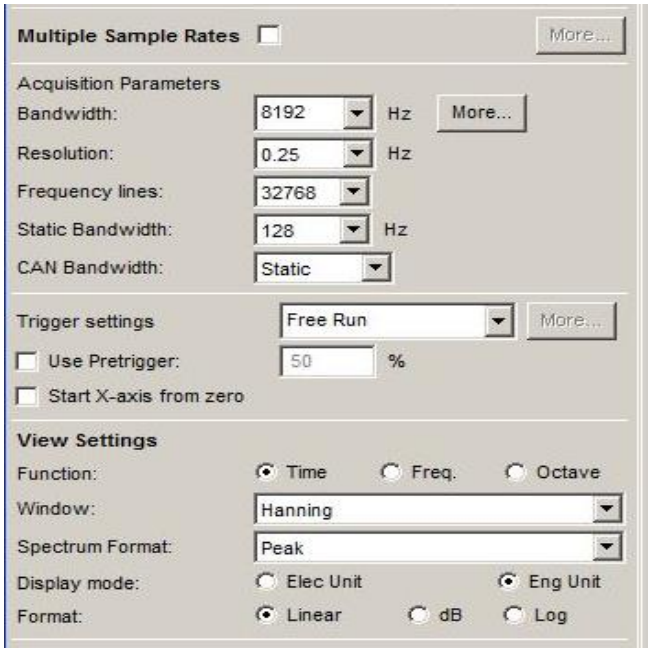

Figure 3.1.3.1 – Test.Lab parameters.

Notes, according to the nomenclature used in [10]:

- the sampling frequency is $f_s = 2 * f_b = 2*8192 = 16384$ Hz;
- the delta-time sample is $\Delta t = 1/16384 = 6.1035 \cdot 10^{-5}$ s;
- setting $f_s/2 = 8192$ Hz → direct relationship is $\Delta t = 1/(2*8192) = 6.1035 \cdot 10^{-5}$ s;
- e.g. case 1, BD2 (Table 3.2.1.1): acquisition time is 80 s, but the acquisition history starts from $t_1 = 3.92179 \cdot 10^{-5}$ s and ends at $t_N = 83.999972$ s. This enlargement of the time history is due to the future windowing of the signals and comes from the parameter "frequency resolution" of Figure 1.3.1, that is 0.25 Hz and corresponds to 4 s. This time is equally splitted and added at the start and at the end of the acquisition resulting in -2 s and 82 s, that are then translated into the values t_1 and t_N of the previous lines. The samples (number of lines in Test.Lab) are $N = 1376256$;
- relationship between 1st and last sample is $t_N = t_1 + (N\text{-}1) \cdot \Delta t$.

More details are shown in Figure 3.1.3.2.

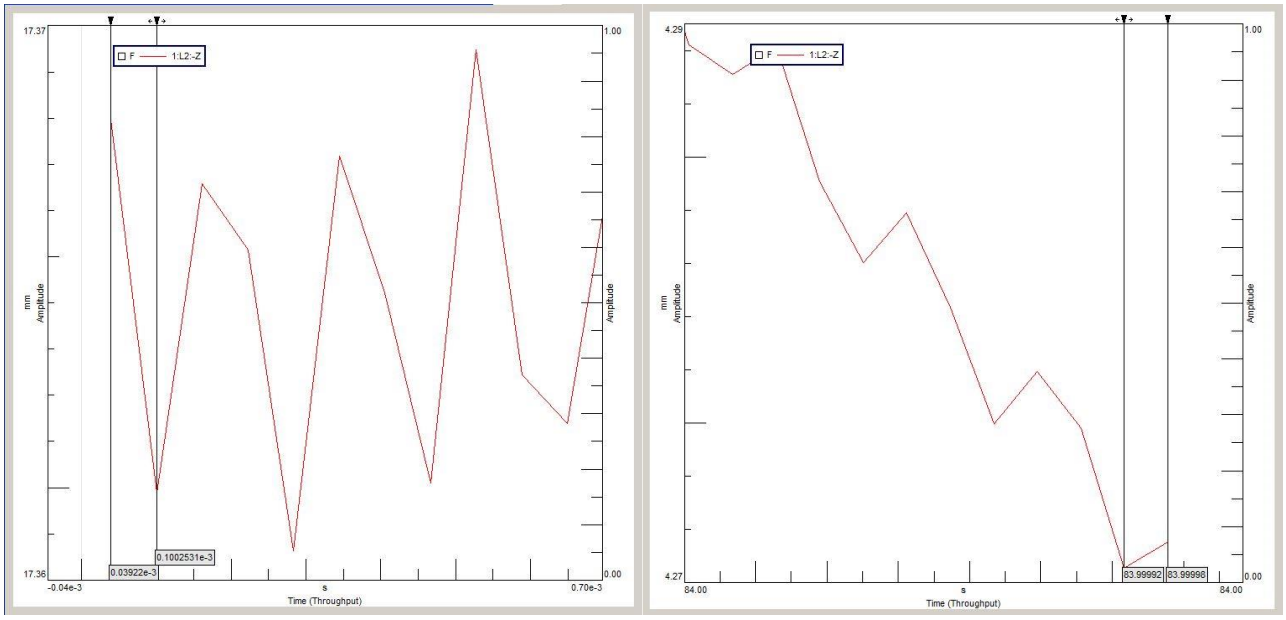

Figure 3.1.3.2 – Example of a Test.Lab acquisition.

It can be seen the values of t_1, t_2, t_N, t_{N-1}, that are consistent with the notes and the delta-time sample Δt.

3.2 Experimental data

Various tests have been carried out with different configuration of the TestRig and IC. Moreover, also the static deformations of the beam are calculated with the use of the lasers.

3.2.1 Experimental static and dynamic tests

In Table 3.2.1.1 are displayed the important data of the experimental tests. In the column "Description" are also written the points used to excite the motion of the beam and the type of test.

Table 3.2.1.1 – Experimental tests layout of 2nd campaign.

#Test	Label	L1 [mm]	L2 [mm]	L3 [mm]	Description	Acquisition Time [s]
1	BS1	+0.385	-1.72	-0.210	Static only beam	-
2	BS2	+0.385	-1.715	-0.21	Static only beam	-
3	BS3	+0.38	-1.715	-0.209	Static only beam	-
4	MaS1	+3.99	+0.57	+0.624	Static beam + attractive magnets	-
5	MaS2	+4.00	+0.57	+0.625	Static beam + attractive magnets	-
6	MaS3	+4.00	+0.57	+0.625	Static beam + attractive magnets	-
7	MaD1	-38.5	n/a	???	Dynamic beam + attractive magnets (P5)	~9
8	MaD2	-29.53	n/a	-6.598 (*)	Dynamic beam + attractive magnets (P5)	~12
9	MaD3	-29.5	n/a	???	Dynamic beam + attractive magnets (P5)	~11
10	MaD4	-29.5	n/a	???	Dynamic beam + attractive magnets (P5)	~14
11	MaD5	-20	???	???	Dynamic beam + attractive magnets (P5)	~10
12	MaD6	-7.76	-6.583 (*)	-1.904 (*)	Dynamic beam + attractive magnets (P5)	~34
13	MaD7	-7.7	???	???	Dynamic beam + attractive magnets (quasi-linear) (P5)	~211
14	MaD8	-2.8	???	???	Dynamic beam + attractive magnets (linearised behaviour) (P5)	~244
15	MrS1	-2.02	-3.17	-0.75	Static beam + repulsive magnets	-
16	MrS2	-1.99	-3.16	-0.755	Static beam + repulsive magnets	-
17	MrS3	-2.01	-3.155	-0.755	Static beam + repulsive magnets	-

18	MrD1	-9 (*)	???	???	Dynamic beam + repulsive magnets = MaD8 (P5)	~105
19	MrD2	-14	???	???	Dynamic beam + repulsive magnets (P5)	~206
20	MrD3	-25.63	-17.54 (*)	-5.802 (*)	Dynamic beam + repulsive magnets (P5)	~125
21	MrD4	-36	n/a	???	Dynamic beam + repulsive magnets (P5)	~167
22	BD1	-35	n/a	???	Dynamic only beam (P5)	~80
23	BD2	-25.3	-17.4 (*)	-5.7 (*)	Dynamic only beam (P5)	~84
24	BD3	-10	???	???	Dynamic only beam (P5)	~84
25	BD4	???	???	???	Dynamic only beam 1^{st}(P5)-2^{nd} modes (P6)	~77
26	BD5	-6.54 (*)	-2.26 (*)	1.93 (*)	Dynamic only beam 1^{st}(P5)-2^{nd} modes (P6)	~41
27	CD1	-35	n/a	???	Dynamic beam + contact (P5)	~39
28	CD2	-25	???	???	Dynamic beam + contact (P5)	~39
29	CD3	-10	???	???	Dynamic beam + contact (P5)	~33
30	CD4	-25.8	-17.7 (*)	-5.8 (*)	Dynamic beam + contact (P5)	~48
31	CD5	???	???	???	Dynamic beam + contact 2^{nd} mode (P6)	~33
32	CD6	-25	???	???	Dynamic beam + contact 1^{st}(P5)-2^{nd} modes (P6)	~35

Notes:

- (*) means “data calculated thanks to the output of the time-histories”;
- in BD5 the supposed L1 IC was -12 mm, but the real acquired measure is -6.54 mm;
- tests that have “Static beam” in “Description” were performed to calculate the static deformation of the beam in the acquired point, so they have not a “Acquisition time”.

3.3 Post-processing results

The data coming from Test.Lab are organised in a MATLAB struct which contains information about time sampling and the actual measurements of the lasers. Time is partitioned with a constant delta-time sample. With the use of the acquired data, it is also possible to fill the missing cells of Table 3.2.1.1 because in the making of the most of experimental tests, only the IC of the Laser L1 has been controlled. In the post-process of the tests are analysed the time histories and the time-frequency contents obtained with both FFT and wavelet method.
Unfortunately, during the postprocessing of the 2nd campaign, it has been discovered that the data acquired by the point lasers are filtered with a low-pass filter that deletes all the information related to frequencies higher than 40÷45 Hz. This happened because of some settings of the devices that were not changed before the preparing of the test setup. Despite this certainly unwanted alteration of the measurements, the tests were analysed.
Luckily, this filter did not happen for the profilometer acquisition, that will be deepened in § 3.3.3.

3.3.1 Analysis of BD2, BD5 and CD4

The first test regards configuration four and an excitation that strongly reproduces the classic 1st mode shape of a cantilever beam. Even if the IC of L1 is about -25.3 mm, it is not enough to cause a visible softening phenomenon that occurs when it is not possible to ensure the small-oscillation simplification. Indeed the time-frequency analysis of the measured signals show a continue line at about 3 Hz, which is the first natural frequency of the system, like can be seen in Figure 3.3.1.1.

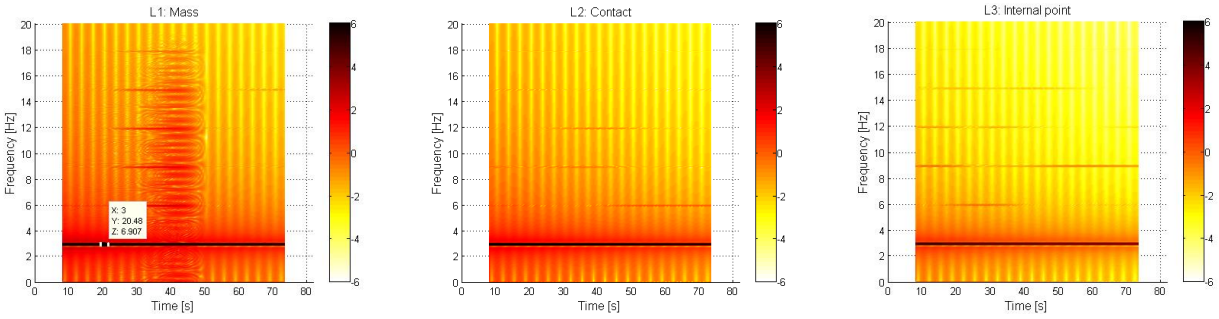

Figure 3.3.1.1 – Time-frequency contents of BD2.
From left to right L1, L2 and L3 are displayed.

To be more precise, with higher frequency resolution the 1st natural frequency is 2.97 Hz, as displayed in Figure 3.3.1.2.

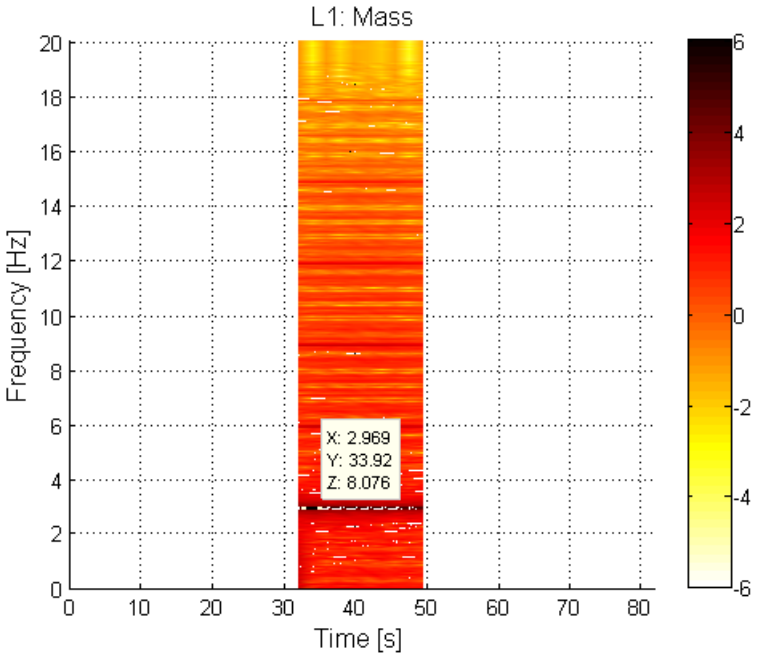

Figure 3.3.1.2 – Zoom of time-frequency content of L1 of BD2.

As can be seen there are two unexpected non-linearity symptoms:

1. superharmonics in L1 multiples of 2.97 Hz, that disappear after about 50 s. This happens because from that instant on, the small-oscillation simplification can be done as a consequence of the decreased amplitude of the oscillations, as shown in Figure 3.3.1.3. This kind of phenomenon will be also visible in BD5 and another explanation will be written using Figure 3.3.1.11;

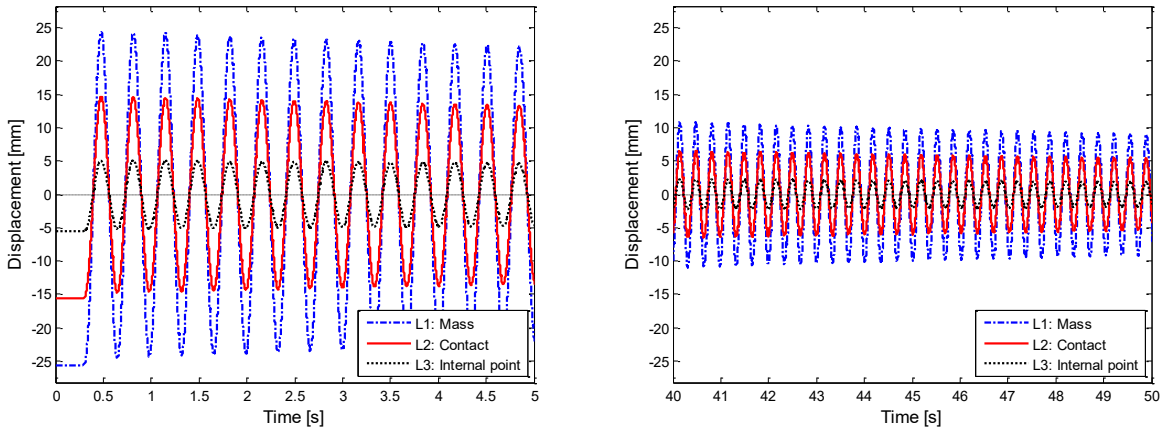

Figure 3.3.1.3 – Time-history of BD2 acquired displacements
0-5 s (left) and 40-50 s (right).

2. in the first 3 superharmonics of L2 and L3 it is clearly visible that the frequency contributions are alternated between the two lasers. But this is not imputable to the mode-shape of 1st natural frequency since the hole beam moves in phase. Indeed it can be interpreted as the so-called “energy path”, which is a typical phenomenon of nonlinear structures that shows internal resonances. A detail of this can be found in Figure 3.3.1.4

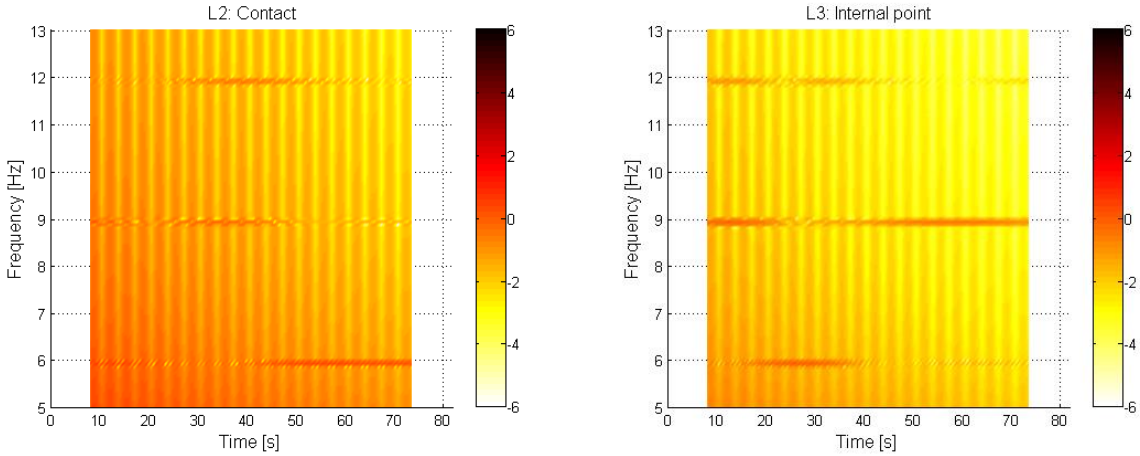

Figure 3.3.1.4 – BD2 Time-frequency contents between 5 and 13 Hz of L2 (left) and L3 (right).

In Figure 3.3.1.5 are shown the time-frequency analysis with the wavelet.

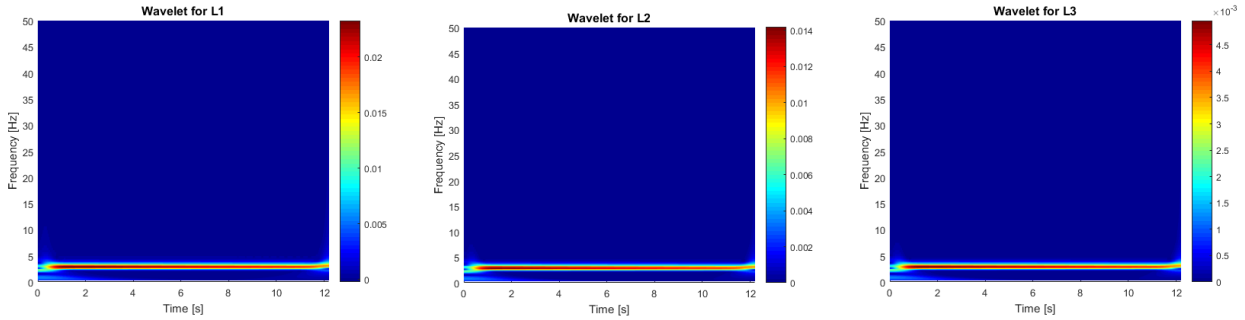

Figure 3.33.1.5 – Time-frequency contents with wavelet of BD2. From left to right L1, L2 and L3 are displayed.

The 3 acquisitions do not highlight any significant distinction but share a good vision of the softening effect owed to the big oscillations, that it presented in Figure 3.3.1.6.

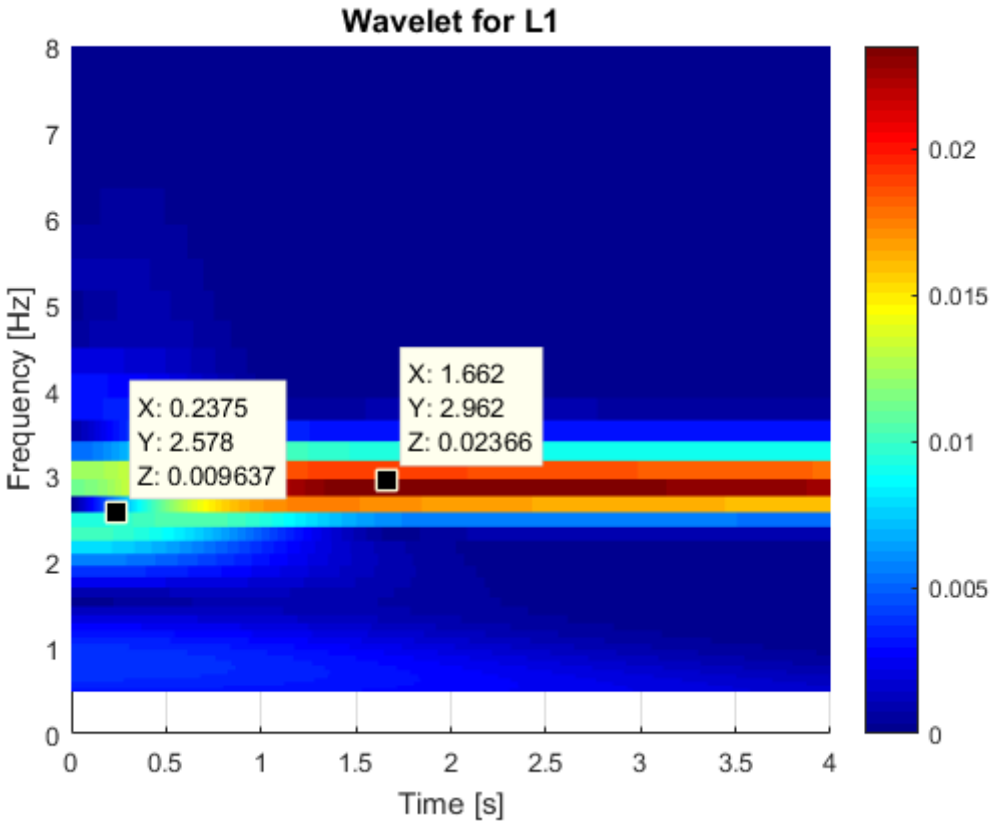

Figure 3.3.1.7 – Detail of the softening effect of BD2 L1.

It is impressive to see how the wavelet analysis is more able to catch this effect than the FFT approach.

Concerning BD5, the excitation is provided through the tension of two wires coming from points P5 and P6, in order to excite both the 1st and the 2nd natural frequencies of the system.
Actually, this excitation results effective as can be seen the first seconds of acquisition and in Figure 3.3.1.8.

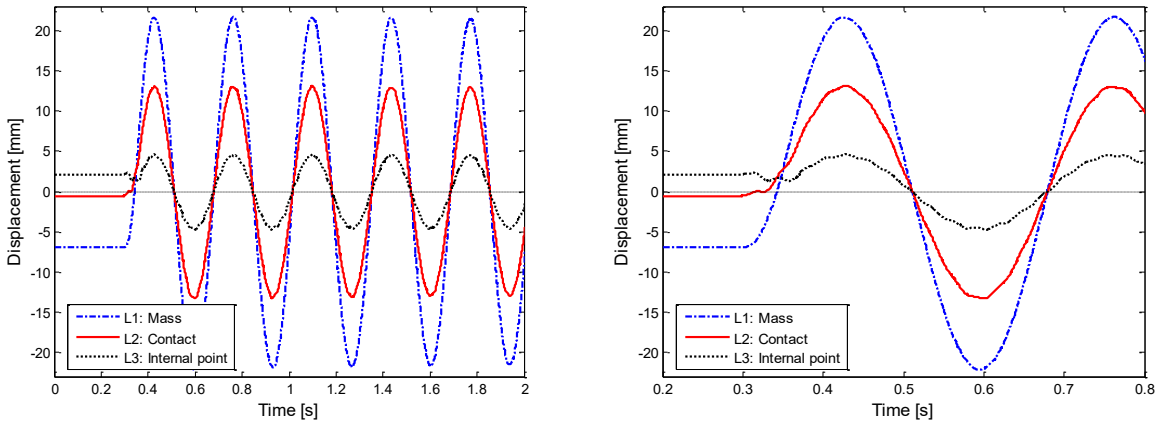

Figure 3.3.1.8 – Time-history of BD5 acquired displacements
0-2 s (left) and 0.2-0.8 s (right).

It is clear how in the starting instants of motion, L3 moves in opposition of phase with respect to the other lasers. Moreover L3, has two high harmonic contributions: the one of the first mode like the rest of the beam and the one of the 2nd mode, because this mode shape particularly shows remarkable displacements of this point.
As regards time-frequency contents, they confirm this interpretation. The results are shown in Figure 3.3.1.9.

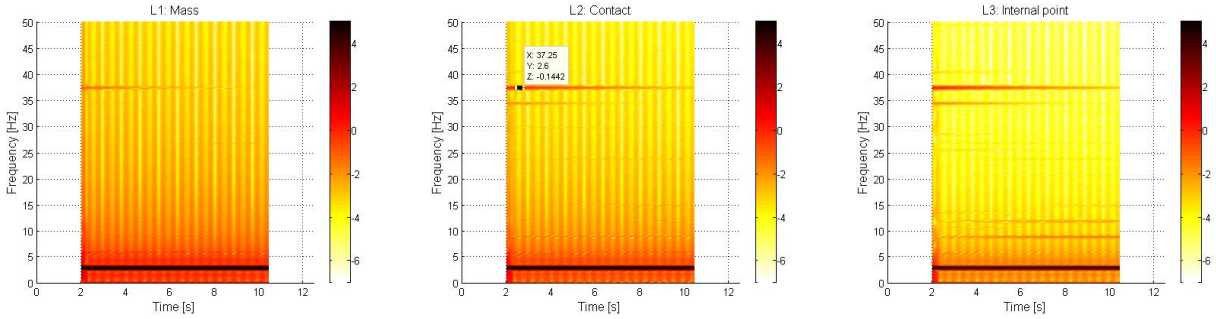

Figure 3.3.1.9 – Time-frequency contents of BD5.
From left to right L1, L2 and L3 are displayed.

It is possible to recognise the 2nd resonance frequency, appearing at 37.25 Hz, that is in agreement with Table 3.4.3. The value depends on the added lumped mass at the end of the beam. If no added mass is considered, from theory the 2nd resonance frequency should be 6.276 times the 1st one at 2.97 Hz, hence at 18.64 Hz.
This 2nd frequency is noticeable with the wavelet as well but with a minor precision, like can be seen in Figure 3.3.1.10.

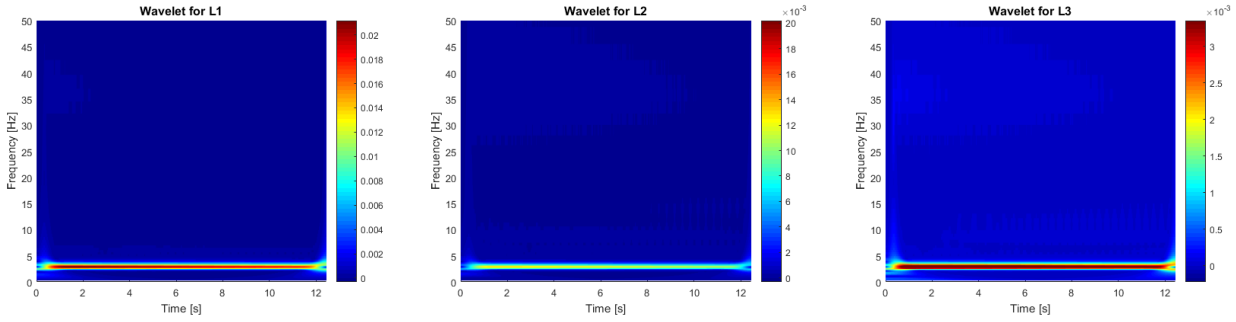

Figure 3.3.1.10 – Time-frequency contents with wavelet of BD5.
From left to right L1, L2 and L3 are displayed.

As regards the superharmonics, it is worth to analyse Figure 3.3.1.11, containing a zoom of the wavelet analysis and time history in a short time range.

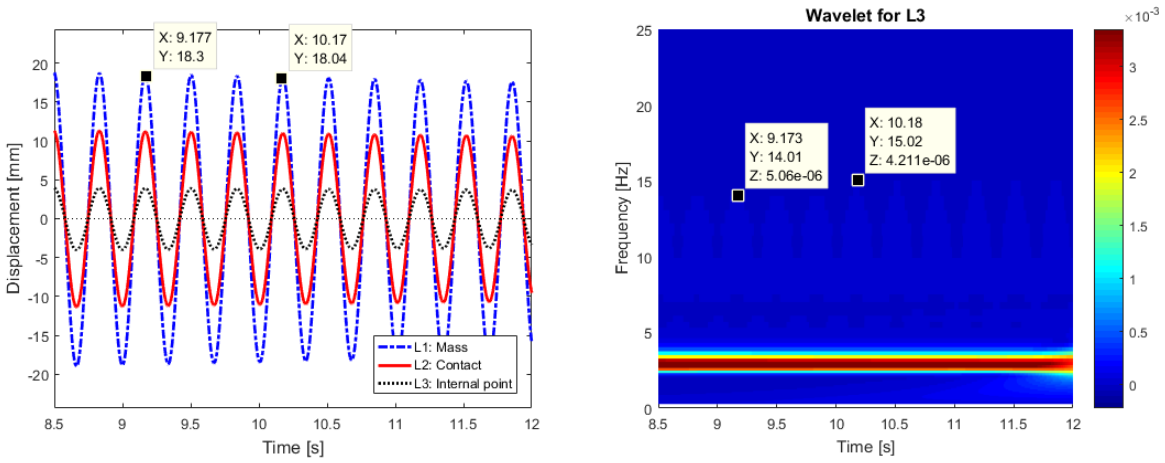

Figure 3.3.1.11 – Detail of time-history and wavelet analysis for BD5 L3.

It is clear that the instants when the presence of the superharmonics is more pronounced is when the beam has the maximum displacements, and it is near to the lasers. This could be a hint of the fact that the superharmonics are caused by the measurements themselves because the lasers acquire points that are on the surface of the beam, but these acquisitions are attributed to the point of the neutral plane. With a great probability, the questioned event would not have happened, if six lasers had been used, with three devices facing the other ones. In this way, the average on the acquisition could have been more exact and representative of the behaviour of the longitudinal axis of the beam.

With the FFT approach, it can be spotted a typical nonlinear phenomenon: the linear combination of the resonances. To be more specific, there are two symmetric contributions (called "sidebands") at ±3 Hz (basically the value of the fundamental) distance from the 2nd natural frequency in L2 and L3, as can be seen in Figure 3.3.1.12.

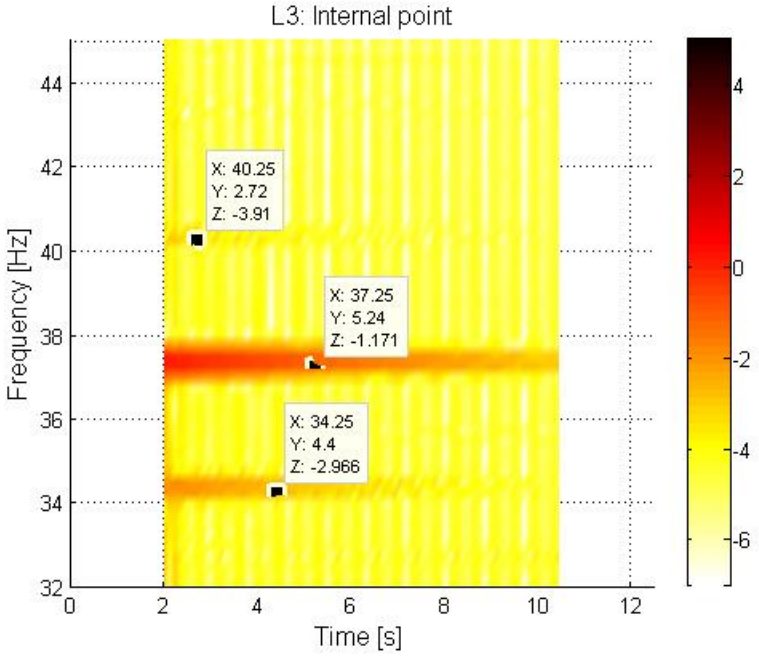

Figure 3.3.1.12 – Detail of BD5 L3 and combination of resonances.

The next experimental test to be analysed is CD4, which matters the 3rd configuration with an initial deformed shape that is related to the 1st cantilever beam mode shape.
In Figure 3.3.1.13 is shown the time-history of the acquired displacements by the lasers in the first 10 s of acquisitions and a detail of the initial instants.

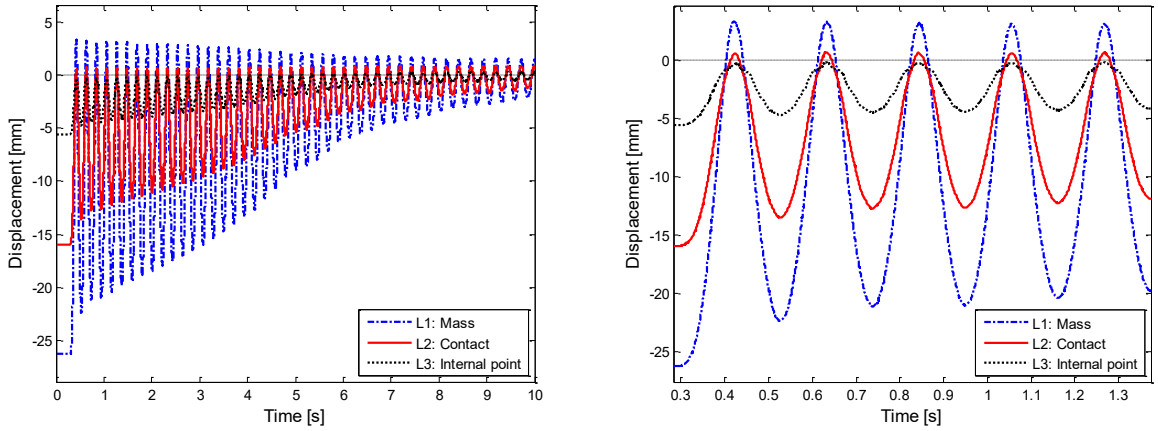

Figure 3.3.1.13 – Time-history of CD4 acquired displacements
0-10 s (left) and 0.3-1.3 s (right).

It is evident that the initial parts of the signals have an oscillation frequency bigger than the remaining part. This happens because there is the contact with the non-holonomic constraint producing a mean major stiffness of the structure and therefore bigger mean resonance frequencies. For further details, the non-holonomic constraint produces an equivalent linearised system with higher resonance frequencies only for a part of the period where the additional contact acts, while in the other part the beam has no additional contact and its natural frequencies are lower. Due to the spectrogram approach a mean value of its natural frequencies can be captured.
In addition to that, L3 appears to have two main harmonic contributions.
To better understand these graphs, in Figure 3.3.1.14 are presented the time-frequency contents of this experimental test.

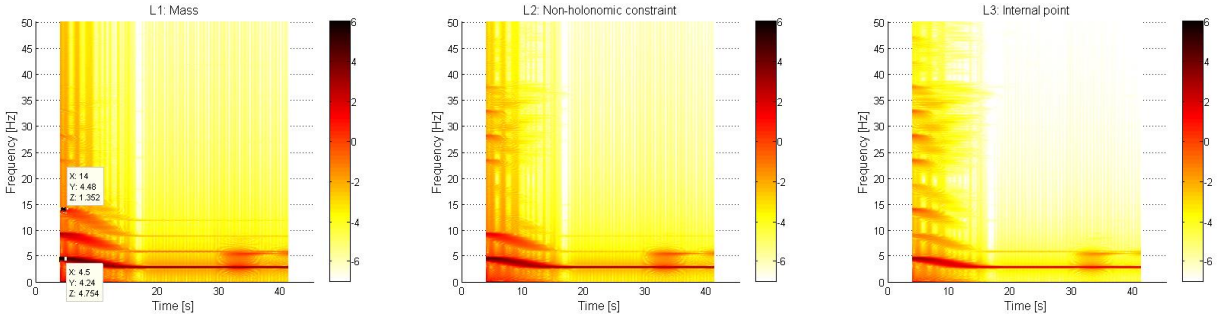

Figure 3.3.1.14 – Time-frequency contents of CD4.
From left to right L1, L2 and L3 are displayed.

The analysis of Figure 3.3.1.14 should be splitted into 2 parts:

- the first 15 s of acquirement: this zone appears to be transition zone where the main frequency contribution slowly changes from 4.5 Hz to 2.97 Hz. Moreover, a typical superharmonic that doubles the value of this main frequency is present. The contribution at 14 Hz is not a superharmonics but it is the 1st natural frequency of configuration 3 (clamped-pinned beam) and it is noticeable only in L1 and L3, since L2 is literally next to P2. Probably a lot of superharmonics of L3 are detected owing to a strong interaction between 2

or 3 natural frequencies of the two linearised systems involved. Furthermore, there also contribution of frequency for L3 that are bigger than 50 Hz, that are possibly related to the 2nd mode of configuration 3, as can be seen in Figure 3.3.1.15.

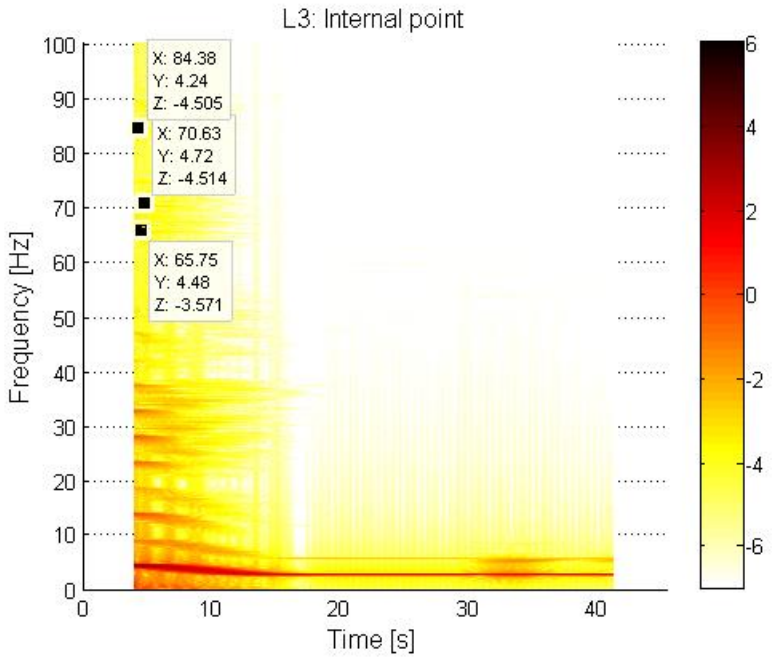

Figure 3.3.1.15 – Detail of CD4 L3.

- the remaining part: the unique participating frequency is 2.97 Hz and its superharmonics are less significant. This event is increasingly remarkable as the measured point becomes nearer to the right end of the beam. That occurs because the values of the displacements progressively grow.

The wavelet method is also utilised, and the results are shown in Figure 3.3.1.16.

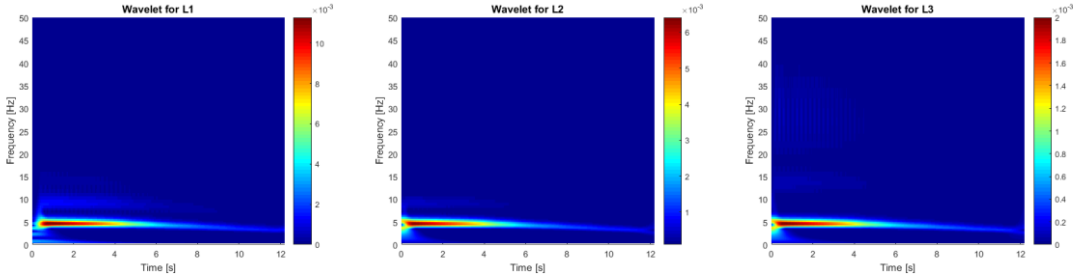

Figure 3.3.1.16 – Time-frequency contents wavelet method of CD4.
From left to right L1, L2 and L3 are displayed.

Here in L3 is visible the already discussed frequency at 14 Hz, the 2nd superharmonic of the fundamental where the contact is present and the evident decrease of the 1st natural frequency of the system.
The frequency contents with this approach for L3 ends at about 40 Hz.

3.3.2 Analysis of MaD2, MaD5 and MrD3

This part is dedicated to three experimental tests with the magnets. The first 2 are related to configuration 1 and the latter to configuration 2.

Concerning MaD2, time-history is presented in Figure 3.2.1.

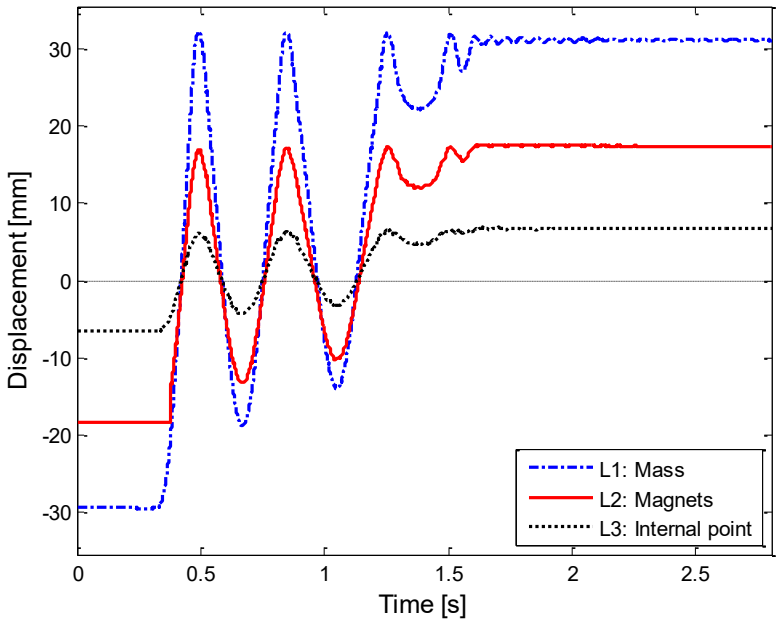

Figure 3.3.2.1 – Time-history of MaD2 acquired displacements.

In this test, the three lasers highlight an in-phase deformed shape, that involves thinking that the beam moves according to its new 1st natural frequency, as supported by the fact that the excitation is only provided through point P5.
The time-history is this short because after 1.2 s of oscillation the beam became stuck to the magnets. Moreover, in first seconds of acquisition L2 is in overload.
Afterwards, time-frequency contents are exhibited in Figure 3.3.2.2.

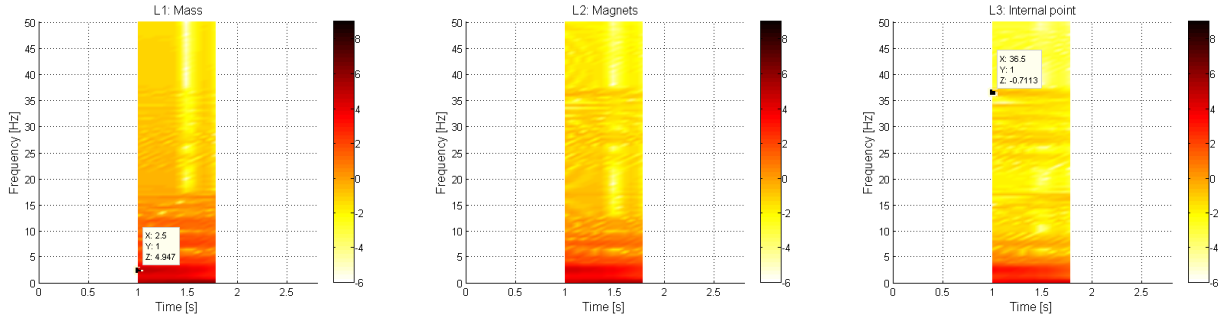

Figure 3.3.2.2 – Time-frequency contents of MaD2.
From left to right L1, L2 and L3 are displayed.

The marked frequencies are the natural frequencies in condition 1: as one would expect they appear to be slightly lower than the other cases because the attractive magnets make the period of

oscillation become higher and as a consequence a decrease of natural frequencies, resulting in a softening effect.

The analysis with the wavelet method is displayed in Figure 3.3.2.3.

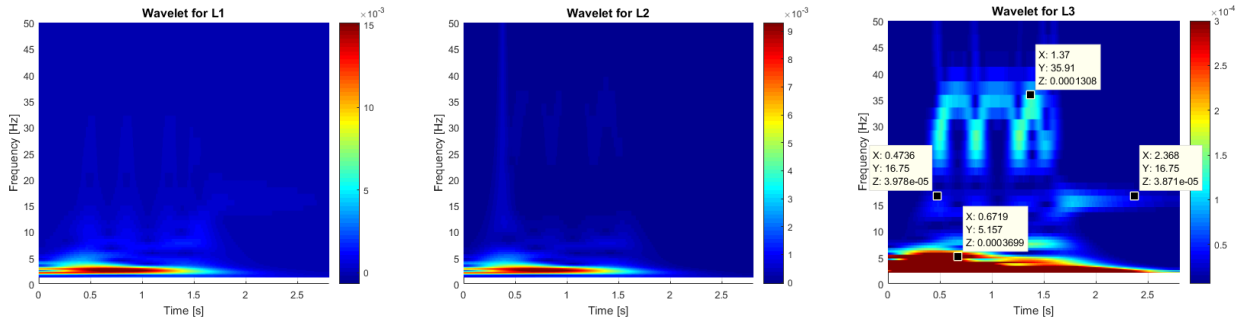

Figure 3.3.2.3 – Time-frequency contents wavelet method of MaD2.
From left to right L1, L2 and L3 are displayed.

The decrease of the natural frequency is clearly noticeable here as well. Moreover, the wavelet analysis better highlights the superharmonics when the beam oscillates.
As regards L3, it can be noticed something related to when the structure hits and leaves the magnets: in the instants of contact the beam can be assimilated to a clamped-pinned beam and so a frequency of 16.75 Hz, that incredibly resembles the first natural frequency of configuration 3 (Table 3.4.3), is visible. This frequency content also continues when the magnets are attached.
While, in the part of the oscillation when the beam is not attached to the magnets, a heavy line at about 36 Hz is present, constituting the 2nd resonance frequency of configuration 3. The values described are probably different from the ones of Table 3.4.3 because of the presence of the magnets.
This kind of alternated frequency contents will be deepened in § 3.3, when the analysis of a configuration 3 test of the first campaign is analysed.
The peak visible in L2 at about 0.4 s is related to the overload phenomenon, as the time-history of Figure 3.3.2.1 confirms.

As regards test MaD6, the given IC was intended to do not make the beam attach to the magnets in order to observe the aspects of a long oscillation time. Some of these features are visible in the time-history of Figure 3.3.2.4

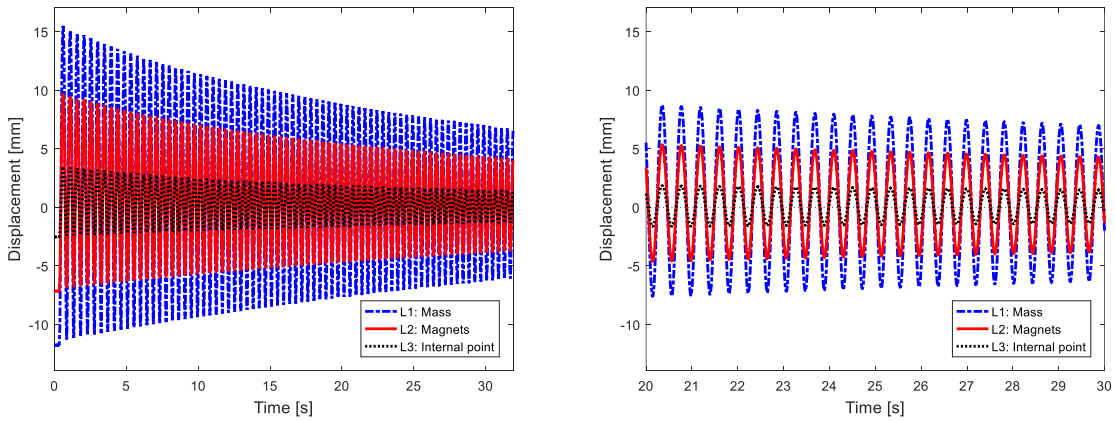

Figure 3.3.2.4 – Time-history of MaD6 acquired displacements
0-32 s (left) and 20-30 s (right).

Here it is evident the phenomenon of the drift, that makes the points of the beam to oscillate around a value that is not 0 mm. This effect is clearer for L1, since the oscillations are bigger.
Time-frequency contents are highlighted in Figure 3.3.2.5.

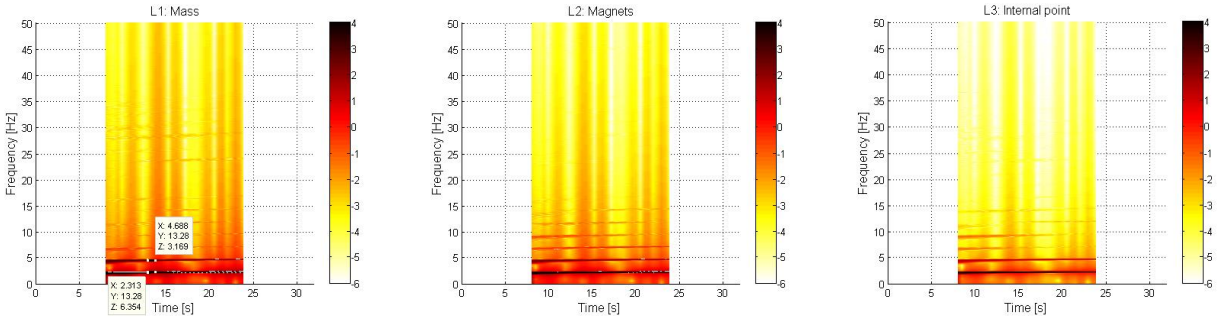

Figure 3.3.2.5 – Time-frequency contents of MaD6.
From left to right L1, L2 and L3 are displayed.

Every laser shows a strong superharmonic of order 2 of 1st natural frequency, which can be spotted more precisely, and it is 2.3 Hz. The fact that only the superharmonics of pair order are present, was predictable due to the deep asymmetry of the system. Moreover, the "energy path" is visible but in minor way than BD2.

Even the wavelet method catches the strong 2nd superharmonic in every laser, like shown in Figure 3.3.2.6.

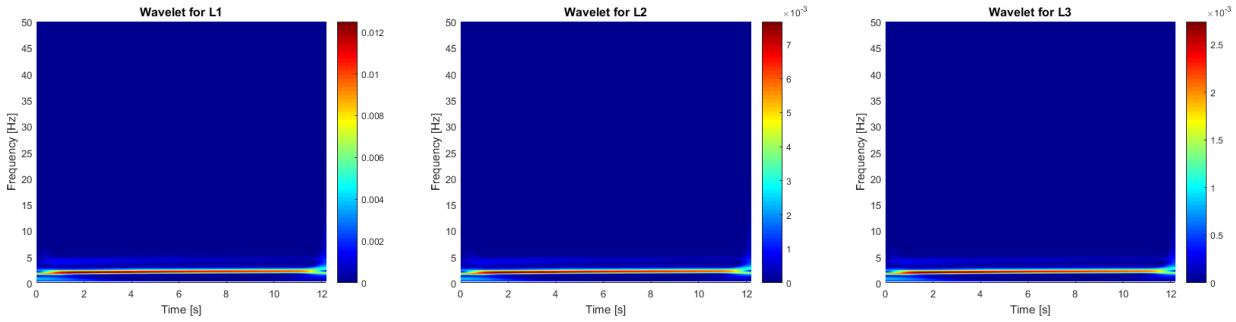

Figure 3.3.2.6 – Time-frequency contents wavelet method of MaD6.
From left to right L1, L2 and L3 are displayed.

The value of the natural frequency is 2.16 Hz in wavelet as can be seen in Figure 3.3.2.7.

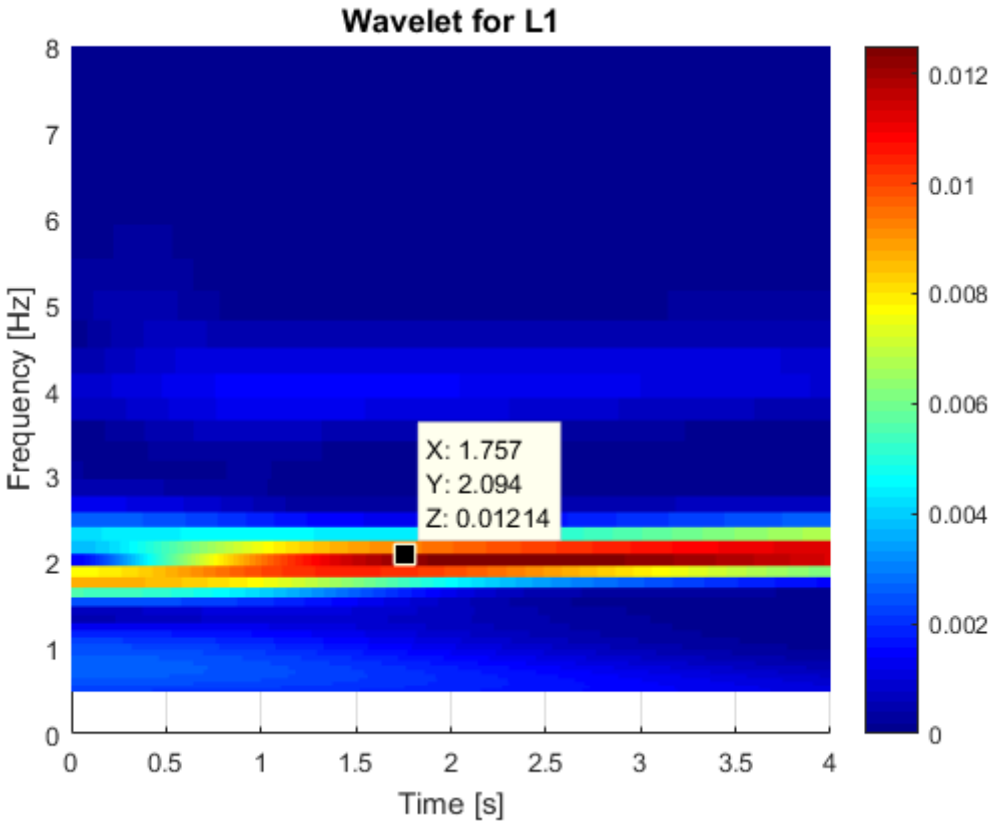

Figure 3.3.2.7 – Zoom of wavelet analysis of MaD6 L1.

The last test to deepened in this paragraph is MrD3, that involves repulsive magnets, i.e. configuration 2.
What is expectable to notice in the time-histories is an opposite drift of the trajectory with respect to condition 1.

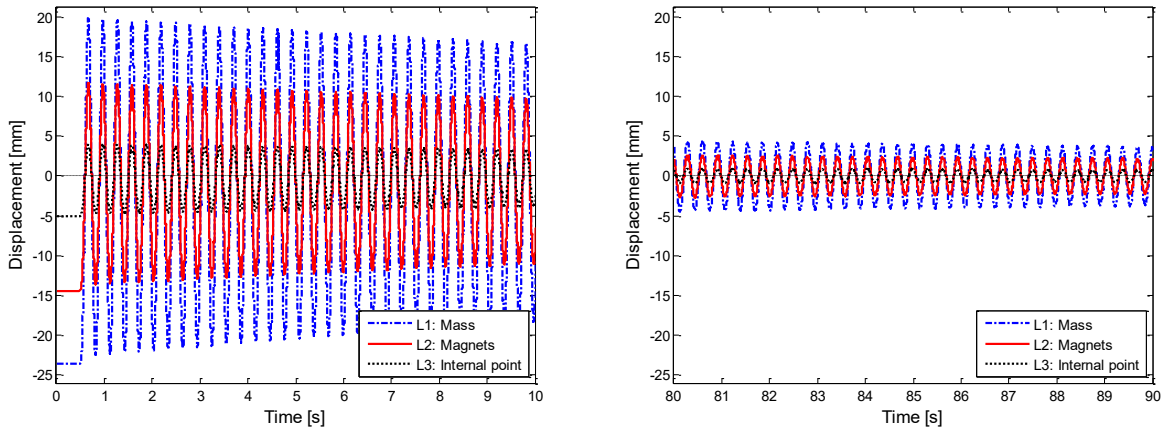

Figure 3.3.2.8 – Time-history of MrD4 acquired displacements
0-10 s (left) and 80-90 s (right).

While the time frequency analysis in Figure 3.3.2.9 shows a hardening phenomenon indeed the 1st natural frequency becomes 3.27 Hz while in configuration 4 is 2.97 Hz. Moreover a strong presence of the superharmonics, especially the 2nd order one, is remarkable.

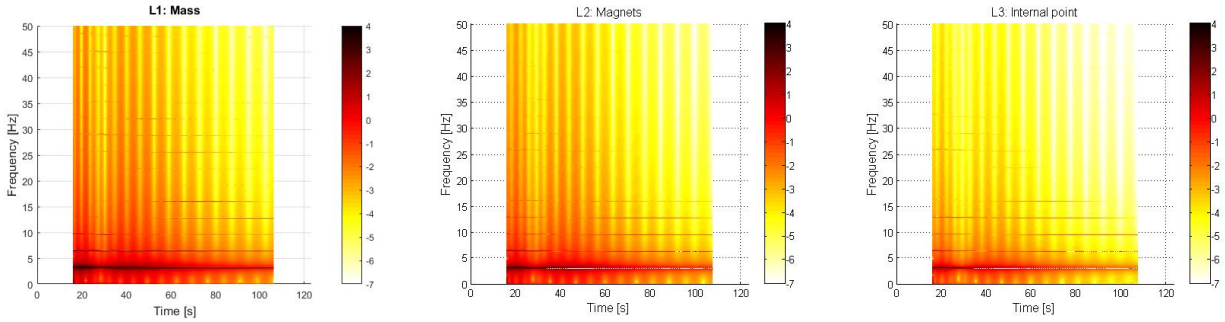

Figure 3.3.2.9 – Time-frequency contents of MrD3.
From left to right L1, L2 and L3 are displayed.

As concerns the wavelet, the results are shown in Figure 3.3.2.10.

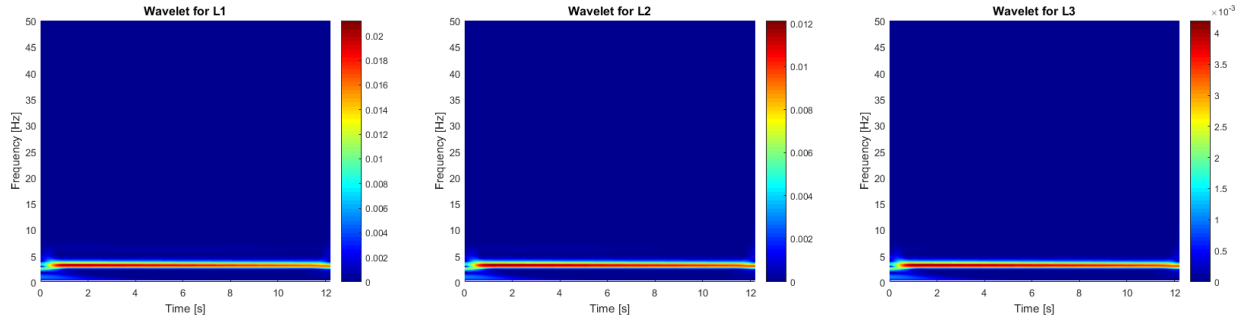

Figure 3.3.2.10 – Time-frequency contents wavelet method of MrD3.
From left to right L1, L2 and L3 are displayed.

The 2nd harmonic is visible, as well as a natural frequency that is bigger than configuration 4, that is shown in Figure 3.3.2.11.

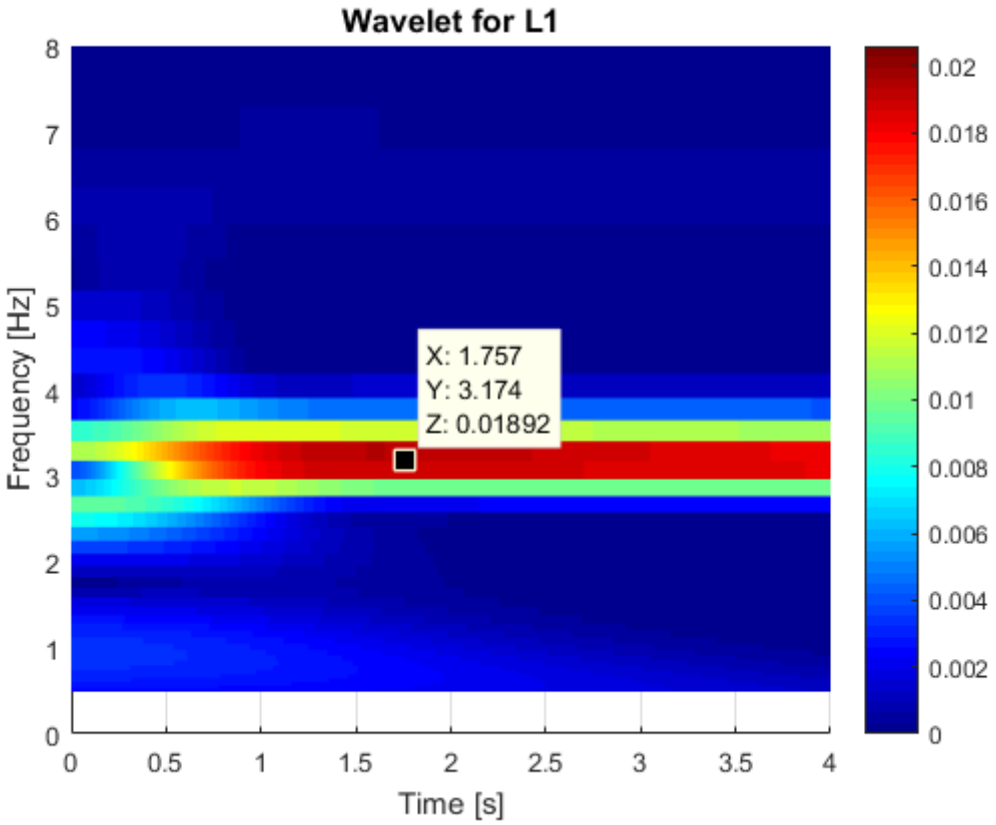

Figure 3.3.2.11 – Zoom of wavelet analysis of MrD3 L1.

3.3.3 Analysis of 1st campaign

It is useful to describe how the setups changes moving back to this configuration.
L1 and L2 are the same of campaign 2.
The important points are reported in Table 3.3.3.1.

Table 3.3.3.1 – Geometry of I/O points of 1st campaign.

Identifier	Exp. point	Model node	x [mm]	y [mm]	z [mm]
Lumped mass centre	P1	156	529	0	0
Non-holonomic constraint	P2	142	399	0	-3.5
Magnets centre in configuration 1	P3A	-	420	0	-43.4
Clamp	P4	100	0	0	0
Hole near lumped mass (1st mode excitation point)	P5	near 152	493	0	0
Middle hole (2nd mode excitation point)	P6	131	295	0	0
Laser L1 (mass)	L1	between 157 and 158	545	-2	-1.5
Laser L2 (contact, non-holonomic constraint, magnets)	L2	141	390	2	-1.5
LP1	LP1	201	-25	0	-1.5
LP2	LP2	104	40	0	-1.5
LP3	LP3	108	80	0	-1.5
LP4	LP4	113	120	0	-1.5
LP5	LP5	117	160	0	-1.5
LP6	LP6	121	200	0	-1.5
LP7	LP7	125	240	0	-1.5
LP8	LP8	129	280	0	-1.5
LP9	LP9	134	320	0	-1.5
LP10	LP10	138	360	0	-1.5
LP11	LP11	142	400	0	-1.5
LP12	LP12	146	440	0	-1.5
LP13	LP13	150	480	0	-1.5
LP14	LP14	between 157 and 158	545	0	-1.5

Note:

- z coordinate of P3A has been calculated in the postprocessing since a measurement of the static deformation of the magnets had not been done. The calculus exploited the fact that the laser L2 kept on staying at a distance of 80 mm from the beam in the 2 configurations. Moreover, the static offset of the laser has been calculated using MATLAB function DigFilt and the vertical extrusion beam containing the constraint magnets moved towards the beam of 10 mm in the 2nd campaign.

- the acquisition of the profilometer last for 20 s. The desired IC is set with the use of the point laser, as described before.

The analysed experimental tests are displayed in Table 3.3.3.2.

Table 3.3.3.2 – Experimental tests layout of 1st campaign.

#Test	Label	L1 [mm]	L2 [mm]	Description	Acquisition Time [s]
1	CD1	-18.53	-11.4 (*)	Dynamic beam + contact (P5)	20
2	MaD1	-19.68	-11.99 (*)	Dynamic \beam + attractive magnets (P5)	20
3	BD1	-15.8	-9.63 (*)	Dynamic only beam (P5)	20

The first test to be deepened is CD1. Just by taking a look at the time-histories acquired it is evident that the data coming from the point lasers are filtered, as can be seen in Figure 3.3.3.1. Only the profilometer acquisition will be deepened because of this.

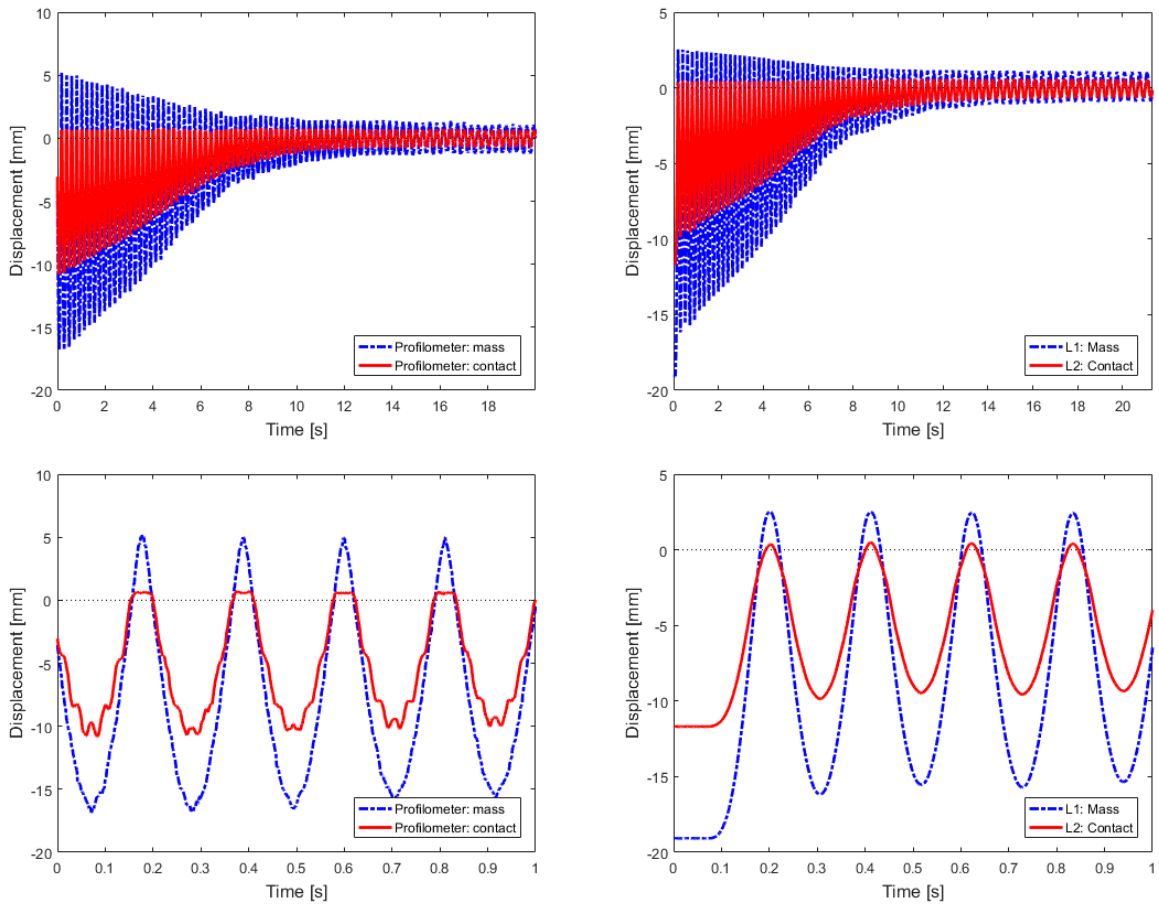

Figure 3.3.3.1 – Comparison of the time-histories of CD1.
In a clockwise direction are respectively displayed profilometer and point laser acquisitions and a zoom of the starting instants of their measurements.

The fact that L1 has the first oscillation peak different from LP14 is owed to the imperfect contemporaneous beginning of the acquisition of the devices.
The 2nd distinction between the 2 time-histories is the different envelop that goes through the maximums of the oscillations of LP14 (left) and L1 (right). The reason of that is the unwanted filtering phenomenon that marked the point laser acquisitions.
As regards the time-frequency contents, it is worth to remind that the points are called LP14 and LP11 and are not exactly coincident with L1 and L2.

In Figure 3.3.3.2, that includes the time-frequency contents of CD1, which is equivalent to experimental test CD4 of 2nd campaign, it is more visible the 1st frequency transition that occurred in Figure 3.3.1.9. Also in Figure 3.3.3.2 the superharmonics of the fundamental are visible.

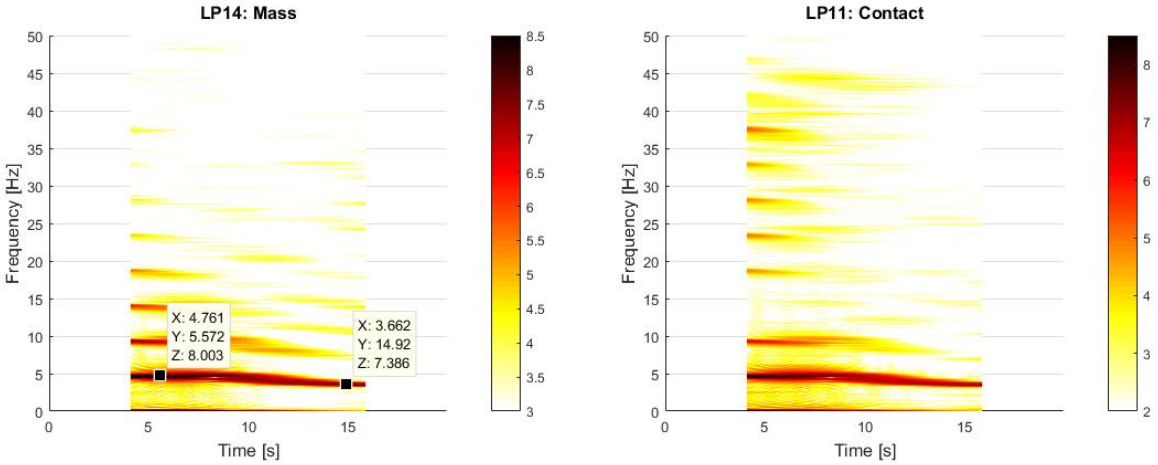

Figure 3.3.3.2 – Time-frequency contents of CD1 with high frequency resolution (k = 13).
From left to right LP14 and LP11 are displayed.

Here happens something unexpected, that is the 1st natural frequency becomes 3.5 Hz when the contact is not more present. This value is also noticeable in all the acquisitions with this laser and is in high contrast to 2.97 Hz that has been detected with the other 1D lasers. Also for the 1st campaign, the 1D lasers show a 1st natural frequency of 2.97 Hz and the time-frequency analysis are not reported for sake of brevity also.

Moreover if the time-frequency transform is applied with lower frequency resolutions and therefore more probability to identify more instantaneous phenomena, it can be seen a strange increase of the natural frequency at about 7 s.

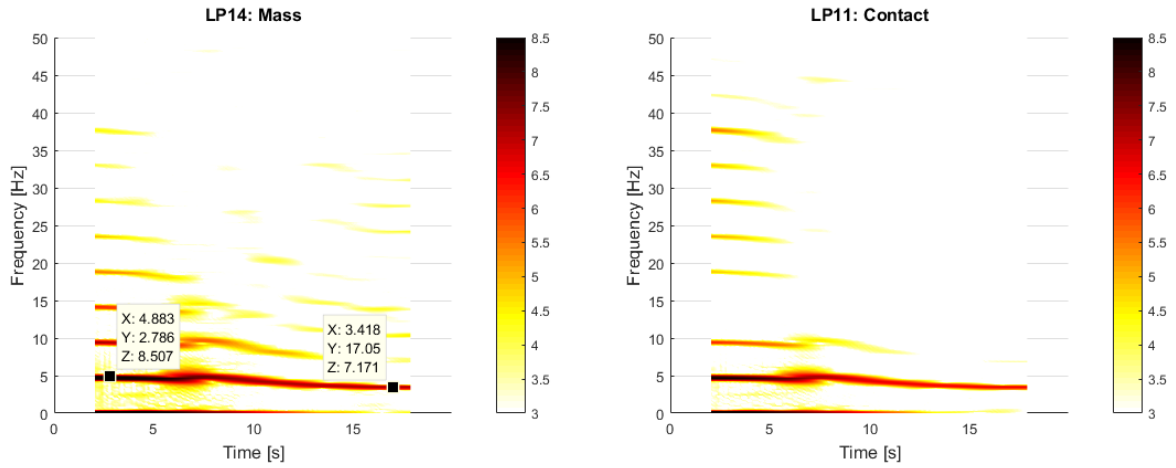

Figure 3.3.3.3 – Time-frequency contents of CD1 with low frequency resolution (k = 12). From left to right LP14 and LP11 are displayed.

Instead, the wavelet analysis is reported in Figure 3.3.3.4.

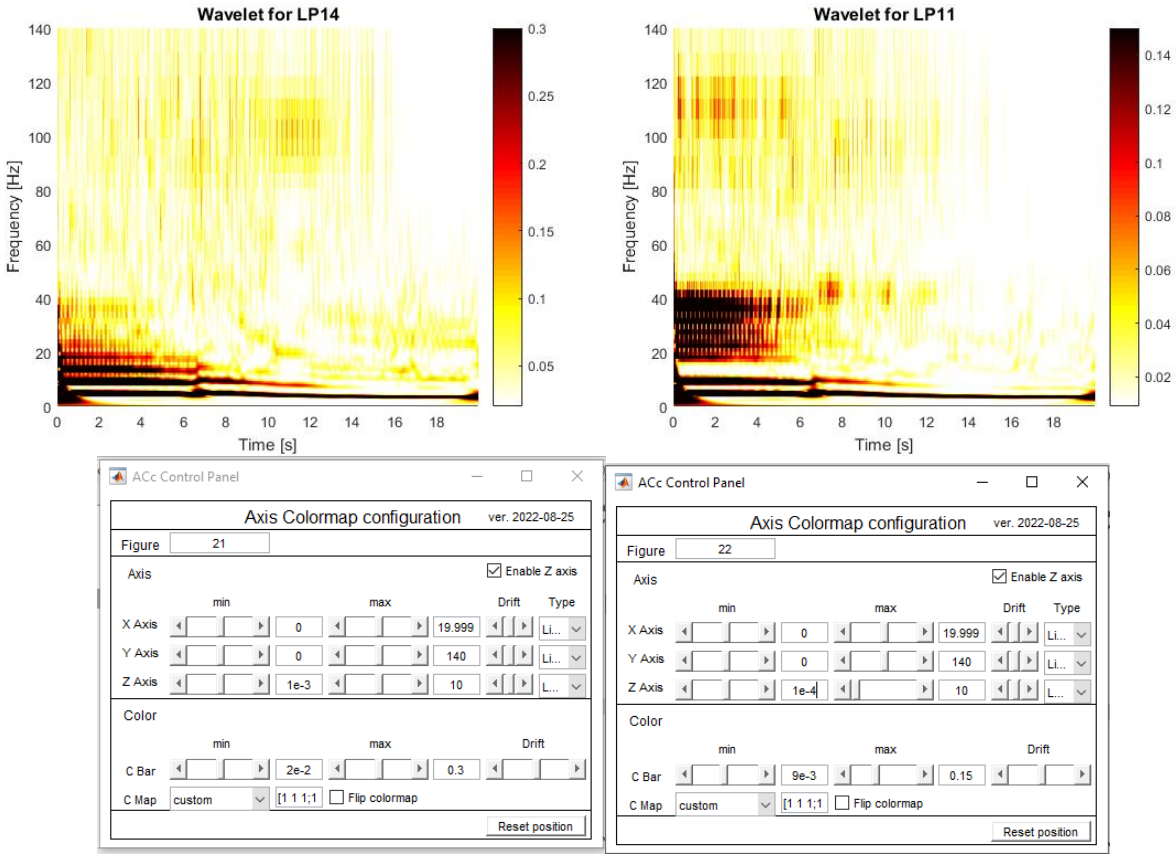

Figure 3.3.3.4 – Time-frequency contents of CD1 wavelet method (k = 12). LP14 (up-left) and LP11 (up-right) with their ACc settings (low).

Even here, the frequency contents are slightly higher than the ones of the LK lasers and the instantaneous peak at 7 s is present as well. In order to better understand this analysis, it is needed a zoom on the first 4 s of LP11, present in Figure 3.3.3.5.

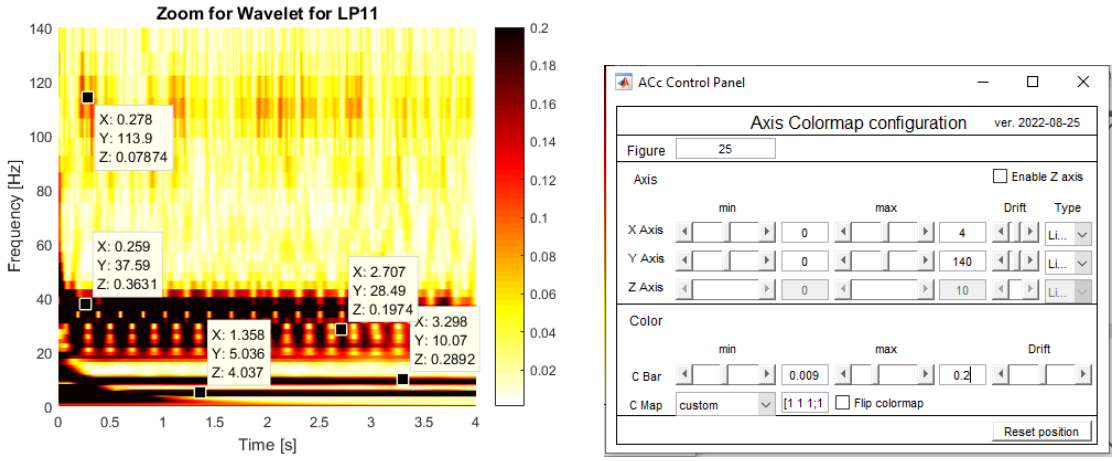

Figure 3.3.3.5 – Zoom of wavelet analysis of CD1 LP11 and its settings in ACc.

Here there are the evidence of the first 3 natural frequencies of the system in configuration 4, i.e. 2.97, 38.75 and 117.9 Hz, as declared in Table 3.4.3. The value of 28.49 Hz is perhaps related to internal dynamic of the beam during the instants of the contact. The highlighted dot at 5.036 Hz is the representation of the first natural frequency of configuration 4 like what is written after Figure 3.3.3.6 could explain.

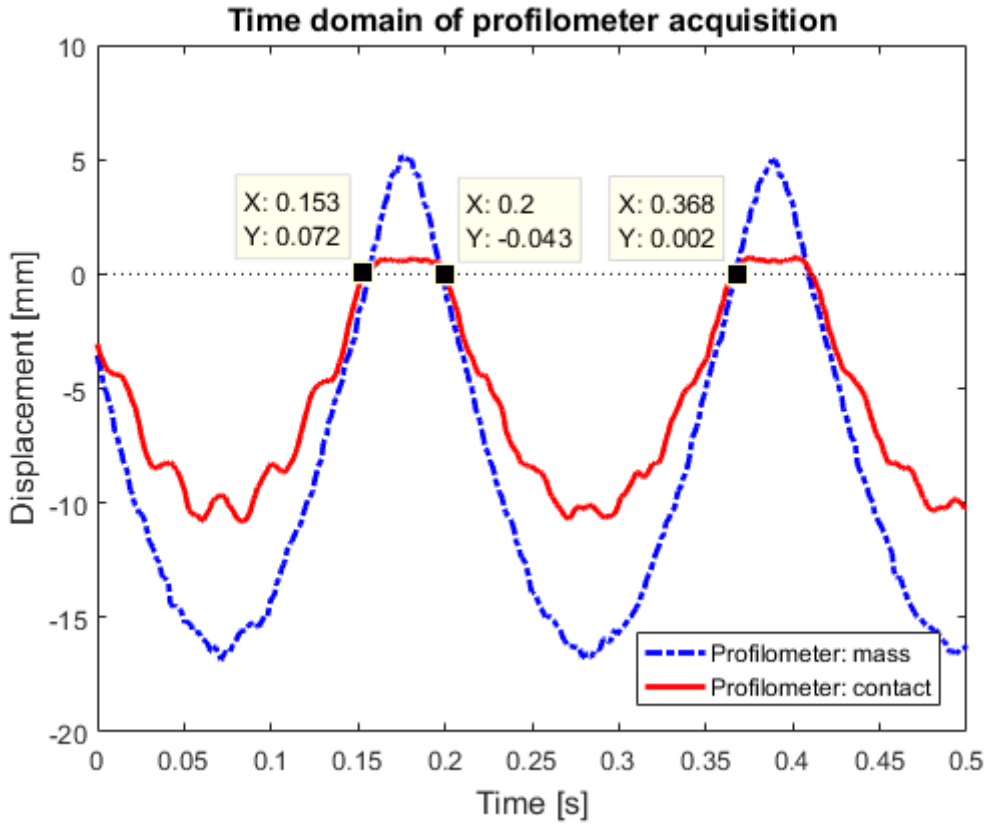

Figure 3.3.3.6 – Instants of contact.

In the picture it is visible that the contact of the beam with the non-holonomic constraint during the first fully acquired oscillation lasts from 0.153 s to 0.2 s while the swinging end at 0.368 s.
Therefore the value of 5 Hz may derive from the Equations 3.3.3.1 and 3.3.3.2.

$$2.97x + 13.88(1-x) = 5.36 \tag{3.3.3.1}$$

Which is a weighted average of the values of the fundamental frequencies of the configurations 4 and 3 respectively. x is computed with the instants marked in Figure 3.3.3.6 and is equal to:

$$x = \frac{0.368 - 0.2}{0.368 - 0.153} = 78.1\% \tag{3.3.3.2}$$

Concerning the 10.07 Hz frequency, it is surely the 2nd superharmonic of the fundamental since 10.07 is basically the double of 5.36 Hz. It is normal to have superharmonic of pair order even if a magnet is not present, indeed this contribution comes the truncation of the displacement when there is the contact.

Since the measured point is in correspondence to the non-holonomic constraint, it is not expected to see a frequency contents of 13.88 Hz, that is the 1st natural frequency of configuration 3, because LP11 does not move in this particular configuration. Different is the case for LP14, whose frequency contents is shown in Figure 3.3.3.7.

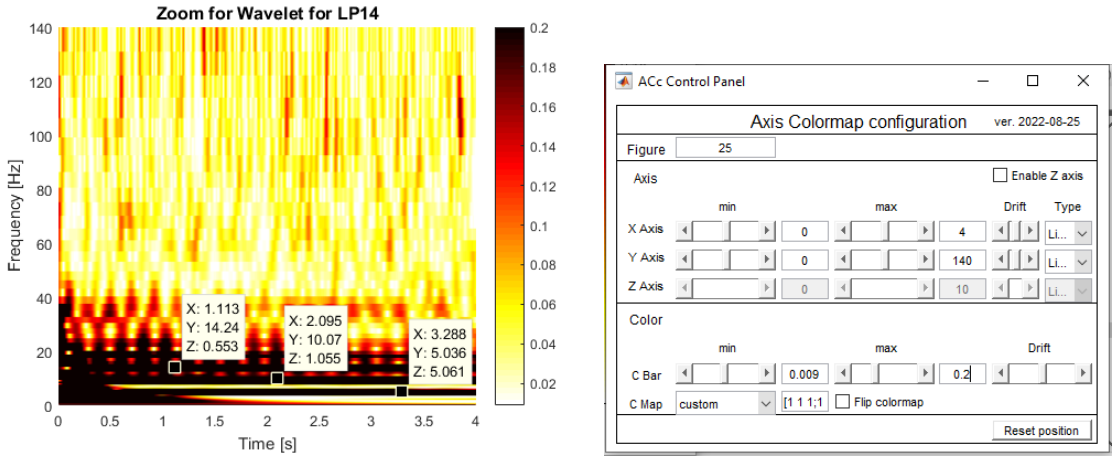

Figure 3.3.3.7 – Zoom of wavelet analysis of CD1 LP14 and its settings in ACc.

As one could predict, a strong black line around 14 Hz is present, but also a contribution deriving from the 3rd superharmonic can be imagined. Even here the 2nd superharmonic is visible.

As regards MaD1, the time-histories are basically equal, as shown in Figure 3.3.3.8. That means that the frequency contents have relatively small values.

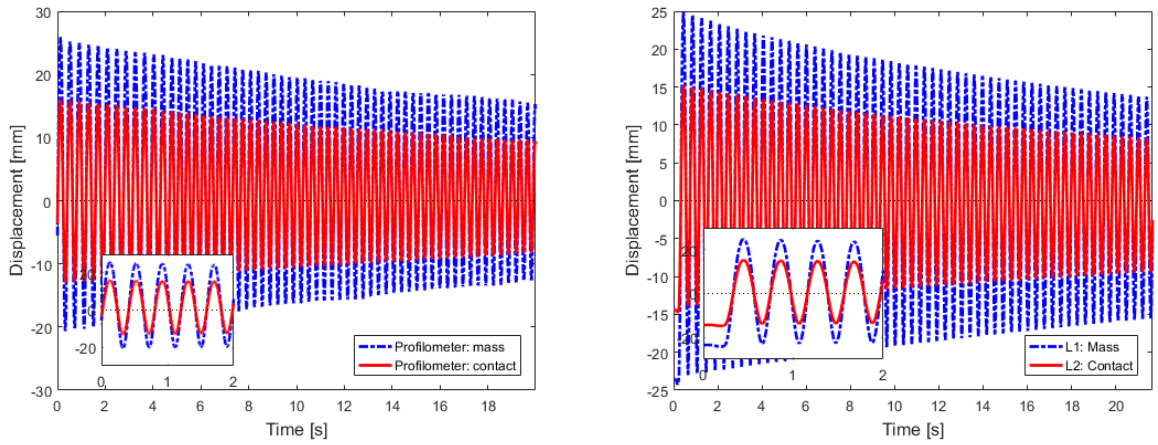

Figure 3.3.3.8 – Comparison of the time-histories of MaD1.
From left to right profilometer and point laser acquisition are displayed.

The spectrogram for this test is contained in Figure 3.3.3.9.

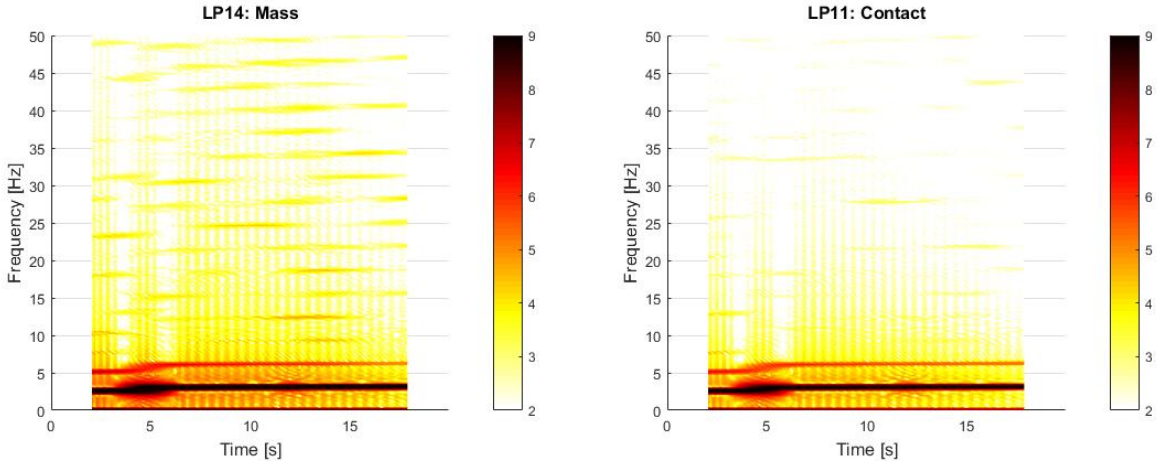

Figure 3.3.3.9 – Time-frequency contents of MaD1.
From left to right LP14 and LP11 are displayed.

The only 2 visible nonlinear effects are the presence of the 2nd superharmonic of the fundamental and the softening effect that derives from the decreasing amplitudes of the oscillations and therefore the decreasing interactions of the magnets.

The wavelet method is displayed in Figure 3.3.3.10.

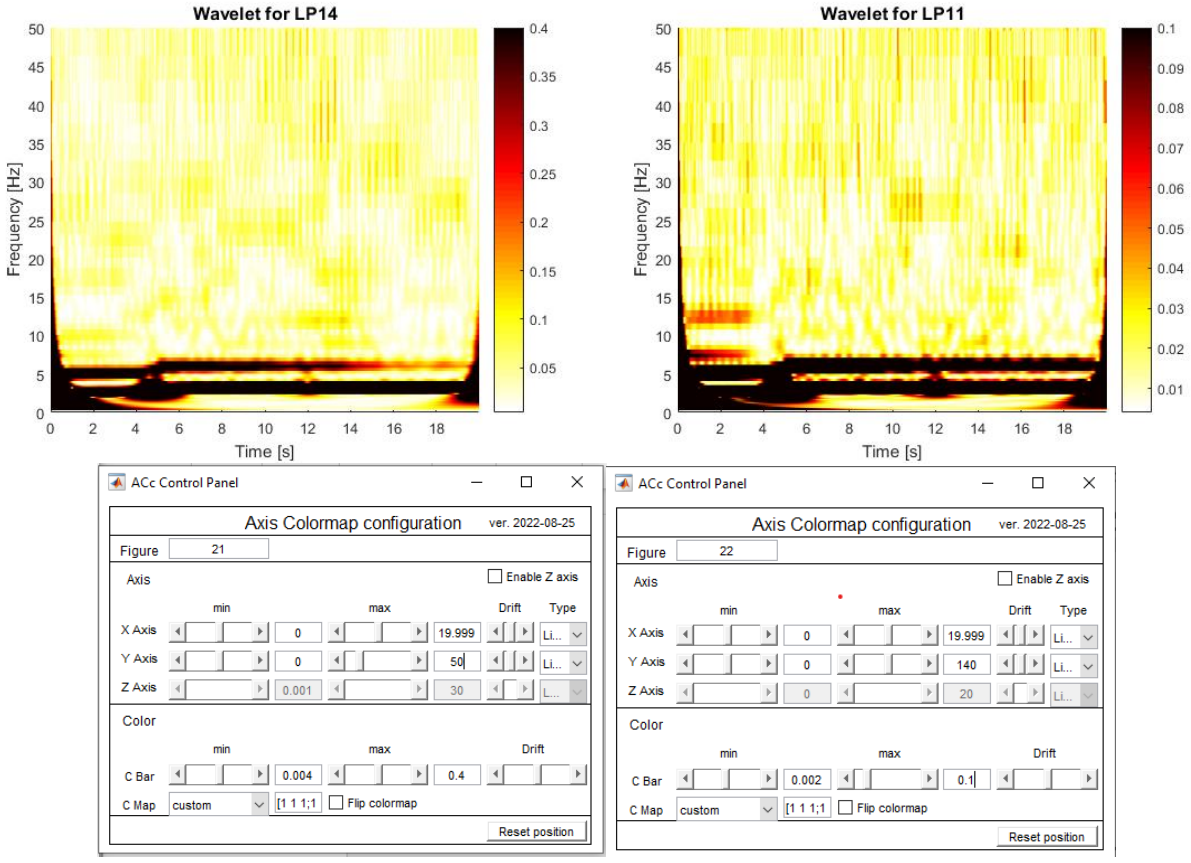

Figure 3.3.3.10 – Time-frequency contents of MaD1 wavelet method LP14 (up-left) and LP11 (up-right) with their ACc settings (low).

Just by looking at LP11, it can be noticed a superharmonic of the 3rd order in the first 4 seconds. This is the confirmation that a nonlinear magnetic force in the equation of motion, if developed up to the 3rd term, completely describes the action of the magnet.
The 3rd harmonic can be seen more easily seen in Figure 3.3.11, where the wavelet method is applied to the derivative of the measured signal LP11. The motivation of that is the fact that the so-called "Mobility FRF" (velocity/input) has a slope after its peaks of about 20 db/decade whereas the "Receptance FRF" (displacement/input) has a 40 db/decade inclination. Thus the frequency contents of the former have many more dark zones than the ones of the latter and the frequency between 10 Hz, i.e. of the third harmonic becomes more visible.

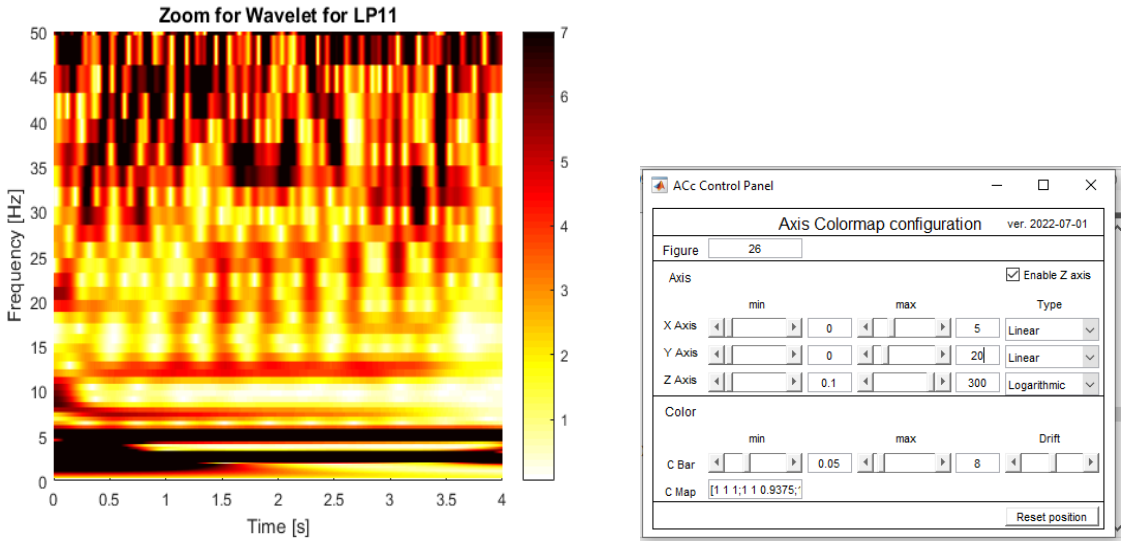

Figure 3.3.3.11 – Time-frequency contents of MaD1 wavelet method for the derivative of LP11 (left) with their ACc settings (right).

For what BD1 concerns, the analysis of the 1st campaign highlights the same aspects already discussed after Figure 3.3.1.7 therefore is not reported for sake of brevity.

3.4 Experimental comparison

Last step is to simulate the structure with Lupos in order to have a correspondence of the natural frequency in configurations 3 (clamped-pinned) and 4 (clamped-free), which are respectively the one with non-holonomic constraint and the one with the only cantilever beam. The representations of these setups are shown in Figure 3.4.1.

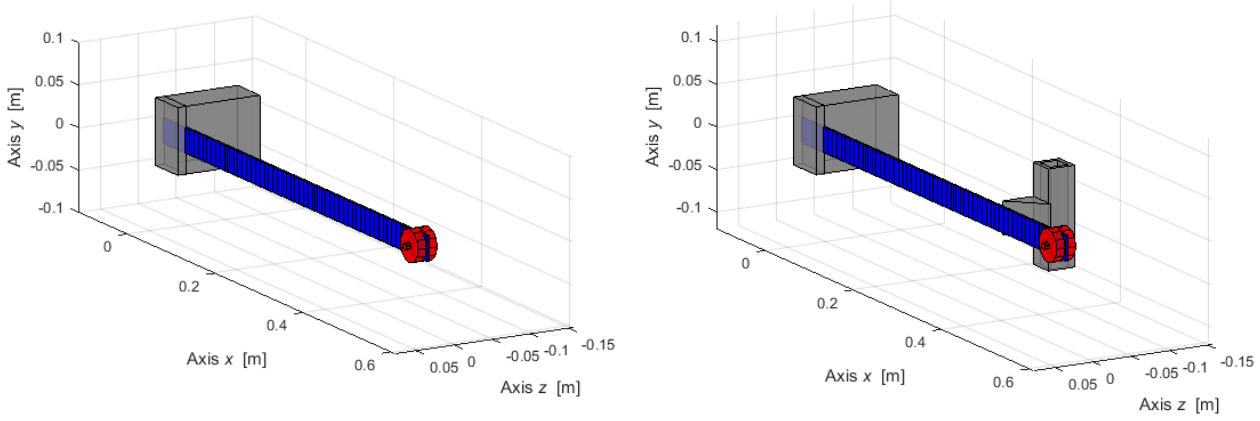

Figure 3.4.1 – Representations of configurations 4 (left) and 3 (right).

The material properties of the elements are chosen accordingly to Table 3.1.2.1 and shown in Table 3.4.1.

Table 3.4.1 – Lupos material properties.

Item	Material	Density [kg/m^3]	Young modulus [GPa]	Poisson ratio [-]
Constraint base	Steel	7800	200	0.3
Constraint plate	Steel	7800	200	0.3
Bosch profiled	Steel	2700	69	0.33
Non holonomic constraint	Steel	2700	69	0.33
Beam	Aluminium	2699.2	69	0.33
Lumped mass	Steel	8300	200	0.3

The density of the lumped mass is chosen to be 8300 kg/m^3 instead of 8225 kg/m^3 in order to take into account the weight of the fasteners.

The lumped mass is chosen to be a rod element as the clamp is modelled with two Timoshenko beams.
Also the Bosch profiled making up the non-symmetric constraint is a Timoshenko beam element, but it is modelled with a hollow section that has the same area, flexional and axial behaviours of the real profiled. The difference between the simulated and actual part is the fact that the section of the former is 34.17x34.17 mm instead of the 40x40 mm of the latter [11].
The triangle making up the non-holonomic constraint is built with two *tria* shells and three *quad* shells, and a total of six nodes.

As regards the beam, it is discretised with Timoshenko beams as well. In particular, the free part has an elements every 10 mm while the locked portion is constituted by two 25 mm long elements.

Concerning the border conditions (BCs), they are reported in Table 3.4.2.

Table 3.4.2 – Border condition for the configurations

Configuration 4		Configuration 3	
Node	DOFs locked	Node	DOFs locked
100	All	100	All
201	All	201	All
202	All	202	All
401	All	401	All
402	All	402	All
-	-	501	All
-	-	142	z-displacement

That, in the clamped-free configuration corresponds to lock the constrained portion of the beam and the clamp. In addition to that, in configuration 3, the new BCs are the one relative to the base of the Bosch profile and the pin that recreates the contact between the beam and the non-holonomic constraint.

The results of the modal analysis for bending in *xz* plane are reported in Table 3.4.3.

Table 3.4.3 – Results of modal analysis.

Mode	Clamped-free [Hz]	Clamped-pinned [Hz]	**Description**
1	2.973	13.88	First bending *xz*
2	38.75	85.18	Second bending *xz*
3	117.9	224.6	Third bending *xz*
4	224.9	280.1	Fourth bending *xz*

Even if the position of Table 3.4.3 in the thesis is at the very end of the work, they were used to justify and proper interpret the graphs of the frequency contents of previous chapter, especially of experimental test CD1 of the 1st campaign. The natural frequency at 2.97÷3 Hz is visible in most of the Figures displayed in the document and it is a solid confirmation of the quality of all the understandings made.

3.5 Conclusions

In this chapter, finally a real nonlinear system is taken into account. The majority of the nonlinear properties highlighted are visible thanks to the frequency content analyses. In particular the wavelet method is much more precise and able to catch instantaneous phenomena at relatively high frequency than the spectrograms owing to the decreasing time windowing needed to have a proper resolution as the frequency grows.
Also there is an exceptional correspondence of the experimental and numerical values of the frequencies, which lends the work a certain prestige.

Conclusions

Chapter § 1 of the work is the perfect representation of how difficult can be to obtain a satisfying result when one has to deal with discretising complex tridimensional automotive structures. In this specific case, many routines affected the final results:

- `PrismaticDiscretisation.m`, where the nodes of an equispaced grid with different distances in the three dimension was created. In particular, the new routine is faster than the previous one;
- `Fea_simpler_Prismatic.m`, where many of the generated nodes were deleted and only the ones near to the initial SW mesh survive. Many attempts to choose properly the "correction factor" were carried out and the best results came with the value of 1;
- `Hex_Mat_assign.m`, where the right material properties were assigned to the surviving Hexs on the base of the material of the nearer Tets. The best way to treat the uncoupled Hexs is to attribute them the most diffuse features of the surrounding cuboid that have the material correctly assigned.

Afterwards, in § 2, an overview of the foremost aspects of nonlinear systems was presented. The presence of the superharmonics of the fundamental frequency in their frequency content is surely one of them. Another important nonlinear characteristic is the hardening/softening phenomenon, i.e. the increase/decrease of the values of the natural frequencies happens when the amplitude of the oscillations grows.
In order to better understand these properties various SDOF damped and undamped system were simulated in Simulink. The most complete equation of motion for this system is:

$$m\ddot{\bar{x}} + c\dot{\bar{x}} + k_1 \bar{x} + k_2 \bar{x}^2 + k_3 \bar{x}^3 = 0 \qquad \text{(C)}$$

The effects of variating one parameter at time were analysed. Due to the fact that k_2 is always negative, instability problems could occur if the system was excited with a too intense IC.
Moreover, it resulted that high damping made more complicated to spot nonlinear symptoms for the used system.
The most appropriate tools used to deepen nonlinear system are:

- Spectrograms: that are based on the FFT, representing structures with summation of sines and cosines. Certainly, a crucial parameter to be set concerning this method is the frequency resolution: the higher it is, the more efficient one is concerning the individuation of the precise values of the frequency contents. Vice versa, the advantage of having a sufficient low resolution is the increasing probability to identify more instantaneous phenomena;
- Wavelet, which employs waves of various shapes and now are widespread in the word of compressing sounds. Here the consequences of varying an input parameter in MATLAB is way minor with respect to the former.

The difference between the two tools is that the spectrograms have a constant delta-time sample Δt and only captures a mean value of the instantaneous frequencies and therefore are less able to catch instantaneous phenomena than the wavelet method. Indeed, the fact that its resolution increases for higher frequencies, does make it more suitable for nonlinear systems.

The theoretical concepts of § 2 were eventually observed in two real experiment campaigns in chapter § 3, where a vibrating beam with various sources of nonlinearity. Unfortunately, the acquirements of the 2nd campaign had been marked with an unwanted low-pass filter that cancelled

the frequency contents of the test over 40÷45 Hz. Nevertheless, many nonlinear symptoms could be highlighted.
The first analysed one was the softening effect owed to the increase of the oscillation period when the hypothesis of little oscillations could not be done, that had been spotted in Figure 3.3.1.7.
Afterwards, the softening and hardening effects noticeable respectively with magnets in attraction and repulsion. Using a test of the first campaign also a validation of what (2.2.2.6) states, i.e. the fact that linearising the expression of a magnet force up to the 3rd order is completely enough to fully reproduce its behaviour. In order to make this, Figures 3.3.3.10-11 were produced to demonstrate that the maximum number of visible superharmonics of the fundamental is 3.
As regards the test involving the non-holonomic constraint, the wavelet method was able to precisely correlate the resonance frequencies calculated using the Lupos simulation tool to the ones visible in the frequency contents. In particular, the first 3 frequencies related to the xz bending modes of the free cantilever beam are clearly visible in Figure 3.3.3.5. The fundamental one was not visible with the value of 2.97 Hz (Table 3.4.3), but with a weighted mean with the 1st natural frequency of the configurations with a clamped-pinned beam (setup 3) that considered the time duration of a complete oscillation and the instants of contact during the oscillation itself. This had been documented with the help of Figure 3.3.3.6.
At the very end of the thesis, the details of the simulation of the systems were reported. It can be said that the frequency contents of the tests were analysed with the use of the final Table of the work, i.e. Table 3.4.3, whose topic is the list of the first 4 natural frequencies of system in configurations 3 and 4 concerning the xz bending modes.

Reference

[1] Bonisoli E., *SolidWorks to LUPOS_2022-04-12*, Politecnico di Torino, Torino, Italy, 2022.
[2] Bonisoli E., *NodesElem*.
[3] Bonisoli E., *Lupos_Tutorial_2022-01-16,* 2022.
[4] Fernandes Reduto A., *MineCraft project: Iveco steering column base,* BSc Thesis, Politecnico di Torino, Torino, Italy, 2021.
[5] https://www.andreaminini.org/chimica/solidi/solidi-cristallini available in 10/05/2022.
[6] https://en.wikipedia.org/wiki/Duffing_equation available in 2022-05-21.
7] Bonisoli E., *Analisi di sistemi dinamici magneto-elastici*, PhD Thesis, Politecnico di Torino, Torino, Italy, 2003.
[8] Nayfeh A.H, Mook D.T., *Nonlinear oscillations,* John Wiley & Sons Inc., New York, 1995.
[9] Bonisoli E., Lisitano D., Conigliaro C., "Experimental-numerical comparison of contact nonlinear dynamics through multi-level linear mode shapes", *Springer*, 2019, EB.
[10] Bonisoli E., "Time-frequency analysis", Politecnico di Torino, Torino, Italy, 2021.
[11] Franco R., *Equivalent mechanical characteristics of a profiled Bosch beam,* BSc Thesis, Politecnico di Torino, Torino, Italy, 2022.

Ringraziamenti

Le prime persone che voglio ringraziare di cuore sono il Professore Bonisoli e il Dottor Luca Dimauro e le nobili menti che hanno condiviso con me la passione per la meccanica vibrazionale. Nonostante i vari "schiaffetti correttivi", alcuni meritati, altri effettivamente no, mi avete accolto nel vostro magnifico ambiente di professionisti e mi avete spronato a fare sempre meglio grazie alle tante volte in cui veniva riconosciuto il mio impegno e la mia passione per la materia.

Grazie a Papà perché "l'arte delu tata è menza mparata" e per tutto il tempo che mi dedicavi in modo potessi concentrarmi al massimo allo studio.

Grazie Mamma per la pazienza, l'amore che mi hai dato e avermi letteralmente fatto mangiare meglio dell'80% degli studenti fuori sede senza farmi impegnare in cucina.

Grazie Francesco e Giulia per aver ammirato il mio percorso di studio e per gli abbracci calorosi che mi davate ogni volta che ci rivedevamo. Vi confesso che, man mano che passano gli anni, sto capendo sempre di più che i fratelli sono le persone più importanti che si hanno, come dice papà.

Grazie a tutti i parenti che hanno creduto in me in modo continuo, ma anche a chi al massimo mi ha chiesto "come ti trovi a Torino?" dopo 4 anni che ci stavo.

Dico un grazie generale a tutti gli amici di Salice, di Canna, di Milano, di Martano, di Andria ecc. per esserci sempre stati sia quando eravamo lontani sia quando eravamo vicini.

E infine, grazie Vincenzo, perché solo tu conosci a pieno cosa hai dovuto fare per questo traguardo e quanto esso vale.